Final Report: Evaluation of Geomorphic Changes of the Little River, Texas

Texas Water Development Board Contract #2300012679

Prepared for:

Texas Water Development Board

Prepared by:

Rebecca Owens, Ph.D.

Raquel Granados Aguilar, Ph.D.

John R. Giardino, Ph.D.

December 2024

This page is intentionally blank.

Final Report: Evaluation of Geomorphic Changes of the Little River, Texas

Texas Water Development Board Contract #2300012679

By

Rebecca Owens, Ph.D., Tyler Junior College

Raquel Granados Aguilar, Ph.D., Tyler Junior College

John R. Giardino, Ph.D., Texas A&M University

December 2024

Table of Contents

List of Figures

List of Tables

List of Equations

List of Acronyms

CTI	Compound Topographic Index
CWT	Continuous Wavelet Transform
DEM	Digital Elevation Model
GIS	Geographic Information System
GPS	Global Positioning System
HUC	Hydrologic unit codes
LiDAR	Light Detection and Ranging
LWD	Large Woody Debris
MStaT	Meander Statistics Toolbox
NHD	National Hydrology Dataset
NRCS	Natural Resources Conservation Service
SfM	MVS Structure from Motion Multi-View Stereo
SPI	Stream Power Index
TWDB	Texas Water Development Board
USGS	United States Geological Survey
WPCA	Wavelet Principal Component Analysis
WPS	Wavelet Packet Spectrum

Executive summary

This study addresses rates of channel migration influenced by varying flow regimes of the Little River from its headwaters at the confluence of the Leon and Lampasas rivers southeast of Belton, Texas, to its confluence with the Brazos River approximately 5 mi (~8 km) southwest of Hearne, Texas. Through its course, the Little River flows generally in a southeast direction for about 107 mi (172 km), measured by its centerline, traversing the Texas Blackland Prairies and East Central Texas Plains physiographic zones. Twelve HUC12 watersheds contribute to the Little River or its immediate tributaries.

Objectives established for the study included: (A) Calculating rates of meander migration along selected reaches of the Little River, (B) correlating these values with varying discharges, (C) determining mechanism of channel migration at temporal intervals from the 1950s to present day, (D) categorizing channel banks for erosion occurrence/potential, (E) examining hydrologic shear stress, bank structure, associated flows, landscape ecological patterns, and sediment category at various bank locations, (F) compiling LiDAR imagery of the Little River Drainage Basin for management use, (G) quantifying rates of planform oxbow development, (H) quantifying rates of meander cutoff for selected sites along the Little River, and (I) categorizing oxbows and meander scrolls based on morphologic and hydrologic properties.

Examination of the Little River included both extensive field work as well as lab and office analysis. The length of the river was examined from the headwaters to its confluence with the Brazos River via canoe. Both aerial and ground-based LiDAR imagery were acquired and used to analyze the river and adjoining banks. ArcGIS® Pro was used to establish and analyze the centerlines of the Little River for the years 1953, 1963, 1974, 1982, 1996, 2004, 2012, and 2018 for purposes of comparison. In addition, the Meander Statistics Toolbox (MStaT), a wavelet-based software that utilizes MATLAB® programming language to provide detailed characterization of large meandering river morphodynamics, was used to examine the length of the Little River.

The findings of this Little River assessment can be summarized as:

- In the Little River watershed, 81% of the area have slope values of 0 to 5%, 16% have slope values greater than 5 to 10%, and ~ 3% of the basin has slope values greater than 10%.
- Eight current oxbow lakes were identified along the ~107 mi (~172 km) course of the Little River
- The Little River experienced migration every 1.2-2.5 mi (2-4 km) in the stretch ~13-31 mi (20-50 km) from its headwaters.
- Using GIS, ten meander bends exhibiting the highest rates of migration

during the years 1953-2022 were identified, eight of these meander bends occurred to the west of Cameron, Texas, which is located near the stratigraphic boundary separating Cretaceous-aged limestone from Paleocene-aged sandstones.

- The average width of the Little River channel is ~95 ft (28.87 m).
    - A chute cutoff has formed, with endpoints at 30° 48' 5.04" N, 97° 7' 27.66" W and 30° 47' 38.76" N, 97° 5' 57.91". The cutoff has created a parcel of land, ~ 618 ac (~250 ha) in area, which sits south of the new Little River channel and north of the former channel. This has the potential to cause frustration among landowners whose property boundaries are defined by the river channel. The new channel was a small creek until 2011, based on remote imagery, at which time it became comparable to the former channel. By 2015, significant sedimentation began to create a plug separating the old channel from the new. As of 2023, the old channel has been plugged, and the cutoff is the main river channel.
- A significant log jam begins at 30° 46' 54.00" N, 97° 3' 56.34" W, and completely blocks the channel for approximately ~233 ft (71 m).
- Channel erosion is most prominent where natural vegetation has been cleared for agriculture. Erosion has produced large woody debris (LWD) in the more actively migrating meander bends, including jams.
- Most of the most rapidly migrating meanders occur west of Cameron, Texas, where the geology changes from Cretaceous-aged limestone to Paleocene—and Eocene-aged sandstones and mudstones.
- The most rapidly moving meander was a chute cutoff with endpoints at 30° 48' 5.04" N, 97° 7' 27.66" W, and 30° 47' 38.76" N, 97° 5' 57.91"
- Aerial LiDAR imagery at ~3 ft (1 m) resolution is available for most of the Little River except for its headwaters through the United States Geological Survey (USGS) National Map Viewer. Aerial LiDAR imagery at ~33 ft (10 m) resolution is available for the entire Little River watershed through the USGS National Map Viewer.
- Ground LiDAR imagery was compiled in this study at specific points of interest along the channel. These points of interest included overpasses and some rapidly migrating meander bends.

1 Introduction

This study addresses rates of channel migration influenced by varying flow regimes of the Little River from its headwaters at the confluence of the Leon and Lampasas rivers southeast of Belton, Texas, to its confluence with the Brazos River approximately 5 mi (~8 km) southwest of Hearne, Texas, (Figure 1-1).

Through its course, the Little River flows generally in a southeast direction for 107 mi (172 km). Discharge in the Little River increases approximately 8 mi (13 km) north of Rockdale where the only tributary, the San Gabriel River, joins the Little River. In addition, this project assesses meander migration rates and patterns, river-bank stability, and landscape-ecological factors associated with river-bank stability for specific locations along the length of the river.

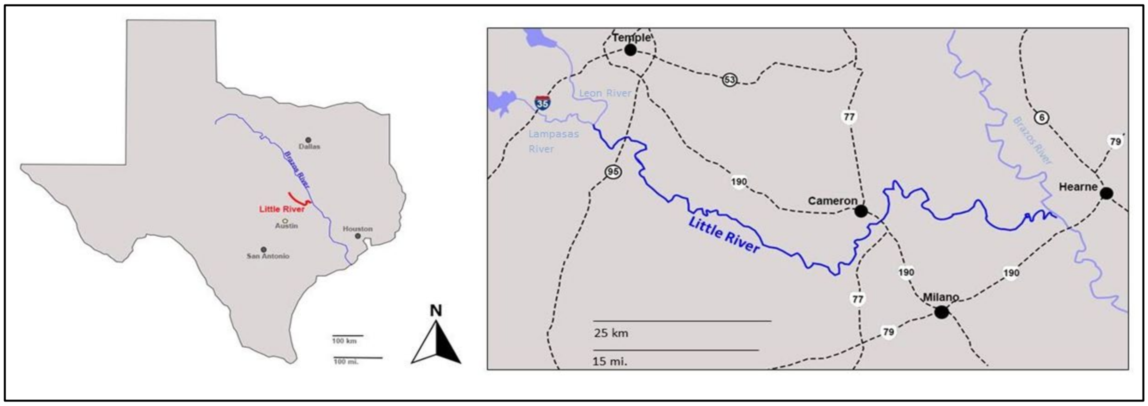

Figure 1-1. Location of the study area.

1.1 Specific Objectives

The specific objectives of this project were:

1) Channel Mechanics

- Calculate rates of meander migration along selected reaches of the Little River and correlate these values with varying discharges.
- Determine the mechanism of channel migration at temporal intervals (i.e., 1950s, 1960s, to 2020) for each selected reach.
- Categorize channel banks for erosion occurrence/potential by examining hydrologic shear stress, bank structure, associated flow, landscape ecological patterns, and sediment category along banks.
- Examine hydrologic shear stress, bank structure, associated flow, landscape ecological patterns, and sediment category along channel banks to categorize them for erosion occurrence/potential.
- Compile LiDAR Imagery of the Little River Drainage Basin for management use.

2) Oxbow Development

- Quantify rates of planform oxbow development.
- Quantify rates of meander cutoff for selected sites along the Little River.
- Categorize oxbows and meander scrolls based on morphologic and hydrologic properties.

2 Background

This section provides background information on the types of river bank erosion included in this report as well as the methodologies used to describe and quantify erosion along the Little River in Texas.

2.1 Assessment of River Bank Erosion

An overview of the methodologies used in this report to assess the erosion of the banks, as well as the processes observed along the Little River follows.

2.1.1 MStat Analysis

Ruben et al. (2021) developed Meander Statistics Toolbox (MStaT), a wavelet-based software which utilizes MATLAB programming language to provide detailed characterization of large meandering river morphodynamics. MStaT fills a gap in the needs of river morphodynamic computation by providing a toolbox with a simple graphical user interface to perform comprehensive analysis through classical measurements such as centerline sinuosity and lateral migration rate, as well as continuous wavelet transform (CWT) and wavelet principal component analysis (WPCA). The CWT identifies dominant wavelength.

Although wavelet analysis has only recently been used in geomorphology studies (van Gerven and Hoitink, 2009) it has been widely used by hydrologists and offers a method of evaluating rivers whose morphology is controlled by multiple factors working on various temporal scales (Mount et al., 2013). As explained by Mount et al. (2013), wavelet analysis involves consideration of bank retreat as a spatial signal of planimetric change. In this approach, varying scales of erosion are equivalent to varying frequencies contained within the signal, and magnitudes of erosion are equivalent to signal amplitude. The erosion signal thus becomes the spatial equivalent of a standard time series signal, with distance substituted for time. This approach is similar to the Fourier analysis approach, which has been used in other geomorphic studies (Ferguson, 1975; Camporeale, 2005) but is dependent upon spatially stationary curvature series (van Gerven and Hoitink, 2009). As natural rivers are not spatially stationary, the Fourier analysis thus leaves great potential for error.

The Fourier transform takes a function as input and produces a function of frequency as output. This output describes how much of each frequency is present in the original function. The concept of wavelet transform uses this same principle to decompose a signal into different frequency components that make it up and identify where a certain frequency or wavelength exists in the temporal or spatial domain (Chen & Zhang, 2023). In the geosciences, the wavelet transform of a signal may represent patterns such as meander curvature (Gutierrez and Abad, 2014). The wavelets of two distinct series (such as a river centerline from two separate years) may be cross-correlated to determine regions with high commonalities. This technique has been utilized in geological studies to assess morphology of sandbars (Tebbens et al., 2002; Short and Trembanis, 2004; Coco et al., 2005; Li et al., 2005; Ruessink et al., 2007), paleoclimatic records (Karimova et al., 2007), and sand transport (Baas, 2006). Wavelet analysis is especially applicable to geomorphic studies, as it does not assume stationarity and is robust toward the intermittent, aperiodic behavior and non-Gaussian distributions typical of sediment transport (Baas, 2006).

The wavelet analysis tool in MStaT performs continuous wavelet transform analysis to determine the spatial distribution and periodicity of a normalized arc-wavelength using the signal derived from curvature fluctuations. It then computes the wavelet spectrum and dominant arc-wavelength at 95% confidence interval (Ruben et al., 2021). An example is presented in Figure 2-1. Note that MStat only runs analysis in metric units; thus, the units in Figure 2-1 are meters.

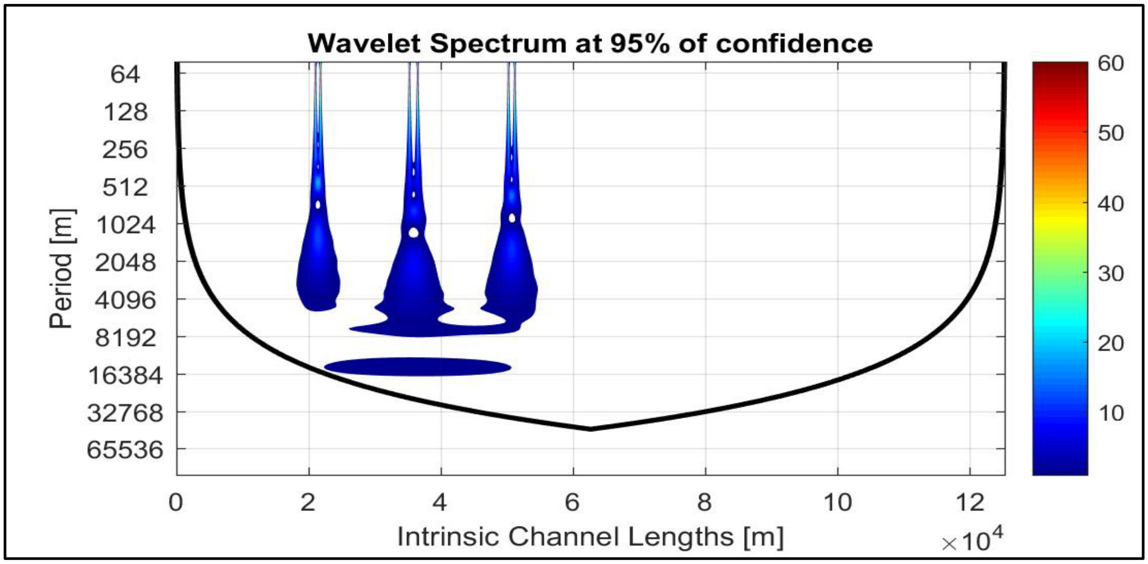

Figure 2-1. Wavelet spectrum depicting highest periodicity of migration at 95% confidence during the years 2004-2012.

Figure 2-1 depicts the wavelet spectrum at 95% confidence for the migration of the Little River between the years 2004 and 2012. The period (left, y-axis) represents the channel length within which a certain magnitude of migration is most commonly detected (Chong et al., 2019). The intrinsic channel lengths (x-axis) represents the full length of the Little River, from headwaters to mouth. The colored scale on the right x-axis represents the Wavelet Packet Spectrum (WPS). The WPS is equivalent to the integration of energy over the period (in meters) of influence (Y. Liu et al., 2007). In this study, the units of the WPS are m^2/Hz, but units will vary by study. The units of the WPS are [unit of time series amplitude]^2/Hz. In this example, the Little River experienced migration every ~1.2-5 mi (2-4 km) in the stretch 12.4-31 mi (20-50 km) from its headwaters.

The curved black line represents the demarcation of 95% confidence in the data.

2.1.2 Qualitative Assessment of Bank Stability

A primary challenge in assessing morphological stability of a river channel is defining what is a "stable" and an "unstable" channel. Brice (1982) considers an unstable channel one whose rate or magnitude of change is great enough to be a significant factor in the planning or maintenance of a bridge, highway, or other structure. Thorne et al. (1996) describes an unstable channel as actively changing its form through time and space and likely to show evidence of serious sustained aggradation, degradation, width adjustment or planform change. Stable streams are subsequently specified as dynamic or moribund, based on whether the channel adjusts in response to natural environmental fluctuations or only to imposed engineering efforts. Whereas dynamic stable streams generally have alluvial channels formed by the river itself, moribund channels often have channels which result from processes and conditions which happened in the past. These channels often exhibit low stream power, low gradients, and erosion-resistant banks. Lagasse et al. (2012) identify stream instability by the presence of lateral bank erosion, aggradation or degradation of streambed progressing with time, and/or short-term fluctuations in the elevation of the streambed usually associated with scour and fill.

Many assessments of river stability were developed to assess the structural integrity of engineering structures which cross river channels (Pfankuch, 1978; Brice, 1982; Brookes, 1987; Thorne et al., 1996; Johnson et al., 1999; Doyle et al., 2000; Lagasse et al., 2012). In the Pfankuch (1978) method, channels are evaluated at the upper banks, lower banks, and bottom. Mass wasting, debris jam potential, and vegetative bank protection are evaluated at the upper banks with rankings of excellent, good, fair, or poor. At the lower banks, channel capacity, bank rock content, obstructions, flow deflectors, cutting, and deposition are assessed similarly. The same evaluation is used at the channel bottom for rock angularity, brightness, consolidation, packing, the distribution of bottom sediment size and percent stable materials, scouring and deposition, and clinging aquatic vegetation. Higher scores indicate lower stability in this evaluation, and each rank is assigned a point value. This differs from Johnson, Thorne, and Booth, in which the final average score is weighted. Later, the Pkankuch (1978) method was found to need more precision of measurement to predict the extent or type of channel change accurately (Morét, 1997). Brice (1982) developed a method for the Federal Highway Administration to assess stream stability based on type. In his method, stream type is based on the variability of width and the presence of bars. He defines stream instability as lateral bank erosion, progressive degradation of the streambed, or natural scour and fill of the streambed. Brookes (1987) studied 46 river channels in England and Wales downstream of channelization works. The study considered how stream power, channel cross-sectional width, shear bed and bank strength, and sediment size affect channel stability, comparing locations of modern channels to former ones using historical aerial photography and maps.

Additionally, empirical measurements were taken over three years using pins inserted into riverbanks. In his summary, measurements are combined to show changes in channel capacity, width, and depth with distance from engineering structures and threshold capacities downstream of channel construction. Historical data revealed occurrences of floods that exceeded the modified threshold, which likely triggered erosion. In their survey of channel stability near engineering structures, Thorne et al. (1996) consider the size of bed material (coarser sediment indicates higher stability), bed protection, stage of channel evolution, percentage of channel constriction, number of piers on channel, percentage of blockage, bank erosion on each bank, meander impact point from bridge in meters, pier skew for each pier, mass wasting at pier, high-flow angle of approach, and percentage of woody vegetation cover. The Federal Highway Administration (2006) developed a detailed method of assessing channel stability in different physiographic regions of the United States. Still, only two reference streams used were in the Gulf Coastal Plain: Alligator Creek and Peace River, both in Florida. Other stability assessments have been developed based on streams in Colorado (Rosgen, 2001), Georgia (Mukundan et al., 2011), and Texas (Owens, 2020).

The method utilized in this study is presented by Doyle et al. (2000) and is a modification of the method by Johnson et al. (1999). Johnson et al. (1999) present a weighted average of 13 stability indicators, each ranked excellent, good, fair, or poor. Each stability indicator was given a pre-assigned weight based on its influence on channel morphology and ranked excellent (1-3), good (4-6), fair (7-9), or poor (10-12).

2.1.3 Stream Power

Shear stress has been used to quantify channel stability in numerous early studies (Graf, 1983; Fischenich, 2001; Phillips, 2013); however, stream power may be a more effective indicator of channel stability (Graf, 1983; Fischenich, 2001; Phillips, 2013; Jha et al., 2022). It is geomorphologically significant because it is directly related to total transport of sediment (Bagnold, 1980). Because stream power is a function of channel dimensions and discharge, it is also more valuable in process analysis than considering individual channel dimensions considered separately (Graf, 1983).

The ability of flowing water to erode sediment determines potential alteration to the channel morphology and is directly correlated to stream power or unit (specific) stream power (Yang et al., 1972; Govers and Rauws, 1986; Phillips, 1989; Wohl, 2000; Fischenich, 2001; Stacey and Rutherford, 2007; Julian et al., 2012). Yang et al. (1972) developed a unitless equation for stream power to estimate total concentration of sediment in alluvial channels in consideration of variable particle size and water depth and temperature. Multiple researchers (Govers and Rauws, 1986; Govers, 1992; Magilligan, 1992; Ali et al., 2011) have found unit stream power to be a valuable predictor of the capacity to transport sediment. Parker et al. (2014) developed a ST:REAM model for the River Taff catchment in South Wales, UK, which closely correlates features associated with erosion or deposition with values for stream power, although not consistently on a regional scale (Parker et al., 2014). Bizzi and Lerner (2015) also used stream power to predict where erosion or deposition will be the dominant force at work in a stream; they showed that the dominant process (i.e., deposition or erosion) can be determined by local stream power and stream power upstream. Deposition is more likely to occur when local stream power was notably lower than that in upstream segments, and erosion is more likely to occur when local stream power was higher than stream power above (Bizzi and Lerner, 2015; Gartner et al., 2015). This observation offers insight to how, specifically, a channel responds to outside forces, based upon stream power.

Wu et al. (2018) found that capacity to transport loess was well predicted by unit stream power on slope gradients above 26.79% and was often a better predictor than shear stress at different gradients in non-erodible conditions (Wu et al., 2016; Wu et al., 2018). Such conditions are rarely encountered in nature, except when channelization has been introduced, as is often found in urban rivers. Candel et al. (2018) utilized potential specific stream power in paleochannels to correlate periods of high potential specific stream power to increased channel migration. When relating stream power to adjustment of a channel, consideration is always taken of external forcings. It is not satisfactory to assume that erosion or deposition is linearly related to stream power or unit stream power in every fluvial setting (Whipple and Tucker, 1999; Fonstad, 2003), but a sufficiently strong correlation exists for consideration as a stability indicator (Yang et al., 1972; Govers and Rauws, 1986; Govers, 1992; Doyle et al., 2000; Fischenich, 2001; Ali et al., 2011; Bizzi and Lerner, 2015; Gartner et al., 2015; Wu et al., 2016; Candel et al., 2018; Wu et al., 2018). Generally, values of stream power and unit stream power decrease with increasing stability and vice versa (Abernethy and Rutherfurd, 1998; Doyle et al. 2000).

Studies of the Canadian River found that specific stream power was the dominant influence on channel widening and channel erosion (Curtis and Whitney, 2003; Julian et al., 2012). Notable feedbacks exist, however, between land usage and channel widening on a temporal scale (Julian et al., 2012). In the Julian et al. (2012) study, as land on the banks of the river was converted to agricultural use, the banks became more susceptible to erosion. A negative feedback loop developed whereby increased erosion from croplands caused an increase in active channel area, eventually causing a decrease in available cropland. In response, farmers reduced cultivation of floodplains, leading to another negative feedback loop: less land clearing and a wider channel promoted native vegetation growth on channel margins, eventually leading to channel narrowing (Julian et al., 2012). Similarly, construction of a hydroelectric/flood control dam was shown to cause a positive feedback loop between channel narrowing and vegetation growth. With the channel already narrowing because of increased vegetation growth, the dam reduced specific stream power further so that vegetation colonized the margins of inactive channels at an increased rate, promoting sediment deposition and further vegetation growth, resulting in continued channel narrowing.

Stream power is a function of stream discharge and slope. Conventionally, discharge increases from the headwaters of a stream to the mouth, whereas slope decreases. It logically follows that stream power should peak in the mid-profile range, and this is observed in some studies (Lecce, 1997; Knighton, 1999). This pattern is inconsistent, however, among rivers. Increase in discharge may be offset by changes to channel slope, width, roughness, or other factors (Phillips and Slattery, 2007). Some studies have found distributions of stream power with multiple peaks, scattered peaks, or even none at all (Graf, 1983; Magilligan, 1992; Fonstad, 2003; Reinfields et al., 2004; Jain et al., 2006). In the Henry Mountains of Utah, stream power decreased in the downstream direction during the 19th century because of region-wide deposition. This changed during the 20th century when, partially in response to catastrophic flooding, system-wide erosion dominated (Graf, 1983). In a study of the Sangre de Cristo Mountains of New Mexico, Fonstad (2003) found underlying geology to influence stream power at least as strongly as channel slope. Allen et al. (2013) found the same level of influence in the northwest Himalayas. Phillips and Slattery (2007), in their studies of the Lower Trinity River, found processes of streamflow were strongly influenced by antecedent topography and river and backwater forcings. Thus, a generalized model of stream power is unlikely; each river's characteristics must be considered individually.

2.1.4 Ground LiDAR

The use of ground LiDAR in geosciences has evolved since its first published studies in the mid-2000s (X. Liu et al., 2007; Hodgetts, 2009). Alho et al. (2011) demonstrated that terrestrial scanners can be used in fluvial geomorphology studies to map river features on a centimeter scale. The advent and affordability of smart devices have made LiDAR's applicability to the geosciences available to a wide spectrum of scientists, students, and practitioners.

Luetzenburg et al. (2021) tested the iPad Pro® 2020 (hereafter iPad) and the iPhone® 12 Pro (hereafter iPhone) for their utility in geomorphologic assessment. Roneklint, a coastal cliff in eastern Denmark on the Island of Zealand, measures ~426 x 49 x 33 ft (130 × 15 × 10 m) and is susceptible to wave erosion. Using the '3d Scanner App' on the iPhone and iPad, scanning the entire coastal cliff and the beach at Roneklint (length: ~426 ft (130 m), width: ~49 ft (15 m), height: ~33 ft (10 m) in December 2020 was completed in approximately 15 minutes (Luetzenburg et al., 2021). The obtained mesh comprised around 1.5 million vertices, textured with approximately 2,500 overlapping images. Image processing was conducted in Cloud Compare.

Luetzenburg et al. (2021) find that the iPad® and iPhone create accurate high-resolution models with accuracy + 0.4 in (+ 1 cm) for small objects. For large objects such as the coastal cliff, an accuracy of + 4 in (+ 10 cm) is obtained, but increased versatility in handling proved a significant benefit over traditional LiDAR methods. After comparing the iPad and iPhone LiDAR capability with traditional LiDAR methods, Luetzenburg et al. (2021) determined that although the accuracy and precision of the iPhone LiDAR models do not reach the standards of state-of-the-art Structure from Motion Multi-View Stereo (SfM MVS), the LiDAR sensor is capable of realistically representing environments like the coastal cliff of Roneklint above a threshold of ~ 4 in (10 cm) and presents a novel, cost-effective and time-efficient alternative to established methods of topographic land surveying. Other studies, primarily in urban forestry, have also found a threshold of ~ 4 in (10 cm) in scanning large objects, such as trees, with the iPad and iPhone (Gollob et al., 2021; Mokroš et al., 2021; Bobrowski et al., 2023).

Gollob et al. (2021) utilized the iPad scanner for tree mapping and found that the iPad showed a detection rate (of small tree stems) of 97.3%, compared to 99.5% with personal laser scanning. Data acquisition time with the iPad was approximately 7.51 minutes per sample plot. This was twice as long as the personal laser scanning approach but 2.5 times shorter than with traditional forest inventory equipment (Gollob et al., 2021). Mokroš et al. (2021) found that range is a drawback of utilizing the iPad for laser scanning, as it has a range of only ~16.4 ft (5 m). Higher accuracy is obtained with proximity. They note a benefit, however, provided by the iPad and iPhone, which is that the point cloud is available immediately in the field. Terrestrial laser scanners (TLS) provided the most accurate results. Still, in the Mokroš et al. (2021) study, the iPad had dimension estimation accuracy and tree detection rate closest to the TLS results, compared to personal laser scanners and multi-camera options.

2.2 Oxbow Development

The Little River is a meandering river in a wide floodplain, prone to oxbow lake production through meander-cutoff-oxbow lake sequencing. LiDAR aerial surveys and orthorectified historical aerial photography in ArcGIS Pro were used to determine the sequence of meander-cutoff-oxbow lake sequencing on the Little River.

Lateral bank migration characterizes meandering rivers, induced by long-term aggradation and degradation of sediment (Sturm, 2001; Turnipseed, 2017). Bank migration results from the interplay of sediment-laden water flowing over an alluvium channel boundary. With time, alluvium will be removed from the channel boundary or sediment will be deposited from the water to the channel boundary. Interaction between these processes leads to lateral channel migration, and the eventual intersection of upstream and downstream river reaches, creating a cutoff and converting the former meander bend to an abandoned channel. Water flow through the abandoned channel is reduced as the cutoff becomes the main flow path, causing sedimentation and plug formation at its connections to the main channel. This separates the abandoned channel from the main channel, converting it to an oxbow lake (Julien, 2002; Turnipseed, 2017).

Guo et al. (2023) classifies oxbow lake evolution into four stages: operational meander-bend (Stage I), cutoff (Stage II), lake (Stage III), and infilling (Stage IV). A detailed discussion of each stage follows.

2.2.1 Operational Meander-Bend (Stage I)

Meander-migration and cutoff processes are fundamental for long-term morphological changes of meandering rivers in alluvial floodplains (Güneralp and Marston, 2012). Prior studies have sought to establish quantitative means to assess the development and propagation of meander bends (Hickin, 1974; Nanson and Hickin, 1983; Hickin and Nanson, 1984; Hooke, 2007; Güneralp and Rhoads, 2009, 2011; Slowik, 2016). Hickin (1974) determined that the ratio of bend curvature to channel width (Rc:W) provides information about the way meanders develop. This information can be interpreted through examination of successive scrolls in the floodplain, formed by successive ridges and swales as the river migrates laterally. Today, these landforms are exceptionally well noted using aerial LiDAR imagery with discrete color ramps (Figure 2-2).

Maximum channel migration rates occur when the value of Rc:W ratio is between 2.0 and 3.0 (Nanson and Hickin, 1983; Hickin and Nanson, 1984; Slowik, 2016). With time, meander bends tend to migrate such that high Rc:W ratios are lowered and low Rc:W ratios are increased (Hooke, 2007). The relationship between the radius of curvature (r) and migration rate is, however, nonlinear. Migration rate (M/w) along a meander bend tends to increase until the r/w ratio reaches a critical value of 2.0 < r/w <3.0, then decreases with increasing value of the r/w ratio (Hickin and Nanson, 1984; Nanson and Hickin, 1983; Güneralp and Marston, 2012).

The planform geometry of the river channel has both local and cumulative influence on the migration rates along the channel. This influence decreases, of course, with increasing distance from the channel location for which the migration rate is determined (Güneralp and Marston, 2012). A freely meandering river, for example, elongates its meander bends, thus increasing its meander amplitude and sinuosity. Conversely, cutoffs cause sudden meander amplitude and sinuosity reductions by shortening the channel length and increasing the channel gradient.

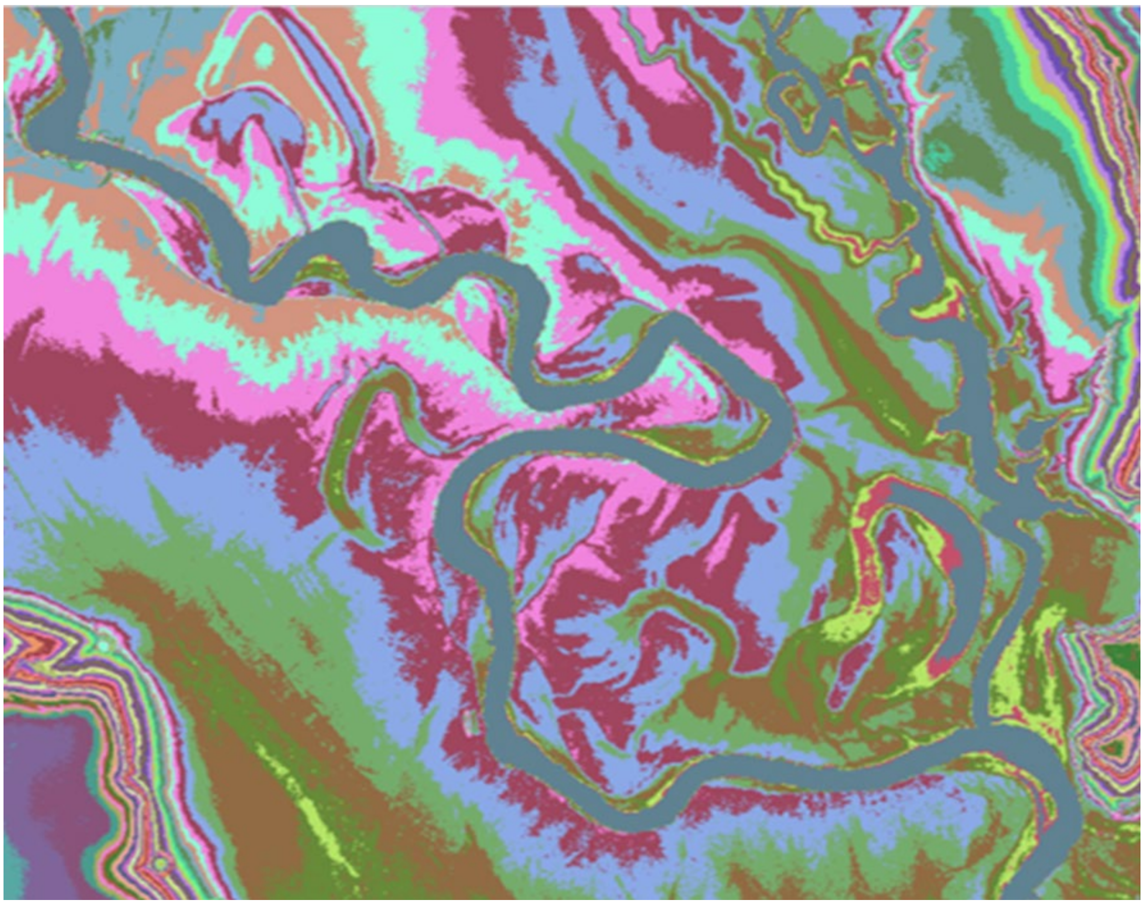

Figure 2-2. Portion of a DEM of the Little River, viewed on a color ramp with discrete boundaries to accentuate oxbow lakes and meander scars.

2.2.2 Cutoff (Stage II)

The cutoff process may occur as a chute or a neck. A chute cutoff forms as a shortcut channel passing through a meander bend and has a length that is longer than a channel width, whereas a neck cutoff forms when the two limbs of a highly sinuous branch touch and has a length that is narrower than a channel width (Julien, 2002; Güneralp and Marston, 2012; Turnipseed, 2017; Gao and Li, 2024). Of the two, chute cutoffs are more common than neck cutoffs (Turnipseed, 2017). Neck cutoffs are more prevalent, however, in low-gradient reaches with high sinuosity and bend curvature, whereas chute cutoffs are more likely to occur in bends with low and intermediate curvatures (Gao and Li, 2024).

The formation of a chute channel at a meander bend requires some mechanism to induce scour and incision in a developing point bar or meander bend (Grenfell et al., 2012). Chute cutoffs can be triggered by four types of mechanisms (Grenfell et al., 2012; Gao and Li, 2024). The first type, headward-erosion chute cutoff, is triggered by upstream overbank flow and subsequent downstream bank erosion. The upstream overbank flow is often triggered by some type of channel blockage or bed aggradation which raises water levels, inducing overbank flows during peak discharge. A chute channel is created once the overbank flow traverses the floodplain and reaches a downstream bend. Further peak flows will, in turn, reinforce headward erosion of the chute channel until it connects with the upstream river limb (Grenfell et al., 2012; Gao and Li, 2024).

A second type of mechanism is the embayment chute cutoff, wherein peak flows have sufficiently high stream powers to excise a pre-existing embayment, carving a new channel through it to a downstream stream reach. This mechanism might be instigated through embayment development by localized channel slumps, swales, or sinkholes (Grenfell et al., 2012; Gao and Li, 2024).

The third type of mechanism is the mid-channel bar chute cutoff, which occurs when the river channel is bifurcated by a central bar. Peak flows arriving at the central bar will be divided, either to the main channel or along the bar itself. The result will be aggradation of the chute bar and narrowing of the channel width, which allows subsequent flows to sustain sufficient shear stress to cut through the bar and form a chute channel. This mechanism is prominent in sand-bed meandering rivers with low bank height and active channel-bar-floodplain dynamics, although it has also been observed in gravel-bed rivers (Gao and Li, 2024).

The fourth mechanism is the scroll-slough chute cutoff, which forms in widening sand-bed bends with laterally growing point bars. The point bars create a series of scrolls and sloughs, with the latter becoming the preferred pathway, even at moderate flow stages. The preferential pathways often become chute channels (Gao and Li, 2024). In reality, none of these processes are mutually exclusive from the others, and chute cutoffs may be initiated using any combination of mechanisms. The time required for full channel adjustment after chute formation varies by river. Hooke (1995) monitored chute cutoffs on the River Bollin and the River Dane and found that channel adjustment continued for 1-3 years with full stabilization after eight years. Blockage of the former channels was established in 1-7 years. Stage II begins when cutoff occurs and can last between one and ten years in an isolated lacustrine environment.

2.2.3 Oxbow Lake Formation (Stage III)

The second stage of oxbow formation is the lacustrine stage, defined by the presence of the fully separated oxbow lake. In a study of oxbow lakes in the Zoige Basin of the

Qinghai-Tibet Plateau, Guo et al. (2023) classifies oxbow lakes based upon four criteria: 1) simple or compound, 2) with or without connecting channels, 3) the shortest distance between the oxbow lake and the main channel (DC), and 4) the distance between the inlet and outlet of the oxbow lake (DL). A simple oxbow lake is one that contains one former meander bend defined as an arc > 60°, whereas a compound oxbow lake has multiple former bends (Guo et al., 2021; Guo et al., 2023). The minimum DL value should approximate the width of the main channel at the time when the oxbow lake was formed by neck cutoff (Guo et al., 2023).

As there are no consistent metrics for directly comparing the magnitude of hydrologic connectivity among oxbow lakes in floodplains of different fluvial systems, a probability-based index, PHC, that quantifies the magnitudes of connectivity in oxbow lakes in terms of recurrence interval (RI) is proposed by Guo et al. (2023). The PHC is defined as: PHC = 1/RI where the RI of each oxbow lake is the magnitude of the main-channel discharge under which the lake is hydrologically connected to the main channel.

2.2.4 Infilling (Stage IV)

During Stage IV, the oxbow lake gradually changes from a lacustrine to a terrestrial setting. During this phase, the sediment source shifts from overbank flows from the main channel to internal deposition within the oxbow lake. Gautier et al. (2007) describes three evolutionary phases of infilling. In the first phase, rapid infilling after plug formation is punctuated by a period of stability. During this phase, the abandoned meander loses about 8–15 % of its area during the first 1–3 years.

Vertical accretion on the plug during this initial stage is accelerated by vegetation growth. After the first accretionary phase, sedimentation slows and the lake stabilizes. During the third phase, accretion may increase as the active meander re-incises the plug and intercepts the abandoned meander, allowing water to flow in the opposite direction than before. The remnant trough will sometimes be infilled within two years (Gautier et al., 2007). The rate of infilling is found by Gautier et al. (2007) to be closely correlated with migration rate of the meander bend.

2.3 Log Jams

Large woody debris (LWD) is defined as logs with either a diameter of ~4 in (0.1 m) or a length of ~3.3 ft (1 m) (Cawthon, 2007; Curran, 2010). According to Montgomery et al. (2003), the length of the tree trunk does not play a significant role in determining transport potential. The ratio of the channel bank full width to the length of the tree trunk has the more significant influence over transport potential, as does the recruitment rate of woody debris (Montgomery et al., 2003; Gurnell et al., 2002; Wohl, 2013; Lombardo, 2017). Meandering rivers with rapid lateral movement recruit large amounts of wood when they erode into wooded areas (Lombardo, 2017). Wood density also affects the likelihood of transport, with dry wood being easier to mobilize than more stable saturated wood (Montgomery et al. 2003). Still more important when considering LWD residence time is the return period of flows capable of moving a large amount of debris (Wallerstein and Thorne 1996).

A jam has formed if enough LWD accumulates to partially or fully block a river channel. LWD jams (or log jams) are defined as jams that are composed of at least one stable "key member" or other obstruction-holding racked LWD (Cawthon, 2007). Jams are initiated by key members, which are larger logs. Smaller logs and debris become wedged against these key members and other obstructions while "loose members" fill the interstitial space within the jam (Abbe and Montgomery, 1996, 2003). Factors that increase the likelihood of LWD jams include narrow channel width, flat topography, and low transport capacity (Lombardo, 2017). LWD jams have been most frequently studied in steep, forested channel reaches where they are often stable channel features, and it is unclear how much of the information on LWD jams from steep forested channels will be relevant to other channel types (Curran, 2010). Low gradient channels tend to exhibit a much higher rate of LWD transport, with jams mobilized on timescales of 100–102 years. This is likely a result of larger channel widths and higher stream order, which are typical of these rivers. The ability of the channel to transport the wood and the range of flows over which the wood moves increase as the channel width-to-log length ratio increases (Curran, 2010). As the watershed area contributing to a channel increases, the channel's size and flow rates increase. The residence time of wood and wood jams, in turn, decreases. This makes understanding the mobility of wood increasingly important (Curran, 2010).

According to Curran (2010), increased LWD and wood jam mobility typical of low-gradient rivers do not necessarily indicate reductions in the influence of wood on channel morphodynamics. Where LWD and wood jams are highly mobile, the frequency of wood mobility and preferred deposition locations are important to understanding channel morphodynamics. When wood jams are recreated in the same locations after each mobilizing flood, for example, the effect on the channel can be similar to that of immobile jams. Low-gradient rivers are also likely to include areas where anthropogenic development interacts with the river, making them subject to active channel and watershed management. In large meandering streams, LWD jams often divert flow toward the bank, causing an increase in local bank scour and channel widening as the channel adjusts to flow around the jam (Keller and Swanson, 1979; Cawthon, 2007).

In a 2007 study of the San Antonio River in Texas (Cawthon, 2007), the sinuosity of the river channel was not found to significantly impact log jam distribution when examining entire reaches. Apparent localized impacts occurred, however. Seven of the ~0.6 mi (1 km) segments studied in the Cawthon (2007) study had sinuosities greater than 2.5, each with a minimum of three jams.

3 Study Area

This section describes the characteristics of the Little River watershed in Texas including the geologic setting, weather and climate, physiographic zones, and a watershed assessment.

3.1 Geologic Setting

The Little River flows through Eocene, Paleocene, and Cretaceous-aged sedimentary deposits from its headwaters southeast of Belton, Texas, to its confluence with the Brazos River southwest of Hearne, Texas (Figure 3-1).

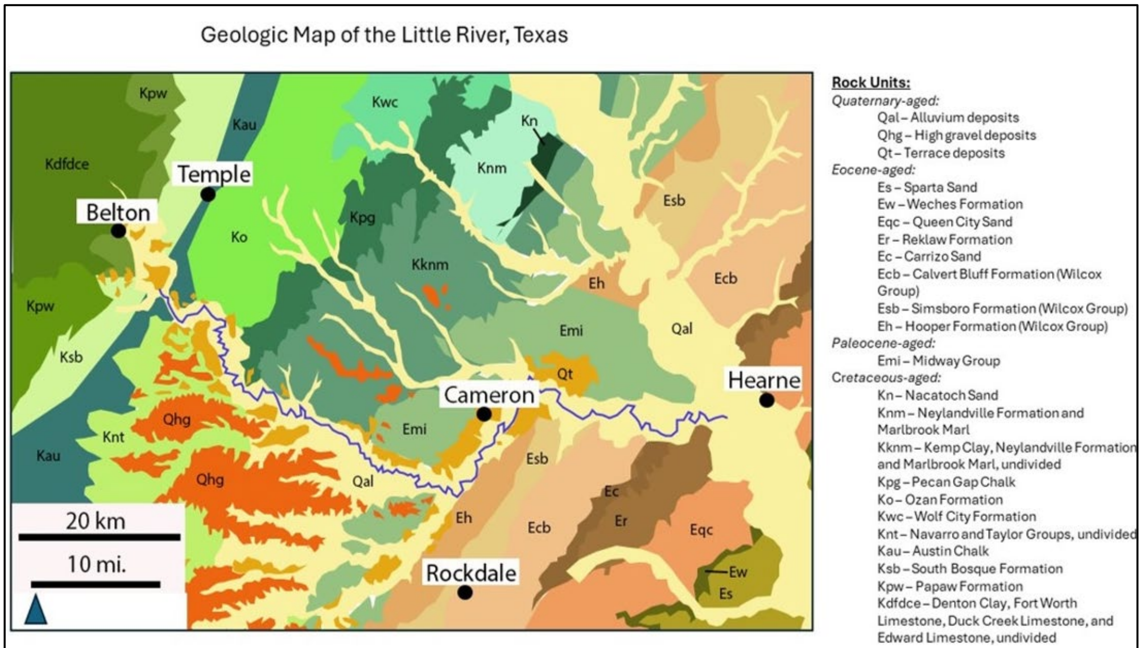

R. Owens, 2024

Figure 3-1. **Geologic map of the Little River region.**

The Little River cuts through the South Bosque Formation and the Austin Chalk at its headwaters. The South Bosque Formation, composed of shale and limestone, ranges in thickness from 35 ft to 150 ft (~10.7 m to 45.7 m). The Austin Chalk is a 150-300 ft (45.7-91.4 m) thick chalk and marl that weathers to form ledges (USGS, 2007).

From there, the river flows through the Navarro and Taylor Groups, the Ozan Formation, and the Pecan Gap Chalk. The Ozan Formation is predominantly clay and is poorly bedded with variable amounts of silt and glauconite. The Pecan Gap Chalk is a true chalk only in the lower portions, grading upwards into a chalky marl and laterally in places to a marl. The Pecan Gap extends into, rather than on top of, the Taylor marl and thus grades laterally to the Navarro and Taylor Groups (Dane and Stephenson, 1928; USGS, 2007).

Downstream of the Ozan Formation, the Little River cuts through the Kemp Clay, Corsicana Marl, Neylandville Formation, and Marlbrook Marl (locally called the Bergstrom Formation or "upper Taylor marl"), with Navarro and Taylor Group still present to the south of the river valley. This rock unit is clayey and calcareous in its upper parts. Its lower part is clay with silt-sized quartz, pyrite, and glauconite. This unit is over 600 ft (182 m) thick (USGS, 2007).

The undivided Kemp Clay, Corsicana Marl, Neylandville Formation, and Marlbrook Marl are the youngest Cretaceous-aged rocks through which the Little River carves its valley. The river enters Paleocene-aged sedimentary rocks downstream, beginning with the Midway Group. The Midway Group is the Wills Point Formation and the Kincaid Formation, mapped together. The Wills Point Formation is primarily clay and silt, with sand becoming more common in the upper portions. Glauconitic near its base, the Wills Point Formation is massive and poorly bedded, with a thickness of over. The Kincaid Formation is sand and clay, with high amounts of glauconite and a greenish-black color in its lower portions. This formation weathers, however, to yellow and yellowish-brown soil. The Kincaid Formation is approximately 150 ft (45.7 m) thick (USGS, 2007).

Progressing to the east, the Little River flows through Eocene-aged rocks, beginning with the Hooper Formation. The Hooper Formation is primarily mudstone, with varying amounts of sandstone, lignite, ironstone concretions, and glauconite. This formation is approximately 500 ft (152.4 m) thick. It is followed by the Eocene-aged Simsboro Formation, mostly sandstone with minor amounts of mudstone, clay, and mudstone conglomerate. This formation is about 300 ft (91.4 m) thick and produces rolling hills that support dense oak growth (USGS, 2007). The Calvert Bluff Formation tops the Simsboro. The Calvert Bluff is mostly mudstone with sandstone, lignite, ironstone concretions, and glauconite. The Calvert Bluff Formation reaches approximately 1,000 ft (305 m) in thickness and supports lignite seams, which can be 1-20 ft (~0.3-6 m) thick (USGS, 2007).

The final two units carved by the Little River are the Carrizo Sand and the Reklaw Formation, both Eocene-aged. The Carrizo Sand is a poorly sorted, thickly bedded sand that weathers yellow to dark reddish brown. It reaches 100 ft (30 m) in thickness and is characterized by ridges that support dense oak growth. The Reklaw Formation is about 80 ft (24 m) thick and is made of sand and clay. Its upper part is silty carbonaceous clay, which weathers from light brown to light gray. Its lower part is fine to medium-grained, grayish-green quartz sand and clay, which weathers moderate brown and dark yellowish-orange. Some clay ironstone ledges and rubble may form. This formation produces deep red soil (USGS, 2007).

3.2 Weather and Climate

The National Climatic Data Center divides Texas into ten climate divisions. The region of the Little River watershed is part of the subtropical and subhumid Division 7: Post Oak Savanna (Texas Water Development Board, 2012). This division receives an annual rainfall of 35-45 inches (89-114 cm) per year, and average temperatures range from 65°-70° F (18°-21° C) ("Post Oak Savannah," n.d.).

The moderate average annual temperatures do not convey the true range of temperatures affecting this region. According to the National Oceanic and Atmospheric Administration (NOAA), average monthly temperatures in Cameron, Texas ranged from 54^{o}-91^{o} F (12.2^{o}-32.8 ^{o} C) in 2023, with a maximum temperature of 110^{o} F (43.3 ^{o} C) and a minimum temperature of 29^{o} F (-1.67^{o} C) (NOAA, 2024).

A summary of temperature values in ^{o} F as reported by NOAA for areas surrounding the Little River during the period of this study is presented in Table 3-1.

Table 3-1. Monthly Temperature Data for Various Locations Reported for 2023 (NOAA, 2024).

2023 Monthly temperature data (°F)	Jan.	Feb.	Mar.	Apr.	May	Jun.	Jul.	Aug.	Sept.	Oct.	Nov.	Dec.
Temple, TX Min.	27	25	27	42	56	64	68	64	60	35	29	27
Temple, TX Max.	84	86	88	90	90	103	107	110	109	97	85	75
Temple, TX Avg.	52.4	53.4	62.1	64.4	74.0	84.5	88.7	90.2	84.3	69.4	57.4	52.8
Cameron, TX Min.	29	30	34	47	55	65	73	69	65	40	34	29
Cameron, TX Max.	80	85	88	89	92	102	105	110	108	97	84	78
Cameron, TX Avg.	54.4	55.3	63.7	65.8	75.3	84.4	89.1	91.3	85.4	68.5	58.8	54.8
Hearne, TX Min.	29	28	33	44	57	65	74	66	63	38	32	28
Hearne, TX Max.	80	86	90	89	92	104	105	111	108	96	86	80
Hearne, TX Avg.	54.1	56.1	64.1	66.3	76.0	84.5	89.0	90.9	85.1	70.9	58.8	54.7

Min. = minimum; Max. = maximum; Avg. = average.

Regional monthly precipitation data in inches for 2023 is presented in Table 3-2.

Table 3-2. Monthly Precipitation Data for Various Locations as Reported for 2023 (NOAA, 2024).

2023 Monthly precipitation data (in)	Jan.	Feb.	Mar.	Apr.	May	Jun.	Jul.	Aug.	Sept.	Oct.	Nov.	Dec.
Temple	0.81	1.97	M	6.11	4.34	0.29	T	0.11	2.29	5.15	1.00	2.77
Cameron	1.58	0.89	NA	5.07	6.62	0.49	0.04	0.00	NA	NA	1.40	2.36
Hearne	2.92	1.31	M	9.36	6.02	1.70	0.00	0.01	1.69	1.77	1.10	3.29

T = minimum; NA = Not applicable.

Climate change is projected to impact mid-latitude grasslands and savannas through a combination of atmospheric warming and changing precipitation regimes. These changing regimes include fewer larger rainfall events, a shift from summer rainfall to increased spring rainfall, increased intervals between rainfall events (Volder et al., 2013). Alteration to precipitation patterns and temperature regimes is expected to have particularly strong influence on the grassland and savannah physiography, as vegetation competes for resources in a new climate. Current monthly temperature regimes are overlain on precipitation values in Figure 3-2.

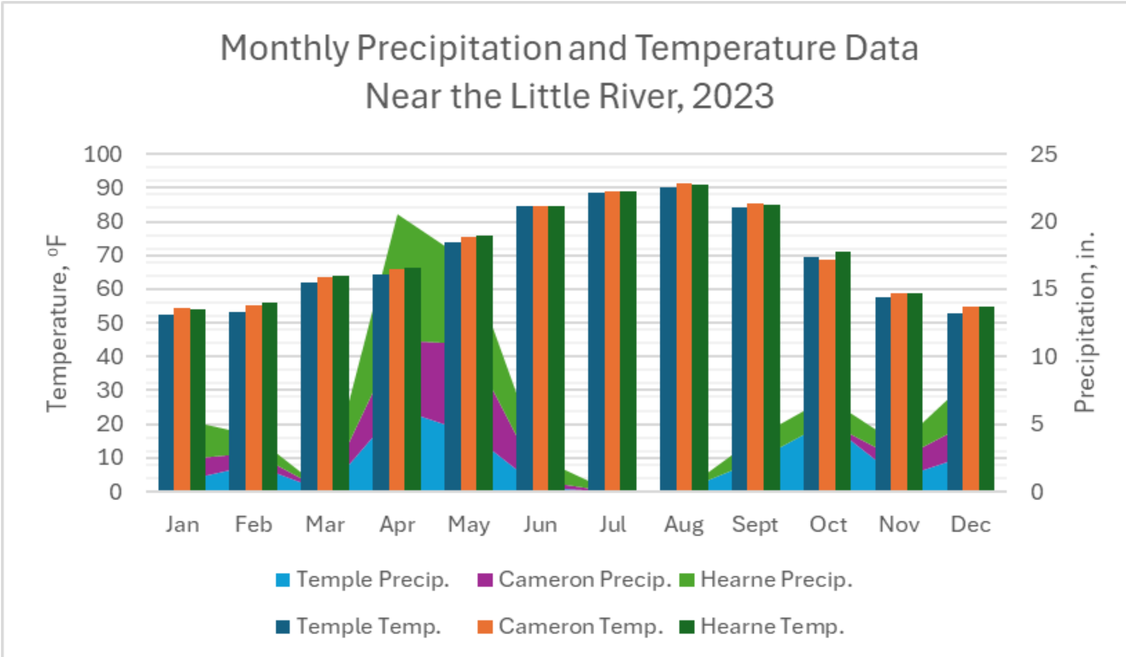

Figure 3-2. Comparison of monthly precipitation and temperature values in the Little River area. The year of reference is 2023. (NOAA, 2024).

3.3 Physiographic Zones

The Little River traverses two physiographic zones from central Bell County to southwestern Robertson County: the Texas Blackland Prairies and East Central Texas Plains. The Texas Blackland Prairies extend from near Sherman, Texas, in the north to San Antonio in the south and are defined by fine, clayey soils. Cretaceous-aged shale, chalk, and marl bedrock produce extensive vertisols, mollisols, and alfisols in this region, supporting prairies as natural land cover. Although much of the Blackland Prairies are now being converted to urban and industrial uses, the natural prairies once supported diverse grasses including little bluestem, big bluestem, yellow Indiangrass, and switchgrass, and a wide range of game including bison, pronghorn antelope, mountain lion, bobcat, ocelot, black bear, collared peccary, deer, coyote, fox, badger, and river otter among others (Griffith et al., 2004).

Most of the Texas Blackland Prairies in the Little River watersheds are Northern Blackland Prairies. Compared to Southern Blackland Prairies, the Northern Blackland Prairies once boasted more tallgrass prairie vegetation. This changed, however, in the late 1800s and early 1900s with the expansion of farming and “breaking the prairie” practices. Large-scale agriculture was introduced, and wooded bottomlands were cleared to the stream banks, a practice still witnessed along the Little River today. Few communities of native Blackland Prairie remain today, having been converted to cropland and non-native pastures of introduced grasses (Griffith et al., 2004). Land cover alteration led to heightened erosion in this region. Historically, the dense tallgrass communities of the Northern Blackland Prairies slowed erosion and trapped water. Today, however, this region experiences one of the highest rates of soil loss of any major area in Texas (Griffith et al., 2004).

The East Texas Central Plains are also commonly referred to as the Post Oak Savanna and are dominated by irregular plains of post oak savanna vegetation. Soils tend to be acidic and range from sand and sandy loams in upland regions to clay and clay loams in low-lying regions. Plant growth is commonly affected by an underlying clay pan, which limits water movement and soil moisture availability. Specifically, the Little River watershed is in the southern portion of this ecoregion, called the Southern Post Oak Savanna. The Southern Post Oak Savanna includes more woods than other plains, consisting mainly of hardwoods over an understory of yaupon and eastern redcedar. Invasive mesquite is common in some southern reaches (Griffith et al., 2004).

The Post Oak Savanna is an ecotone in transition, as woody trees displace native grasses and vegetative composition changes by the restriction of fires (Zimmerman et al., 2008; Thompson, 2011) and the influence of climate change (Volder et al., 2013). Although the region has historically been dominated by post oak and tallgrass, the eastern redcedar common in its modern-day understory has encroached in the last century as wildfires have been restricted. This encroachment results in the decline in grasses, as the post oaks thrive in transition zones where they do not compete with the native grasses, and cedars outcompete the grasses for water (Thompson, 2011). Climate change further complicates the competitive makeup of this ecotone. For example, competition between trees and grasses for resources is magnified during initial tree establishment. Physiological tolerances among growth forms of these vegetation types will mean further evolution of one type's success over another (Volder et al., 2013).

3.4 Watershed Assessment

Twelve HUC12 watersheds contribute to the Little River or its immediate tributaries. A brief assessment of each follows. This information is summarized in Table 3-3.

3.4.1 Fryers Creek – Leon River

The Fryers Creek - Leon River watershed contains the most downstream portion of the Leon River, one of three flowing channels whose confluence creates the Little River. This watershed stretches for 17.2 mi^2 (44.6 km^2) over Austin Chalk limestone, Ozan Formation claystone, Eagle Ford and Woodbine Formations, and extensive alluvium and terrace deposits. Bedrock is overlain predominantly by mollisols, with pockets of entisols, vertisols, and inceptisols.

3.4.2 Mitchell Branch – Lampasas River

The Mitchell Branch watershed contains the most downstream portion of the Lampasas River. This watershed covers 26.5 mi^2 (68.5 km^2) and is composed of claystone, limestone, shale, and marlstone from the Fredericksburg Groups, Austin Chalk marlstone, chalk, and shale, and extensive alluvium and terrace deposits. Bedrock in the area is overlain by mollisols, with pockets of entisols, vertisols, and inceptisols.

3.4.3 Moon Branch – Salado Creek

Extending over 22 mi^2 (~ 57.5 km^2) the Moon Branch watershed contains the most downstream portion of Salado Creek. In this watershed, entisols comprise a larger proportion of soil cover than in the more northern watersheds, but mollisols continue to dominate. Small pockets of vertisols and inceptisols are present. The bedrock in this watershed is predominantly chalk, mudstone, and claystone of the Austin Chalk. Siltstone and mudstone of the Navarro and Taylor Groups are also present, and quaternary alluvium.

3.4.4 Boggy Creek – Little River

The Boggy Creek watershed contains the headwaters of the Little River, formed by the confluence of the Leon River, Lampasas River, and Salado Creek. The Boggy Creek watershed covers 26.8 mi^2 (69.4 km^2) of land, overlain by vertisols and mollisols with small amounts of inceptisols and entisols. Bedrock is predominantly alluvium and terrace deposits from the Little River, with lesser amounts of Ozan Formation claystones and Austin Chalk chalk, marlstone, and claystone.

3.4.5 Runnells Creek – Little River

The Runnells Creek watershed covers 20.5 mi^2 (53 km^2) of land containing mostly alluvium and terrace deposits from the Little River and Runnells Creek, a small tributary. Other bedrock in this watershed includes limestone, marlstone and siltstone from the Navarro and Taylor Groups. Bedrock is overlain by entisols and vertisols, primarily, with small amounts of mollisols present.

3.4.6 Knob Creek

The Knob Creek watershed contains Knob Creek, a minor tributary to the Little River. This watershed extends over 37.6 mi^2 (97.4 km^2) of land underlain by limestone, marlstone and siltstone from the Navarro and Taylor Groups in its northern regions and alluvium, terrace deposits, and Austin Chalk claystone, marlstone, and chalk in its southern portions nearer the Little River. Small amounts of limestone and other carbonates from the Pecan Gap Chalk are also present in the far southeastern portion of this watershed. Bedrock is covered primarily by vertisols throughout this watershed, with small amounts of mollisols and inceptisols present.

3.4.7 Cutoff Slough – Little River

The Cutoff Slough watershed extends over 52 mi^2 (~135.3 km^2) of land. Soils in this watershed vary between mollisols and vertisols, primarily, with smaller amounts of entisols and inceptisols. Alluvium and terrace deposits from the Little River are deposited on claystone from the Ozan Formation and clay, siltstone, and sandstone from the Navarro Group and Marlbrook Marl. Small amounts of limestone and other carbonates from the Pecan Gap Chalk are present in the far northwestern portion of this watershed.

3.4.8 Cattail Creek – Little River

The Cattail Creek watershed encompasses 55.8 mi^2 (144.6 km^2) of land underlain by claystone and sandstone of the Hooper Formation and quaternary alluvium and terrace deposits. Mollisols most closely follow the river channel, whereas vertisols, entisols, and inceptisols intermix through the non riparian zone.

3.4.9 Bear Creek – Little River

The Bear Creek watershed has an area of ~35 mi^2 (90 km^2) and contains an even mix of entisols, mollisols, inceptisols, and vertisols. Mollisols most closely follow the river channel. Geology consists of quaternary alluvium and terrace deposits overlain on sandstone and claystone of the Hooper Formation.

3.4.10 Maysfield Creek

The Maysfield Creek watershed has an area of ~37 mi^2 (96.4 km^2)· Entisols follow the creek, with few patches of vertisols scattered along the drainage divides and sparsely along the creek bed. Mollisols are most common in this watershed, and inceptisols appear infrequently near the divides. The underlying geology is predominantly Austin Chalk, with terrace deposits along the creek and Navarro and Taylor Groups sporadically on the eastern and western edges.

3.4.11 Pin Oak Creek

The Pin Oak Creek watershed has an area of ~36.7 mi^2 (95 km^2) and overlies the Carrizo Sandstone. Alluvium deposits are present within the main river channel and its immediate floodplain. This bedrock is overlain by mollisols closest to the Little River and alfisols beyond. Inceptisols follow the smaller tributaries within this watershed.

3.4.12 Polecat Creek

The Polecat Creek watershed extends over ~28 mi^2 (73 km^2) over the Carrizo Sandstone, with alluvium deposits within the river channel and floodplain. Mollisols are the most common soil type nearest the Little River until it approaches the Brazos River. At this point, the mollisols grade to vertisols. Alfisols predominate on the land beyond the river channel, followed by inceptisols following the smaller tributaries.

Table 3-3. Description of Watersheds Contributing to the Little River.

Name	Area	Geology	Soil	Landcover
Fryers Creek – Leon River	17.22 mi^2	40% - Austin Chalk 26% - Alluvium 12% - Terrace deposits 7% - Terrace Deposits 6% - Undivided parts of Washita and Fredericksburg Groups 6% - Ozan Formation 2% - Austin Chalk	61% - Mollisols 24% - Vertisols 10% - Alfisols 6% - Entisols	21% - Herbaceous 21% - Cultivated Crops 17% - Hay/Pasture 8% - Developed, Open Space 7% - Developed, Low Intensity 7% - Evergreen Forest 6% - Woody Wetlands 5% - Deciduous Forest 4% - Developed, Medium Intensity 2% - Developed, High Intensity
Mitchell Branch -	26.45 mi^2	21% - Georgetown Limestone	77% - Mollisols 16% - Vertisols	45% - Herbaceous 17% - Hay/Pasture

Lampasas River		9% - Edwards and Comanche Peak Limestones, undivided 35% - Undivided parts of Washita and Fredericksburg Groups 7% - Terrace Deposits 1% - Austin Chalk 1% - Edwards and Comanche Peak Limestones, undivided	4% - Alfisols 2% - Inceptisols 1% - Entisols	12% - Evergreen Forest 10% - Deciduous Forest 6% - Developed, Open Space 6% - Woody Wetlands 4% - Cultivated Crops
Moon Branch - Salado Creek	22.2 mi^2	1% - Eagle Ford Formation 16% - Georgetown Limestone 11% - Buda Limestone and Del Rio Clay, undivided 2% - Navarro and Taylor Groups, undivided 5% - Alluvium 63% - Austin Chalk 2% - Terrace deposits	67% - Mollisols 15% - Vertisols 2% - Entisols 1% - Inceptisols	54% - Herbaceous 11% - Deciduous Forest 11% - Cultivated Crops 10% - Hay/Pasture 8% - Evergreen Forest 5% - Woody Wetlands 2% - Developed, Open Space
Boggy Creek	26.8 mi^2	51% - Ozan Formation 23% - Alluvium 19% - Austin Chalk 2% - Terrace Deposits	46% - Vertisols 43% - Mollisols 9% - Alfisols 3% - Entisols	44% - Cultivated Crops 19% - Herbaceous 19% - Hay/Pasture 6% - Woody Wetlands 5% - Developed, Open Space 4% - Deciduous Forest 2% - Evergreen Forest
Runnells Creek	20.46 mi^2	37% - Navarro and Taylor Groups, undivided 6% - High gravel deposits Trace - Terrace deposits 24% - Alluvium 1% - Austin Chalk 30% - Terrace deposits	44% - Vertisols 35% - Mollisols 20% - Alfisols 1% - Inceptisols	32% - Cultivated Crops 25% - Herbaceous 24% - Hay/Pasture 8% - Woody Wetlands 5% - Deciduous Forest 3% - Developed, Open Space
Knob Creek	37.6 mi^2	68% - Ozan Formation 18% - Austin Chalk 14% - Pecan Gap Chalk 12% - Alluvium 3% - Terrace Deposits	83% - Vertisols 16% - Mollisols 1% - Alfisols	41% - Herbaceous 23% - Cultivated Crops 22% - Hay/Pasture 5% - Developed, Open Space 2% - Deciduous Forest 2% - Developed, Low Intensity 1% - Developed, Medium Intensity
Cutoff Slough	52.24 mi^2	36% - Alluvium 39% - Navarro Group and Marlbrook Marl, undivided 10% - Terrace Deposits 4% - High Gravel Deposits 3% - Midway Group, undivided 2% - Pecan Gap Chalk	54% - Vertisols 35% - Mollisols 12% - Alfisols	31% - Cultivated Crops 24% - Hay/Pasture 22% - Herbaceous 6% - Developed, Open Space 6% - Woody Wetlands 5% - Deciduous Forest 4% - Evergreen Forest 2% - Shrub/Scrub
Cattail Creek	55.83 mi^2	30% - Alluvium 19% - Hooper Formation 15% - Midway Group, Undivided	37% - Alfisols 36% - Vertisols 27% - Mollisols	34% - Hay/Pasture 18% - Shrub/Scrub 18% - Cultivated Crops 8% - Deciduous Forest

		13% - Terrace Deposits 5% - Simsboro Formation 4% - Midway Group, Undivided		6% - Developed, Open Space 5% - Herbaceous 5% - Woody Wetlands 4% - Evergreen Forest
Bear Creek	34.75 mi^2	34% - Midway Group, Undivided 24% - Alluvium 22% - Terrace Deposits 7% - Hooper Formation 3% - Simsboro Formation 2% - Midway Group, Undivided 1% - High Gravel Deposits	49% - Alfisols 30% - Vertisols 21% - Mollisols	36% - Hay/Pasture 20% - Shrub/Scrub 12% - Developed, Open Space 10% - Cultivated Crops 9% - Deciduous Forest 4% - Herbaceous 3% - Woody Wetlands 3% - Evergreen or Mixed Forest
Maysfield Creek	37.22 mi^2	31% - Terrace deposits 38% - Alluvium 3% - Simsboro Formation Wilcox Group, undivided 5% - Calvert Bluff Formation 2% - Hooper Formation 3% - High gravel deposits	75% - Alfisols 16% - Vertisols 7% - Mollisols 1% - Entisols	41% - Hay/Pasture 24% - Cultivated Crops 15% - Shrub/Scrub 7% - Deciduous Forest 4% - Developed, Open Space 3% - Mixed Forest 2% - Woody Wetlands 1% Open Water
Pin Oak Creek	36.68 mi^2	23% - Alluvium 18% - Reklaw Formation 3% - Wilcox Group, undivided 30% - Calvert Bluff Formation 26% - Carizzo Sand	74% - Alfisols 20% - Mollisols 4% - Entisols 2% - Inceptisols 1% - Vertisols	27% - Hay/Pasture 21% - Deciduous Forest 16% - Shrub/Scrub 11% - Mixed Forest 11% - Cultivated Crops 5% - Woody Wetlands 3% - Developed, Open Space 3% - Evergreen Forest 3% - Emergent Herbaceous Wetlands
Polecat Creek	28.11 mi^2	7% - Reklaw Formation 4% - Terrace deposits 41% - Alluvium 40% - Wilcox Group, undivided 8% - Carizzo Sand	52% - Alfisols 31% - Mollisols 13% - Vertisols 3% - Inceptisols	30% - Cultivated Crops 19% - Hay/Pasture 19% - Deciduous Forest 13% - Shrub/Scrub 7% - Mixed Forest 4% - Developed, Open Space

4 Methods

This study utilized four techniques of assessing the dynamics of the Little River to determine its regions of greatest lateral migration: MSTaT analysis, GIS analysis, stream power and stream power index analysis, and channel assessment based on qualitative field observations. The results of all four methods are correlated to provide recommendations of those meander bends most prone to geomorphic change.

4.1 MStat Analysis

The MStat Analysis was carried out by following these steps:

a. Acquire XY Coordinates for the Little River

b. ArcGIS Pro derived centerlines for the Little River in 1953, 1963, 1974, 1982, 1996, 2004, 2012, and 2018. For 1982-2022, this was accomplished using orthorectified imagery from the United States Geological Survey (USGS) Earth Explorer and the National Hydrology Dataset (NHD). For 1953-1972, single-frame aerial photographs were downloaded from the USGS Earth Explorer and manually digitized in ArcGIS Pro. In each image, the river valley was first traced as a polygon, and then the “Polygon to Centerline” tool was launched to reveal the centerline of the Little River for the represented year. (Before progressing to step b, ensuring that the centerline is one continuous segment is essential. If not, MSTaT cannot read the XY coordinates appropriately. The user should select one portion of the centerline in ArcGIS Pro. If the entire centerline is not highlighted, then the “Merge” tool needs to be employed to merge all segments before continuing.)
c. The “Points Along Line” tool was then employed to create a series of points on the centerline. These were evenly spaced at 0.31 mi apart, and endpoints were also created.
d. Two new fields were added to the Attribute Table for the Points Along Line layer: X-coordinate and Y-coordinate. For the “Coordinate Format,” “Same as Input” should be selected. This should ensure that the coordinates are recorded in UTM format.
e. The Attribute Table is exported to Excel®, and all columns except X-coordinate and Y-coordinate are deleted. All headings must also be deleted. Only the data should remain.
f. This process was repeated for each year of centerline data for the Little River.
g. Spreadsheets were uploaded to MstaT, and computational analysis was run.

4.2 GIS Analysis of Meanders

Using ArcGIS Pro, the centerlines of the Little River for the years 1953, 1963, 1974, 1982, 1996, 2004, 2012, and 2018 were compared (Figure 4-1). Centerlines from two sets of successive data sets were selected, and polygons were constructed using the “Construct Polygons” tool (Figure 4-2). The area and perimeter of each polygon were then calculated in ArcGIS Pro and added to the attribute table, with the X— and Y coordinates of the polygon centroid.

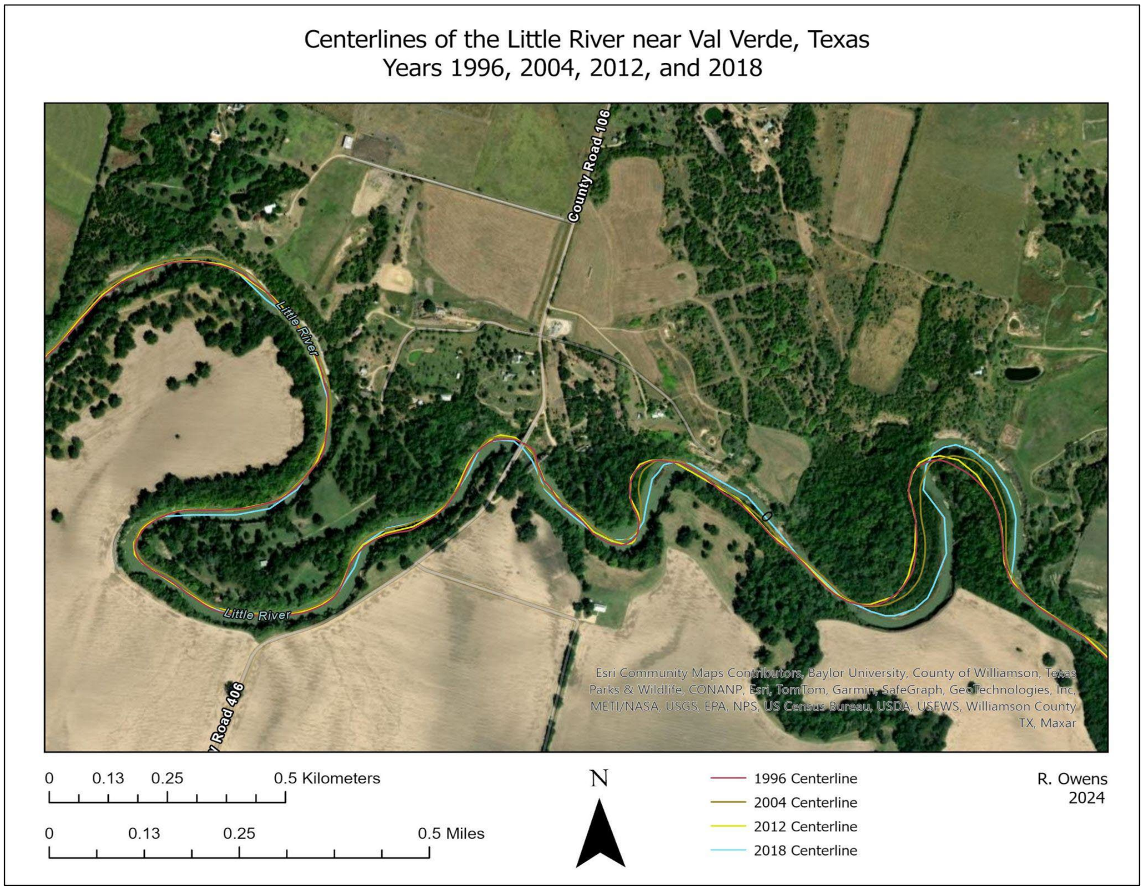

Figure 4-1. **Overlay of centerlines from 1996-2018 on a portion of the Little River.**

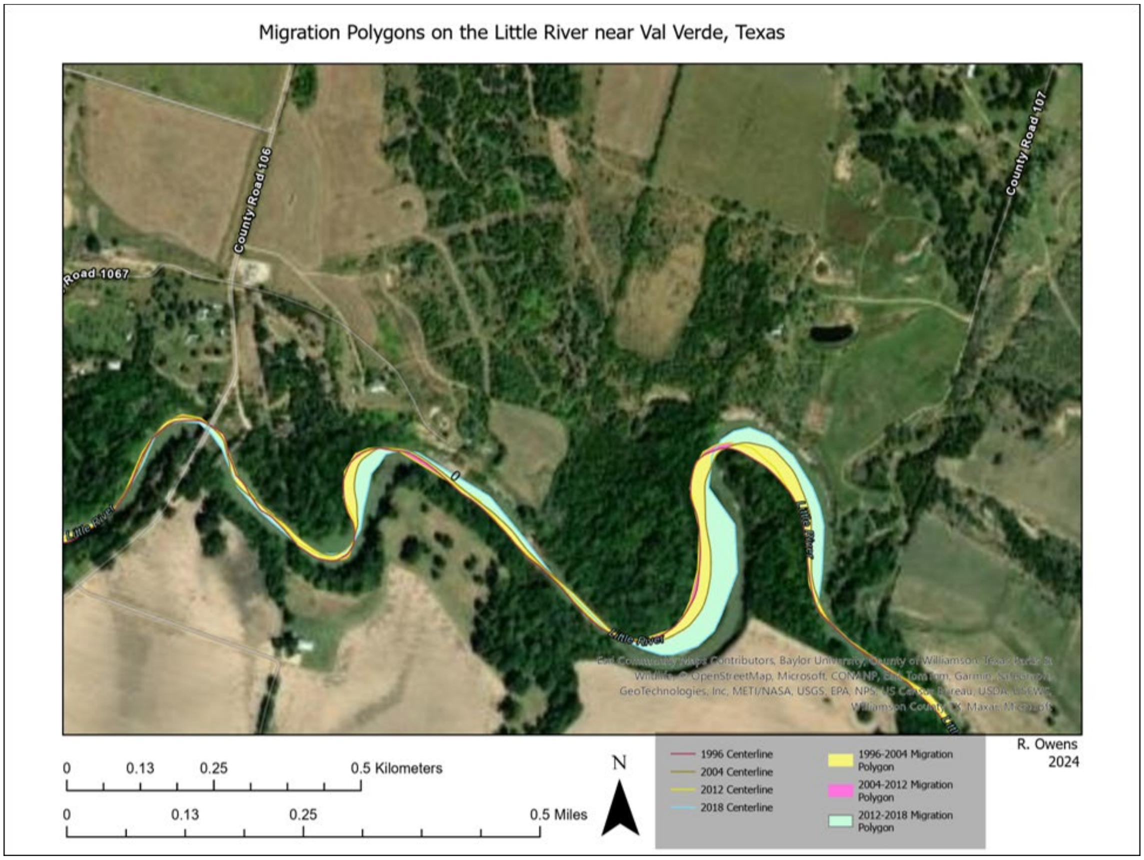

Figure 4-2. Migration polygons from 1996-2018 on a portion of the Little River.

The total migration of centerlines is calculated from the polygons using the following equation:

$$Mn = A / (0.5*P) \qquad \text{Eq. 1}$$

where Mn is the total rate of migration, A is the area of the polygon, and P is the perimeter of the polygon (Giardino and Rowley, 2016). To accommodate errors associated with digitizing imagery of various scales, migration values less than 19.7 ft (6 m) were eliminated from the data.

4.3 Qualitative Assessment of the Little River

Field assessment of the Little River was conducted during August and September of 2023. The Little River was traversed by canoe, and assessment was performed using traditional field methods and ground LiDAR. Gage height at USGS gage station 08104500, located within this segment, ranged from 0.79-0.92 ft (0.24-0.28 m), with discharge values ranging from 27-34 cfs (0.76-0.96 cms).

Qualitative descriptions were based on the method of channel stability assessment by Doyle et al. (2000) and modified by Benson et al. (1999). This method calculates a weighted score based on observations of bank angle, sediment size, bank cutting, mass wasting, vegetative cover, bar development, debris-jam potential, and shear-stress ratios (Table 4-1). In this study, shear-stress ratios have been replaced with stream power values. Classification of stream power values is based on findings from a study of stream power and its influence on bank stability throughout the contiguous United States by Jha et al. (2022). In this assessment system, high scores correspond to low bank stability.

Table 4-1. Qualitative Stability Indicators Utilized in this Study.

Stability indicator	Excellent (1-3)	Good (4-6)	Fair (7-9)	Poor (10-12)
Bank soil texture and coherence (0.6)	Clay and silty clay; cohesive material	Clay loam to sandy clay loam	Sandy clay to sandy loam	Loamy sand to sand; noncohesive material
Average bank angle (0.6)	Bank slopes 18° or 33%	Bank slopes up to 27° or 50% on one or occasionally both banks	Bank slopes to 31° or 60% common on one or both banks	Bank slopes over 31° or 60% common on one or both banks
Vegetative bank protection (0.8)	Wide band of woody vegetation with at least 90% density and over; primarily hard wood, leafy, deciduous trees with mature, healthy, and diverse vegetation located on the bank; woody vegetation oriented	Medium band of woody vegetation with 70% to 90% plant density and cover; a majority of hard woody, leafy, deciduous trees with maturing, diverse vegetation located on the bank; woody vegetation oriented 80° to 90° from horizontal with minimal root exposure	Small band of woody vegetation with 50% to 70% plant density and cover; a majority of soft wood, piney, coniferous trees with young or old vegetation lacking in diversity located on or near the top of bank; woody vegetation oriented at 70° to 80° from horizontal often with evident root exposure	Woody vegetation band may vary depending on age and health with less than 50% plant density and cover; primarily soft wood, piney, coniferous trees with very young, old and dying, and/or monostand vegetation located off of the bank; woody vegetation oriented at less than 70° from horizontal with extensive root exposure
Bank cutting (0.4)	Little or none evident; infrequent raw banks less than 6 in (15 cm) high generally	Some intermittently along channel bends and at prominent constrictions; raw banks may be up to 12 in (30 cm)	Significant and frequent; cuts 12 in – 23.6 in (30 to 60 cm) high; root mat overhangs	Almost continuous cuts, some over 23.6 in (60 cm) high; undercutting, sod-root overhangs, and side failures frequent
Mass wasting or bank failure (0.8)	No or little evidence or potential or very small amounts of mass wasting; uniform channel width over the entire reach	Evidence of infrequent and/or minor mass wasting; mostly healed over with vegetation; relatively constant channel width and	Evidence of frequent and/or significant occurrences of mass wasting that can be aggravated by higher flows, which may cause undercutting	Frequent and extensive mass wasting; the potential for bank failure as evidenced by tension cracks, massive undercuttings, and

		minimal scalloping	and mass wasting of unstable banks; channel width quite irregular and scalloping of banks is evident	bank slumping is considerable; channel width is highly irregular and banks are scalloped
Bar development (0.6)	Bars are more mature, narrow relative to stream width at low flow, well vegetated and composed of coarse gravel to cobbles	Bars may have vegetation and/or be composed of coarse gravel to cobbles, but minimal recent growth of bar evident by lack of vegetation on portions of the bar	Bar widths tend to be wide and composed of newly deposited coarse sand to small cobbles and/or may be sparsely vegetated	Bar widths are generally greater than one-half the stream width at low flow; bars are composed of extensive deposits of fine particles up to coarse gravel with little to no vegetation
Debris jam potential (0.2)	Debris or potential for debris in channel is negligible	Small amounts of debris present; small jams could be present	Noticeable accumulation of all sizes; moderate downstream debris potential possible	Moderate to heavy accumulations of various size debris present; debris-jam potential significant
Stream power (1.0)	$\Omega \leq 35$ W/m^2	35 W/m^2 < $\Omega \leq 100$ W/m^2	100 W/m^2 < $\Omega \leq 300$ W/m^2	$\Omega > 300$ W/m^2

4.4 Stream Power, Stream Power Index, and Compound Topographic Index

This section describes the steps followed to calculate stream power and develop the stream power index and compound topographic index maps.

4.4.1 GIS Analysis for Stream Power Calculation

Stream power for the Little River was calculated by adapting Gartner (2016)'s workflow as follows:

1. Obtain DEMs from the USGS 3D Elevation Program (3DEP). Coverage for the entire Little River watershed is available in the 1/3 arc-second dataset, with a resolution of approximately 32.8 ft (10 m). Note: other DEMs available for the area include the NHDPlus Data with a resolution of ~98 ft (30 m), and 3.28 ft (1 m) LiDAR DEMs from 3DEP, which only cover approximately 60% of the study area.
2. In ArcGIS Pro, the four DEM files USGS_13_n31w097_20240229.tif, USGS_13_n31w098_20211103.tif, USGS_13_n32w097_20211103.tif, and USGS_13_n32w098_20211103.tif are combined using the "Mosaic to New Raster" tool (Data Management Tools) and projected to NAD 1983 UTM Zone 14N Coordinate System using the "Project Raster" tool.
3. The projected raster is clipped to the watershed boundary using the "Clip Raster" tool. Here we used the file WBDHUC8_Texas_NHD_TWDB_2020 from ArcGIS®

Online which corresponds with the Little River HUC8 watershed.

4. After installing the Arc Hydro Toolbar, the “Fill Sinks” tool was used to remove the errors from the DEM.
5. The Fill DEM was then used as input in the “Flow Direction” tool (ArcHydro) to create the Flow Direction map, which in turn was used to create the Flow Accumulation map.
6. The upstream point on the main channel and the “Flow Direction” map are used in the “Flow Path Tracing Arc Hydro” tool to produce a single stream line for the Little River.
7. Using the “Generate Points Along Lines” tool, points were created along the Little River stream line with a spacing of 1,640.4 ft (500 m) and an upstream starting point (Figure 4-3).
8. New columns in the attribute table of the points layer created in the previous step were populated with values from the Flow Accumulation map and the Fill DEM (elevation) using the “Extract Multi Values to Points” tool.
9. The coordinates for each point were added using the “Calculate Geometry” tool in the attribute table of the Little River points layer.
10. The “Table to Excel” tool was used to convert the attribute table from the Little River points layer into a .xlsx file.

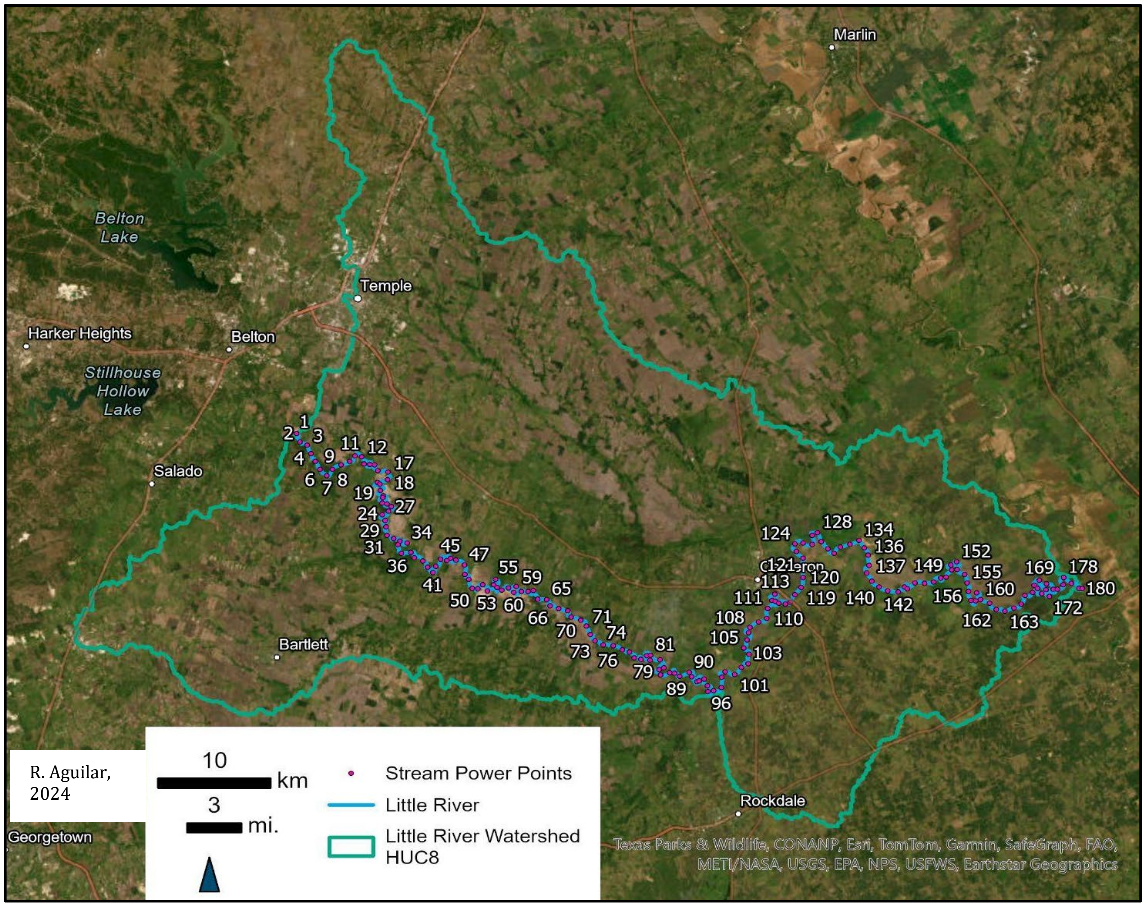

Figure 4-3. **Location of the data points resulting from step 7 of the Stream Power GIS analysis.**

4.4.2 Stream Power Computations

According to Bagnold (1966), stream power is the product of the river discharge, stream slope, and weight of water

$$\Omega = \rho \, g \, Q \, S \qquad \textbf{Eq. 2}$$

where Ω is stream power, ρ is the density of water 62.4 lb/ft^3 at 39° F (1,000 kg/m^3 at 4° C), g is gravity 32.2 ft/s^2 (9.8 m/s^2), Q is river discharge, and S is energy gradient or stream slope in uniform flow.

Stream slope was calculated using the slope function in Microsoft Excel for each point of the Little River table. The slope function uses the elevation difference over the distance between consecutive points.

Gartner (2016) recommends smoothing the stream slope values to reduce DEM errors. Here we used a moving average (rolling mean) function with a window of 10 unit segments or 6.2 mi (10 km) in R. The rollmean function calculates the smoothed values from ordered observations centered 3.1 mi (5 km) upstream and 3.1 mi (5 km) downstream. Here we used the following script in an online version of R rolling_mean <- rollmean (observations, k = 10, fill = NA, align = "center")

The entire stream slope values were included in the “slope values range” in order (i.e., top of the reach to bottom of the reach).

Drainage area was calculated using the flow accumulation values in the units of several raster cells extracted in step 8 of the GIS analysis (section 4.4.1) and multiplying by the area of each raster cell. Here, we used an area of 1030.6 ft^2 (95.75 m^2) for a cell size of 32.1 ft (9.78 m) by 32.1 ft (9.78 m).

We used aerial pictures to measure the width of the river and to calculate the average width of the channel to be W = 94.72 ft (28.87 m).

Discharge was calculated using the following regression equations:

$$\mathbf{Q = 10^{2.339} A^{0.5158}} \qquad \textbf{Eq. 3}$$

developed by Asquith and Thompson (2008) for undeveloped small watersheds in Texas, where Q is the peak streamflow for 2-year recurrence interval in cubic feet per second and A is the drainage area in square miles.

$$\mathbf{Q = 0.92 A^{0.7}} \qquad \textbf{Eq. 4}$$

proposed by Finlayson & Montgomery (2003) for small- to mid-sized watersheds where Q is in m^3/s and A in km^2.

$$\mathbf{Q = 174.66 A^{0.458}} \qquad \textbf{Eq. 5}$$

by Dutnell (2000) where Q is bankfull discharge in cubic feet per second and A is contributing drainage area of the watershed in square miles.

The stream power computations for the Little River watershed, including the discharge calculations, are shared with the Texas Water Development Board through Dropbox®.

4.4.3 Stream Power Index

The digital terrain analysis methodology described by Timm, 2016 was adapted to calculate the Stream Power Index (SPI) using the NRCS Engineering Toolbox for ArcGIS Pro.

1. Obtained DEMs from the USGS 3D Elevation Program (3DEP). Coverage for the Little River watershed is available in the 1/3 arc-second dataset, with a resolution of approximately 32.8 ft (10 m). LiDAR DEMs with a resolution of 3.28 ft (1 m) are available for a large area of the watershed. The high resolution DEMs were used for the hydrologic conditioning of the data.
2. In ArcGIS Pro, the four DEM files USGS_13_n31w097_20240229.tif, USGS_13_n31w098_20211103.tif, USGS_13_n32w097_20211103.tif, and USGS_13_n32w098_20211103.tif are combined using the “Mosaic to New Raster” tool (Data Management Tools) and projected to NAD 1983 2011 Texas Centric Mapping System Albers using the “Project Raster” tool.
3. The projected raster was clipped to the Little River watershed boundary running the “Define Area of Interest” script (Terrain Analysis Tools - NRCS Engineering Toolbox). Here we used the file WBDHUC8_Texas_NHD_TWDB_2020 from ArcGIS

Online which corresponds with the Little River Hydrologic Unit Code 8 watershed. Running the "Define Area of Interest" script created elevation contours every 10 ft (~3 m), a hillshade map (Figure 4-4), and a depth grid of the watershed.

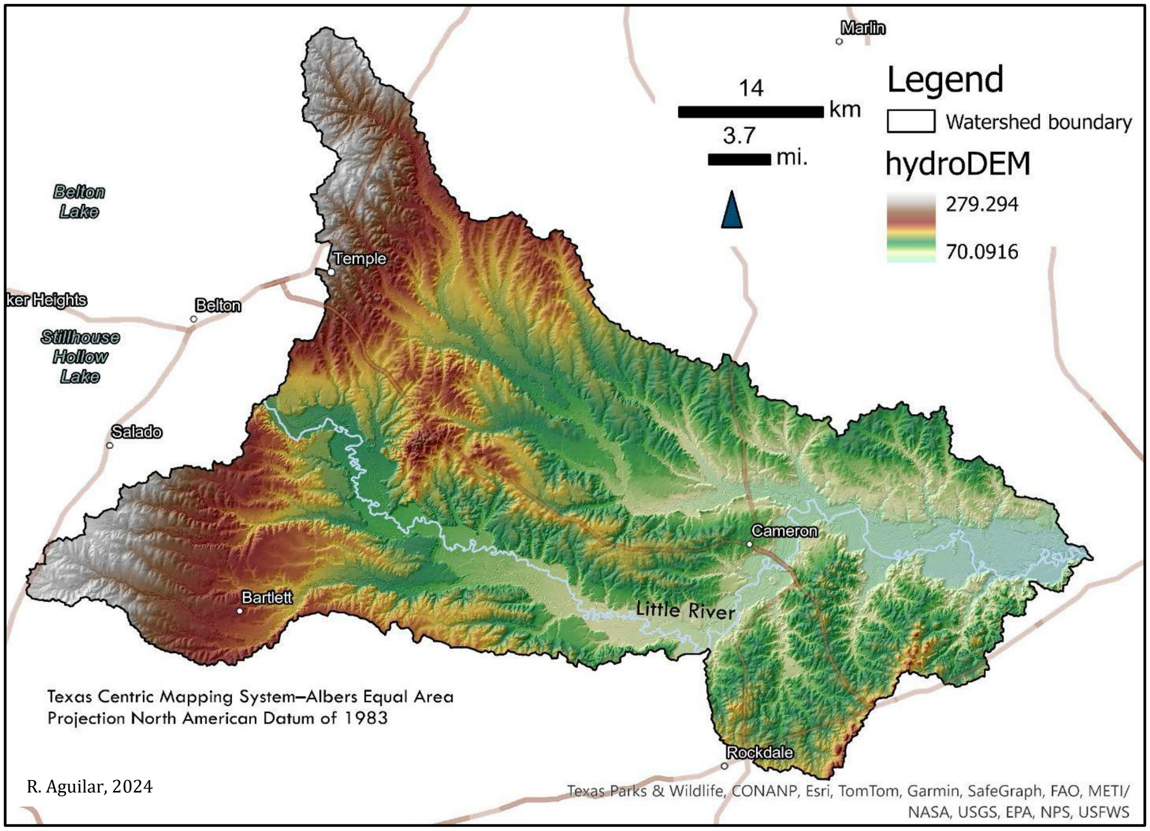

Figure 4-4. HydroDEM displayed over hillshade to show exaggerated 3D surface of the Little River watershed.

4. Used the "Mosaic to New Raster" tool (Data Management Tools) to combine the 35 DEM files with 3.28 ft (1 m) resolution, and the "Project Raster" tool to project the new DEM. A hillshade map of the 1m projected DEM was created to use in the hydrologic conditioning of the data. Note: these DEMs do not cover the entire Little River watershed and were only used to remove "digital dams".
5. Created Culverts feature class layer (polylines) using known bridge locations downloaded from ArcGIS Online, as well as the 3.28 ft (1 m) hillshade created in the previous step and aerial imagery to remove "digital dams" (Figure 4-5) evident in the depth grid map.

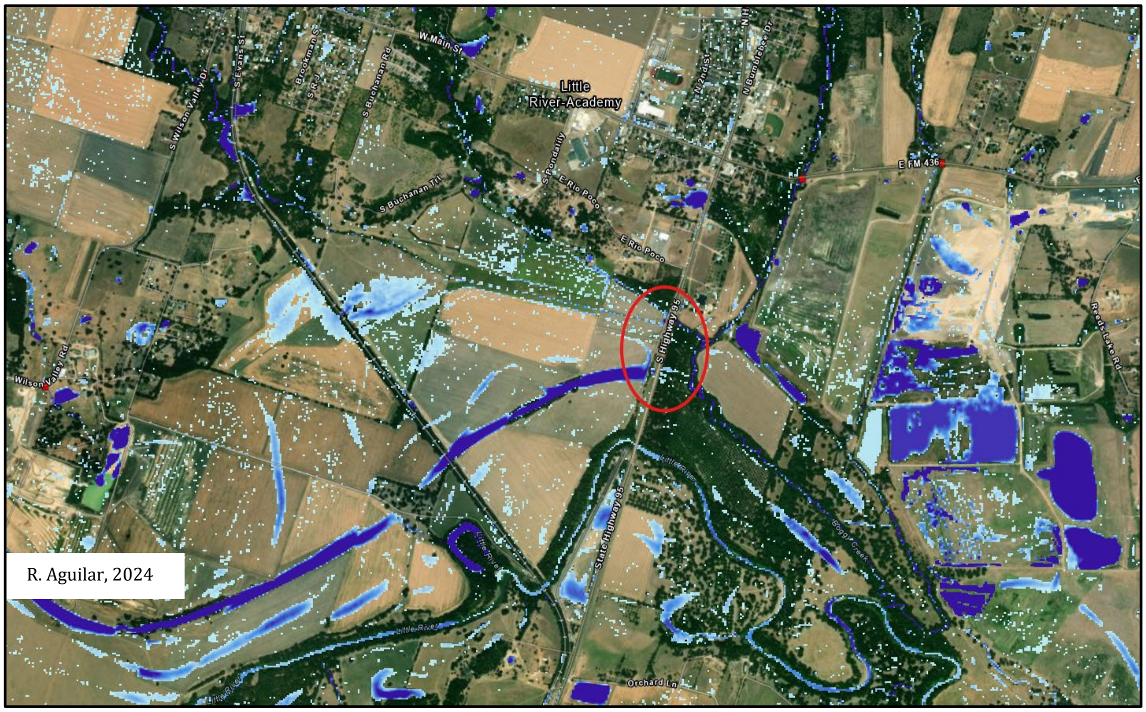

Figure 4-5. **An example of a digital dam is circled in red. The blue areas correspond to the depth grid.**

6. Running the “Create Stream Network” script (Terrain Analysis Tools - NRCS Engineering Toolbox) fused the Culverts layer and the 32.8 ft (10 m) DEM to create a hydroDEM in which sinks were filled to remove errors (Figure 4-4). The hydroDEM is used in this operation to produce the “Flow Accumulation” (Figure 4-6) and “Flow Direction” maps, as well as a stream linear network using a flow accumulation value >= 42.

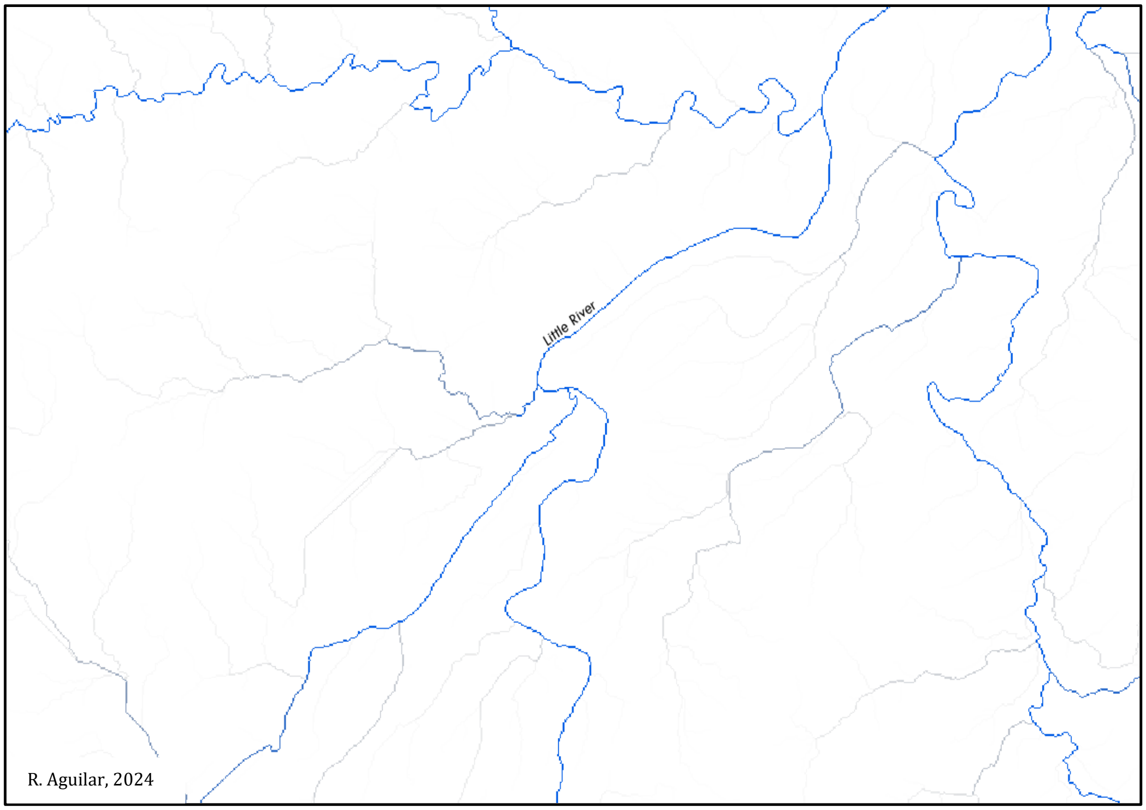

Figure 4-6. **Example of the Flow Accumulation south of Cameron, Texas.**

7. The Stream Power Index (SPI) script (Terrain Analysis Tools - NRCS Engineering Toolbox) uses the “Flow Accumulation” and “Slope” rasters to determine SPI by multiplying the natural logarithms of slope and flow accumulation, as shown in the following formula:

$$\mathbf{SPI} = \ell n(A * \tan\beta) \qquad \textbf{Eq. 6}$$

where A is flow accumulation and β is percent slope.

Figure 4-7 shows an example of SPI signatures indicating areas of potential erosion south of Cameron, Texas.

Figure 4-7. **Example of Stream Power Index (SPI) signatures indicating areas of potential erosion south of Cameron, Texas.**

4.4.4 Compound Topographic Index

The Compound Topographic Index (CTI) was computed using the NRCS Engineering Toolbox for ArcGIS Pro and an adaptation of the digital terrain analysis methodology described by Timm et al. (2014) and Timm (2016).

The CTI script (Terrain Analysis Tools - NRCS Engineering Toolbox) uses the "Flow Accumulation" and "Slope" maps created following steps 1-6 in the SPI section to produce the CTI map, which helps identify areas where water tends to pond and accumulate as shown in Figure 4-8.

CTI is derived by dividing slope by flow accumulation, and it is computed using the following equation:

$$\mathbf{CTI = \ell n(A / tan\beta)} \qquad \textbf{Eq. 7}$$

where A is flow accumulation and β is percent slope.

Figure 4-8. **Example of Compound Topographic Index (CTI) signatures indicating areas of impounded water.**

4.5 Ground LiDAR Collection

LiDAR scans were taken of the banks of the Little River at each highway or farm-to-market overpass using an iPad or iPhone and 3D Scanner App. Image processing was completed through CloudCompare®.

To more closely assess the rapidly migrating meanders, the results of GIS analysis, stream power analysis, MSTaT and qualitative bank assessment were correlated to determine the most unstable meanders. These were scanned in the field using ground LiDAR with a 12.9-inch iPad Pro (6th generation) and iPhone 14 Pro Max. Data were processed using CloudCompare. The resulting DEMs are provided to the Texas Water Development Board through Dropbox.

3D Scanner App was selected for use because this application was previously tested by Luetzenburg et al. (2021) for use in geosciences with favorable results. Other applications, such as Pix4D, were considered but were ultimately not tested because of logistical problems with purchasing. 3D Scanner App is a free application, rendering such issues nonexistent. Like Luetzenburg et al. (2021), this study utilized CloudCompare for image processing because of its ease of utility.

Ground LiDAR scans of the upper portions of banks are best collected in the winter, when vegetation is minimal, and air temperature is less likely to cause overheating of smart devices. An exception exists if the purpose of the scans is to assess erosion beneath road overpasses. In this situation late summer is recommended, as the shade of the overpass reduces the likelihood of overheating and low water levels will expose more of the lower banks around the bridge support columns.

The user should ensure that GPS and location services are enabled on the smart device before scanning. In 3D Scanner App, scans were taken in the "LiDAR" setting and saved to the devices. In this setting, a triangulated surface model creates a mesh from the raw point cloud data. Although 3D Scanner App also offers a "Point Cloud" mode which records raw data and does not triangulate to a mesh, the LiDAR setting typically allows for a larger spatial extent. Some smaller areas were scanned in one scan, but larger areas were scanned in segments which were combined during processing. All scans were shared to Google Drive® directly from the smart devices as "LAS Geo-Referenced" files. These can then be downloaded as .las files to a device for processing.

As the georeferenced scans will have undefined coordinate systems, it is necessary to first use a GIS software to project them. This was accomplished in ArcGIS Pro using the Extract LAS tool. Using Extract LAS, the .las file is selected, and under the "Environments" tab a coordinate system is selected to which the .las file will be projected. This step must be completed before opening the files in CloudCompare.

In CloudCompare, the projected .las files are opened for processing. As the point clouds are unclassified, classification is necessary before conversion to raster. If any scene requires the combination of multiple scans, this step must be completed before classification of the point clouds. To combine multiple point clouds, two projected .las files showing overlapping areas are opened simultaneously in CloudCompare. To rotate or translate one without the other, it is necessary to select the file to be manipulated from the table of contents and deselect the other file. Then, the translate tool is selected from the upper toolbar. On most devices, clicking and dragging the image will rotate it and right-clicking and dragging will translate it. This is not made clear in most online tutorials.

Through clicking and dragging each individual image and the entire scene, the two point clouds can be manually aligned. CloudCompare offers a tool called Finely Register Already Roughly Aligned Entities which purports to precisely align point clouds after manual alignment. This tool exhibited only moderate success when attempted in this study. Rather, it was found that after extensive manual alignment, CloudCompare automatically fuses the two georeferenced point clouds together without the use of this tool. Once the two point clouds are combined, the Merge Point Clouds tool is used to combine them to one point cloud. No reclassification should occur at this point, if the user is so prompted.

The preceding steps are repeated until all overlapping point clouds are combined into one. After combination, the resulting point cloud must be cleaned to meet the needs of the user. If a digital elevation model (DEM) is desired, all non-ground points such as vegetation or anthropogenic structures should be removed. If a digital surface model (DSM) is desired, it may be necessary to classify points based upon their type (ground, vegetation, structure, etc.). In this study, non-ground points such as vegetation, temporary reference markers, and litter were removed. Some permanent structures such as bridge support columns were left in the image, however, as a reference. This is accomplished using the Segment tool, which can be used to select non-ground points and segment them into a new point cloud.

The resulting point cloud of non-ground points can then be deleted or reclassified, depending on the needs of the user. This was repeated with careful manipulation of the image until the remaining image showed only ground points and selected permanent structures. The point cloud is then converted to a DEM using the workflow Tools → Projection → Rasterize. In this study, the resulting rasters opened in ArcGIS Pro without issue and accurately geolocated.

4.6 Assessment of Oxbow Development

Assessment of oxbow development followed the methodology of Giardino and Lee (2012). Using data from DEMs and historical imagery in ArcGIS Pro, attributes of each oxbow lake were recorded and input into models to evaluate the evolution of each lake over time.

Oxbows were identified from the most current DEM of the Little River, dated to 2022. Historical aerial imagery was manually georeferenced to the 2022 DEM, allowing a visual record of change from 1953 to 2022 in roughly decadal intervals. A major drawback encountered was the lack of historical aerial imagery from before 1953 for this area. Eight current oxbow lakes were assessed along the course of the Little River. Their respective dates of formation were estimated by determining the median of the years just before and just after oxbow formation, based on aerial imagery. Imagery from the years 1953, 1963, 1971, 1982, 1994, 2004, 2012, 2018, and 2022 were used. Of the eight current oxbows, three formed before 1953 and so their ages of formation could not be accurately determined. One was exceptionally recently-formed in the imagery from 1953, and so the year 1950 was used as an approximation for its date of formation.

ArcGIS Pro was used to determine the diversion angle, length of each oxbow and the length of the river meander between the endpoints of each oxbow. The diversion angle was measured as the angle between the upstream portion of the oxbow and the main channel in the downstream direction. Length of the oxbow and length of the channel between oxbow endpoints were used to calculate the cutoff ratio by the following formula:

$$\mathbf{C_R = O_L / M_L} \qquad \textbf{Eq. 8}$$

where C_R is the cutoff ratio, O_L is the length (ft) of the oxbow, and M_L is the length (ft) of the main channel between the oxbow endpoints. The cutoff ratio is considered because in a linear geomorphic system, a greater cutoff ratio in oxbows of equal depth and width results in lower sedimentation rates (Giardino and Lee, 2012). Similarly, a larger diversion angle results in an abandoned channel entrance farther away from the main channel flow and subsequent reduction in sedimentation rates (Giardino and Lee, 2012).

The thickness of sediment deposition at the plug of each oxbow lake was calculated by determining the difference in elevation of the plug, identified as the accumulation of sediment at the most upstream portion of the oxbow, and the elevation of the main channel. The date of the DEM from which elevation data were measured was compared to the date of oxbow formation to determine the age of the oxbow at the time sediment deposition thickness was determined. This information was used to calculate the rate of sedimentation using the following equation:

$$S_R = (O_E - M_E) / O_A \qquad \textbf{Eq. 9}$$

where S_R represents the rate of sedimentation (ft/yr), O_E is the elevation of the upstream oxbow surface, M_E is the elevation of the main channel, and O_A is the age of the oxbow in years.

From this, equations developed by Giardino and Lee (2012) were utilized to calculate the number of days of connection from each oxbow lake to the main channel and the flow required to establish connection between the oxbow lake and the main channel. The following equation is used to calculate the number of days of connection for all dated oxbows using the rate of sedimentation:

$$C\# = 28.255 * \ln(S_R) + 91.638 \qquad \textbf{Eq. 10}$$

where C# is the number of days of connection between the main channel and oxbow and S_R is the rate of sedimentation. The following equation is used to calculate the flow required to maintain connection between the oxbow lake and the main channel:

$$F_F = -674.5 * \ln(C\#) + 3306 \qquad \textbf{Eq. 11}$$

where F_F is the flood-flow (connection flow) required to connect the main channel to the oxbow lake and C# is the number of days of connection between the main channel and the oxbow.

5 Results

The results of this study are described in detail in this section.

5.1 MStaT Analysis

Using the points from centerlines generated in GIS, spaced evenly at ~820 ft (250 m) apart, MSTaT generated centerlines for the Little River for each year assessed (Figure 5-1).

For each year assessed, MSTaT determined points of maximum curvature for each bend in the river and indicated the line of inflection which runs the length of the river, following the meander curves.

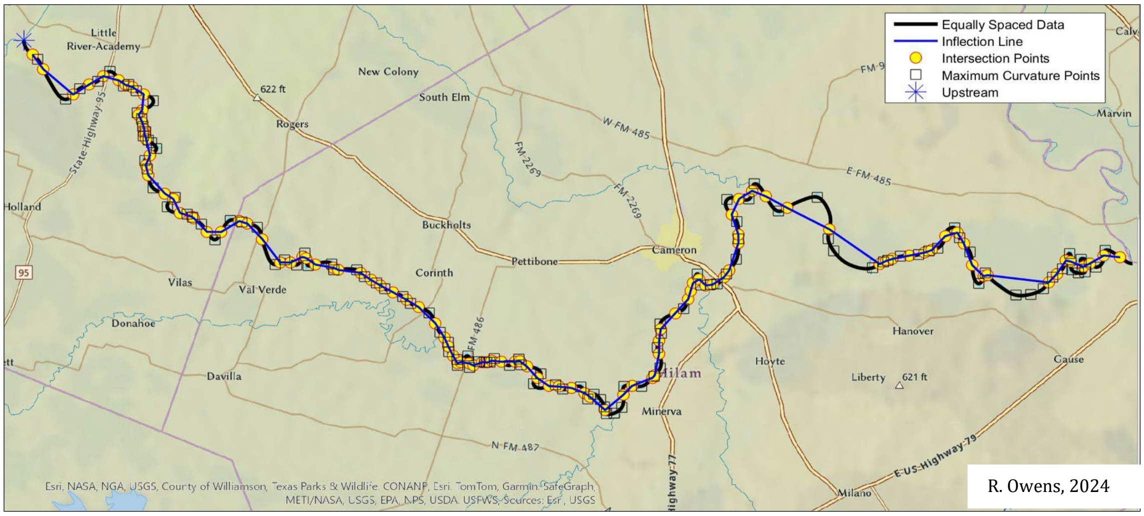

Figure 5-1. **Centerline generated by MStaT for the Little River. The blue inflection line connects points at which the curvature changes direction, represented in yellow.**

Data for the Little River, years 1953, 1963, 1974, 1982, 1996, 2004, 2012, 2018, and 2022 were analyzed in MStaT for channel morphodynamics, wavelet analysis, and meander migration rate. The results for channel morphodynamics are presented in Table 5-1.

Table 5-1. **Channel Morphodynamics of the Little River calculated in MStaT. The average channel width is 82 ft (25 m)**

Year	Total length analyzed (mi)	Bends found	Mean sinuosity	Mean amplitude (ft)	Mean arc-wavelength (ft)	Mean wavelength (ft)
1953	73	99	1.22	710	3860	3220
1963	73	101	1.22	698	3810	3170
1972	72	101	1.23	705	3740	3100
1982	63	91	1.25	697	3630	2970
1996	75	107	1.26	717	3700	3020
2004	77	122	1.29	637	3300	2650
2012	75	111	1.25	702	3600	2890
2018	76	107	1.28	742	3700	2990
2022	74	100	1.27	749	3860	3100

For each set of years assessed, reach length was compared to migration rate. These results are presented in Figures 5-2 to 5-9. Please note that meters are the only available units using MStat; thus, Figures 5-2 to 5-9 all use meters. From 1953 until the early 1970s, a positive correlation is observed between reach length and migration rate. From 1974 to 1982, this relationship is less distinct as spikes in migration are observed on some shorter lengths. Wavelength spectra were determined for each set of years assessed.

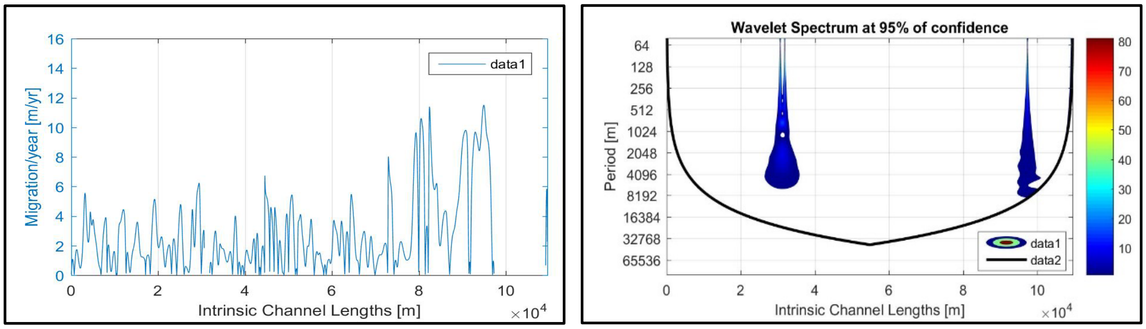

Figure 5-2. Annual migration rate of the river for the years 1953-1963. The wavelet spectrum demonstrates migration peaks at the end of the river's course and at approximately 19 mi (30 km).

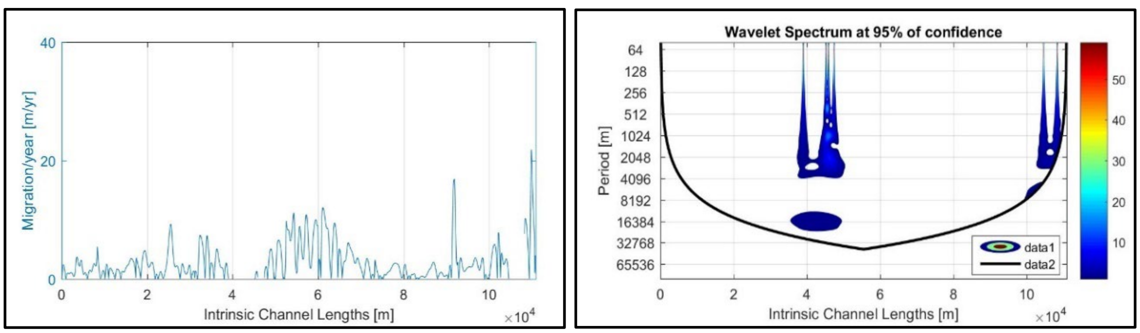

Figure 5-3. Annual migration rates for the Little River for the years 1963-1974. Wavelet analysis indicates maximum migration rates shifting downstream since 1953-1963.

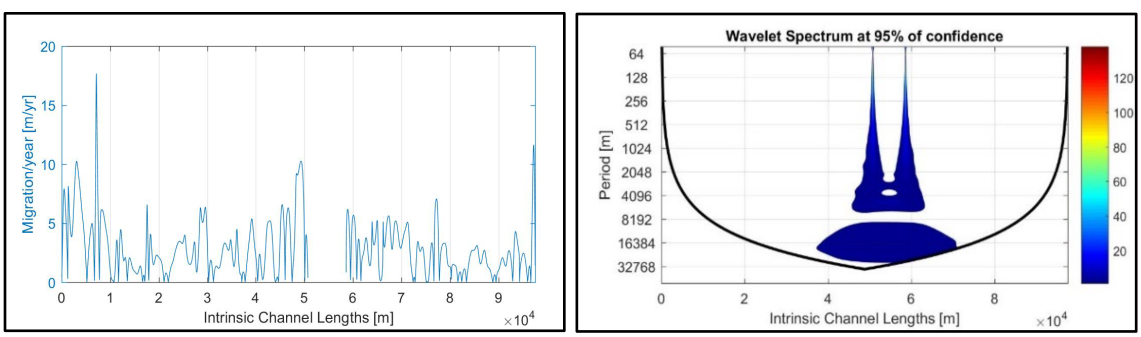

Figure 5-4. Migration rates and wavelet analysis for 1974-1982.

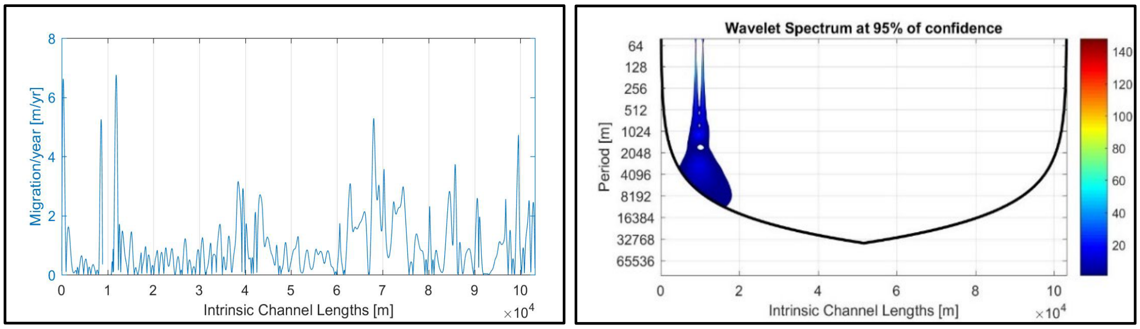

Figure 5-5. **Annual migration rates and wavelet analysis for the Little River for the years 1982-1996. Here, most notable migration has shifted upstream in the 95% confidence interval.**

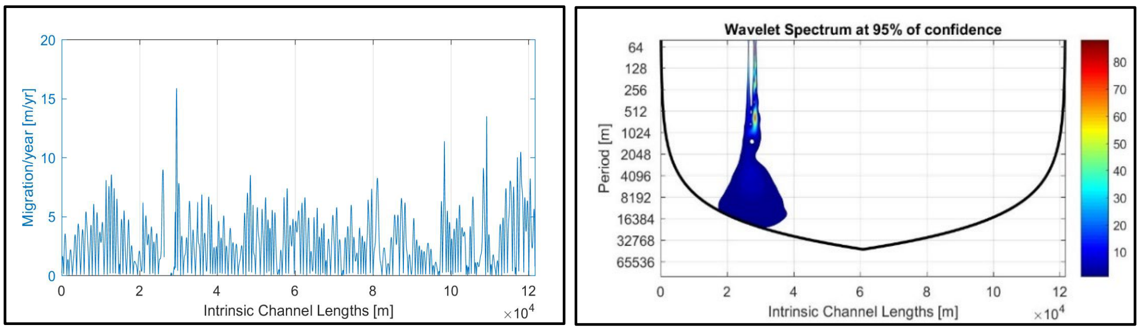

Figure 5-6. **Annual migration rates and analysis for the years 1996-2004. It is interesting to note here that, although migration that occurs on a periodicity of 210-3360 ft (64-1024 m) is less common, it occurs with higher power.**

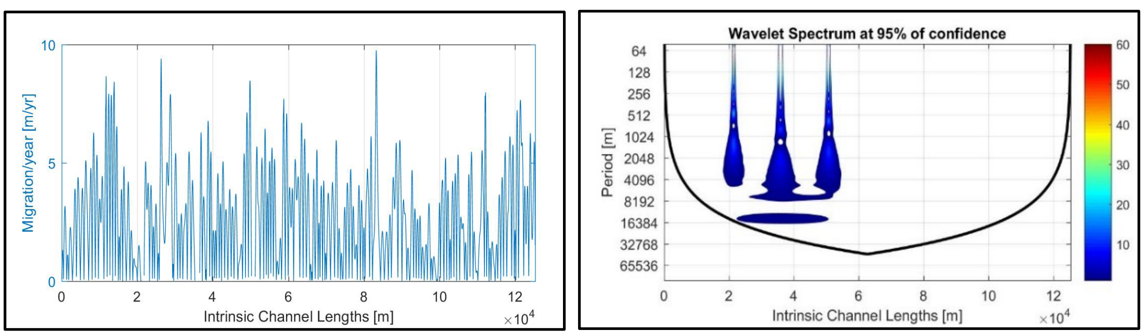

Figure 5-7. **Annual migration rates and analysis for 2004-2012. High power values persist at the lower periodicities.**

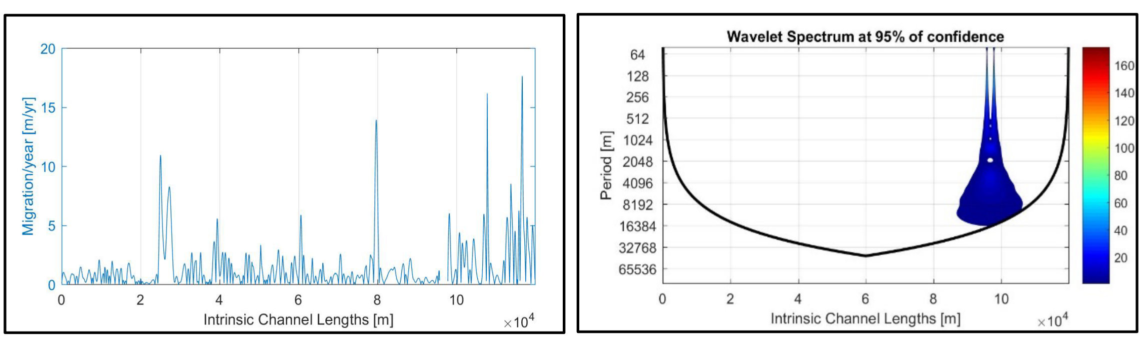

Figure 5-8. **Analysis for the years 2012-2018. Here, migration has again shifted**

downstream. High migration rates persist in this region today.

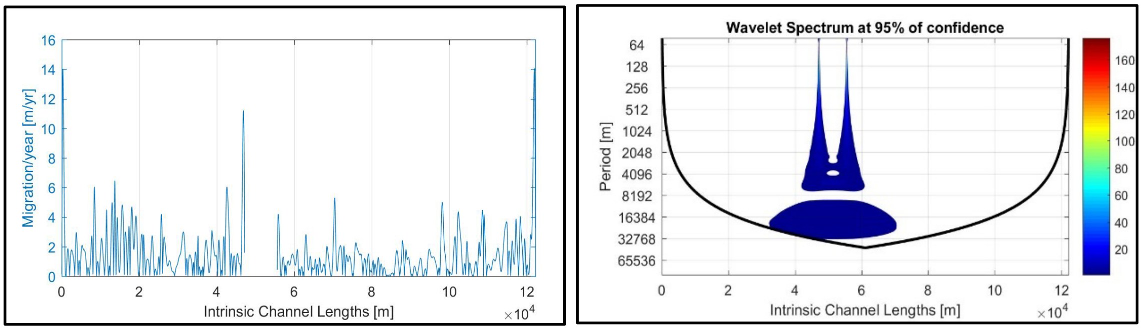

Figure 5-9. In the 2018-2022 time interval, the chute cutoff is apparent in both the migration rate graph and the wavelet analysis.

5.2 GIS Analysis of Meanders

The number of migration polygons for each time interval are presented in Table 5-2.

Table 5-2. Summary of migration polygons constructed for time intervals in GIS.

Study years	Reaches with migration 19.7-32.8 ft	Reaches with migration ≥ 32.8 ft	Reaches with migration ≥ 19.7 ft
1953-1963	38	173	211
1963-1972	32	164	196
1972-1982	34	150	184
1982-1996	73	118	191
1996-2004	82	57	139
2004-2012	86	68	154
2012-2018	107	122	229
1996-2018	134	101	235
2018-2022	134	103	237
1953-2022	39	227	266

For each time interval, river meanders were analyzed for migration greater than 10 m (~32.8 ft) and between 6-10 m (~19.7-32.8 ft). The full data are available in Appendix A. In total, 227 reaches experienced migration equal to or greater than 10 m (~32.8 ft) during the years 1953-2024. 39 reaches experienced migration equal to or greater than 6 m (~19.7 ft) but less than 10 m (~32.8 ft) during that same time period. The low number of reaches (39) for 1953-2022 compared to individual time periods is a result of aggradation that slowed or reversed the expansion of some migration pathways that had previously been active.

GIS analysis demonstrated that of the ten meander bends exhibiting the highest rates of migration during the years 1953-2022, eight occurred to the west of Cameron, Texas (Figure 5-10). This is noteworthy, as Cameron sits very near the stratigraphic boundary separating Cretaceous-aged limestone from Paleocene-aged sandstones.

The most rapidly-moving meander was a chute cutoff with endpoints at 30° 48' 5.04" N, 97° 7' 27.66" W and 30° 47' 38.76" N, 97° 5' 57.91". The cutoff has created a parcel of land approximately ~250 ha (618 ac) in area which sits south of the current Little River channel and north of the former channel. The current channel was a small creek until the year 2011, based on remote imagery, at which time it became comparable in size to the former channel. By 2015, significant sedimentation began to create a plug separating the old channel from the new. As of 2023, the old channel has been plugged and the cutoff is the main river channel.

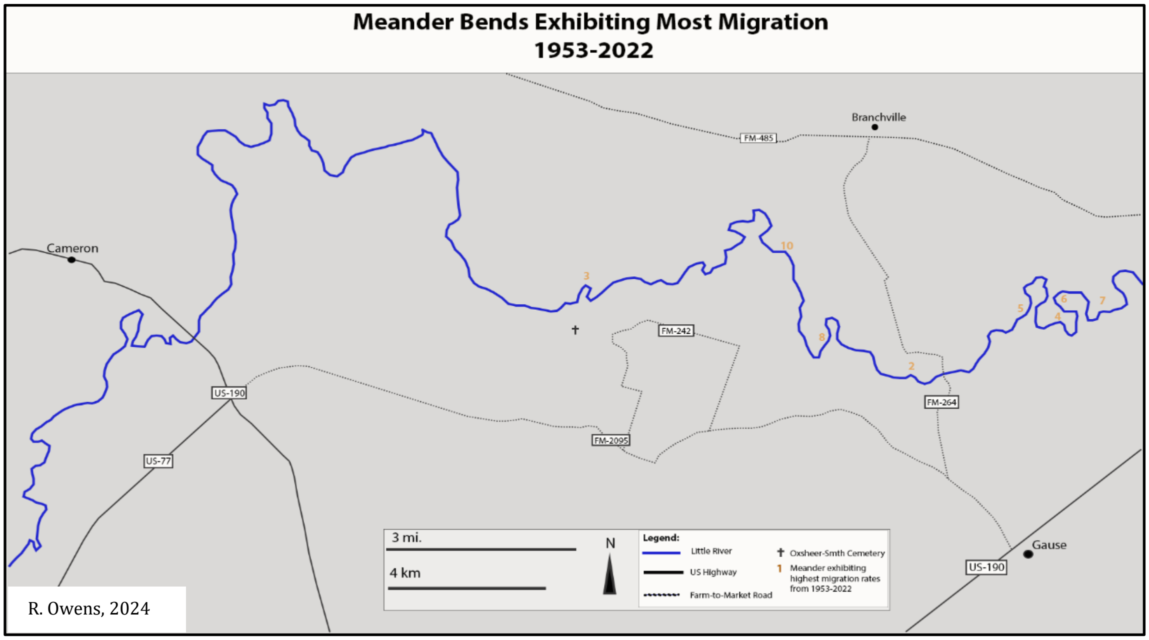

Figure 5-10. **Locations of highest migration for the entirety of available data on the Little River: 1953-2022.**

In addition to assessment of meander migration, a longitudinal profile was developed for the Little River from headwaters to mouth (Figure 5-11).

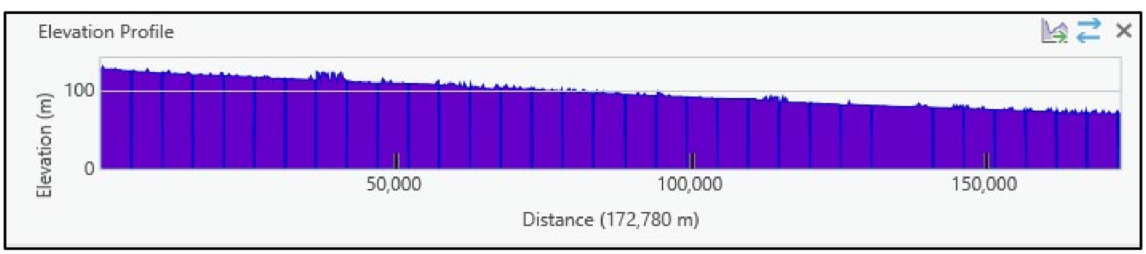

Figure 5-11. **Longitudinal profile of the Little River from headwaters to mouth.**

The maximum elevation of the river channel is found to be 429.7 ft (130.97 m) and minimum ~230 ft (70.24 m). The average slope of the channel is 7.34%, or 4.2º.

5.3 Qualitative Assessment of the Little River

A qualitative description of each segment studied on the Little River follows. All photographs by R. Owens (2024).

The locations of segments 1-6 are presented in Figure 5-12.

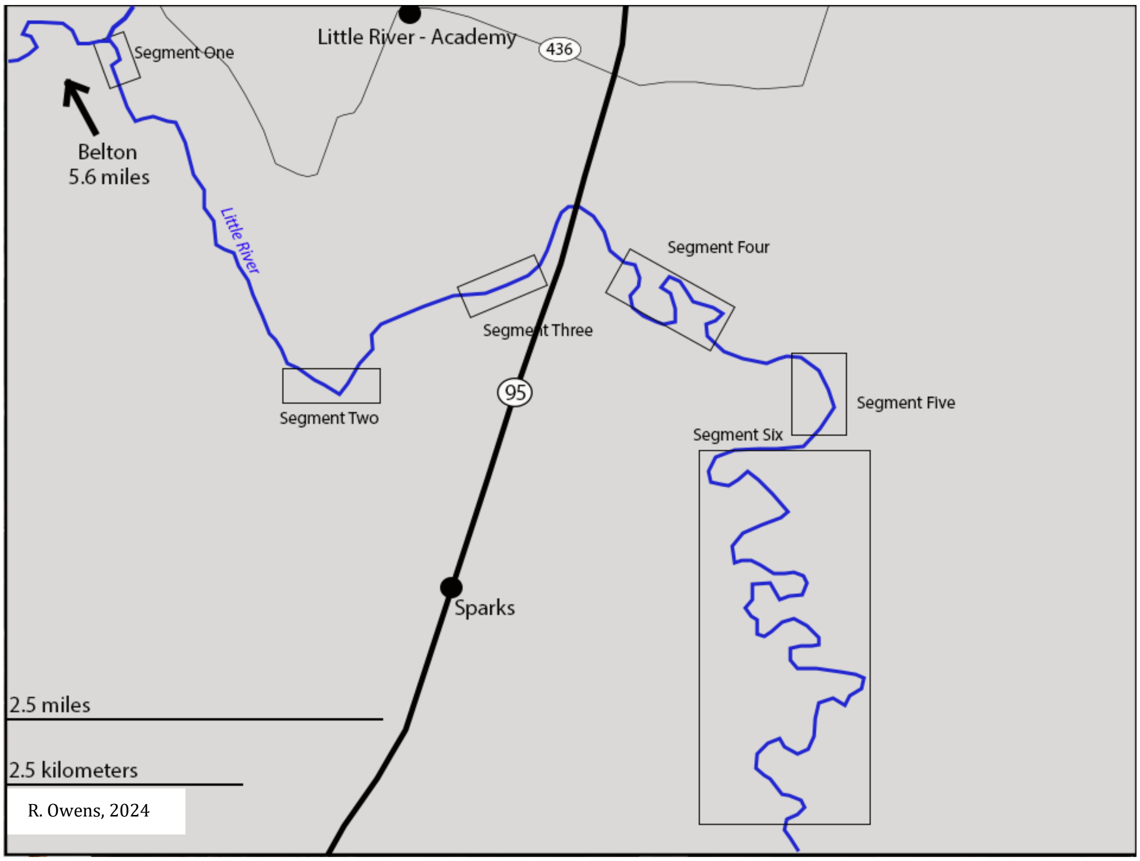

Figure 5-12. Locations of Segments 1-6 assessed by qualitative properties on the Little River.

5.3.1 Segment One

Location: 30° 58' 58.8" N, 97° 24' 0" W

Just downstream from the headwaters of the Little River, formed by the confluence of the Leon and Lampasas rivers southeast of Belton, Texas, the river channel is experiencing significant lateral erosion. A cutbank on the northeastern side of the river exhibits bare, earthen walls and evidence of slumping (Figure 5-13).

Figure 5-13. Barren cutbank in Segment One.

Active point bars are accumulating in the river channel in this stretch and are visible in aerial imagery. The river winds with a sinuosity of approximately 1.13 within its main channel in this location among active point bars. Point bars are predominantly clay with cobble-sized limestone accumulations and light vegetation and extend 65.6-98.4 ft (20-30 m) into the channel. Potential for debris jams was low, but high for sediment trapping as evidenced by the extensive point bars. Channel width here is approximately 141 ft (43 m). The texture of the bank material was predominantly clay, and bank angles on the cutbank side approached 88°. Point bars are sparsely vegetated and composed predominantly of clay and sand.

5.3.2 Segment Two

Location: 30° 56' 52" N, 97° 22' 23" W

Approximately 3.4 mi (5.5 km) downstream of its headwaters, the Little River makes a sharp turn to the northeast. Between its headwaters and this bend, the river exhibits a sinuosity of approximately 1.08 and meanders exhibit migration rates of approximately 12.14 ft/ yr (3.7 m/yr). Point bars, while present, do not extend to half the width of the channel. Cutbanks exhibit bank angles of 87° and moderate vegetation (Figure 5-14).

Figure 5-14. Moderate vegetation typical of Segment Two on the Little River.

At the northeastern bend, bank angles and vegetation levels remain similar to those immediately upstream. The river, however, is trifurcated by central bar formation within its channel and exhibits a jam of large woody debris (LWD) which spans 45% of the channel width for a length of ~180.5 ft (55 m) (Figure 5-15).

Figure 5-15. Large woody debris typical of Segment Two.

5.3.3 Segment Three

Location: 30° 57' 36" N, 97° 21' 19.16" W

0.75 mi (1.2 km) upstream of the Hwy 95 overpass south of Little River-Academy, the river makes an abrupt meander to the north. This is a rapidly-progressing meander, exhibiting vertical, barren banks on the cutbank and a wide, lightly-vegetated point bar. Soil texture at this location is clay, and bank angles of the cutbanks are 88^{o}. This location showed little threat of debris jams or flow disruption. Moderate vegetation developed on the narrow bars, whereas the cutbanks were completely barren. This meander is in an agricultural area. Moderate and heavy vegetation remains on the northwestern side of the meander, but the northeastern edge has been cleared to the channel's edge.

5.3.4 Segment Four

Location: 30.95753 N, 97.34017 W

A series of rapidly migrating meanders occur beginning at 0.88 mi (1.41 km) downstream of the Hwy 95 overpass south of Little River-Academy. The first meander is progressing to the West. The cutbank side exhibits evidence of rockslide and a LWD jam blocks approximately half of the river channel (Figure 5-16).

Figure 5-16. Rockslide (left) and large woody debris (right) in Segment Four.

At the point of maximum curvature, the cutbank exhibits vertical walls with minimal vegetation. LWD remnants persist in the channel, though no jams are present. A subsequent meander progresses to the north. It exhibits similarly barren cutbanks with bank angles of 71^{o}. The growing point bar exhibits moderate vegetation. At the end of this series of meanders, the channel is narrow (92.8 ft or 28.3 m) and exhibits moderate to heavy vegetation on its banks (Figure 5-17).

Figure 5-17. Moderate to heavy vegetation in Segment Four.

5.3.5 Segment Five

Location: 30.94462 N, 97.31802 W

This straight segment of the river exhibits a clear channel with heavily vegetated banks (Figure 5-18). Average channel width in this segment is 82 ft (25 m). No debris jams nor sediment traps are evident, and only two point bars are present. These are unvegetated and predominantly clay and sand. Landcover is agricultural in this stretch, but a moderate to heavily wooded treeline remains at the channel edge. This treeline averages 85.3 ft (26 m) in thickness on the southeastern bank and 180.5 ft (55 m) on the northwestern bank.

Figure 5-18. Heavy vegetation on Segment Five.

5.3.6 Segment Six

Location: 30.94265 N, 97.32232 W to 30.8824 N, 97.29659 W

This is a southward-trending segment of active meanders. In this stretch, banks become progressively more barren as one progresses south, evidence of mass wasting is visible, and LWD resulting from bank undercutting becomes more prominent (Figure 5-19).

Figure 5-19. Large woody debris and severe bank cutting in Segment Six.

Landcover in this region is agricultural. Although light vegetation remains on either side of the river, land has been cleared for agriculture to the channel's edge. Channel sinuosity is 2.22 in this stretch, and channel width averages 108 ft (33 m). The location for segment seven is presented in Figure 5-20.

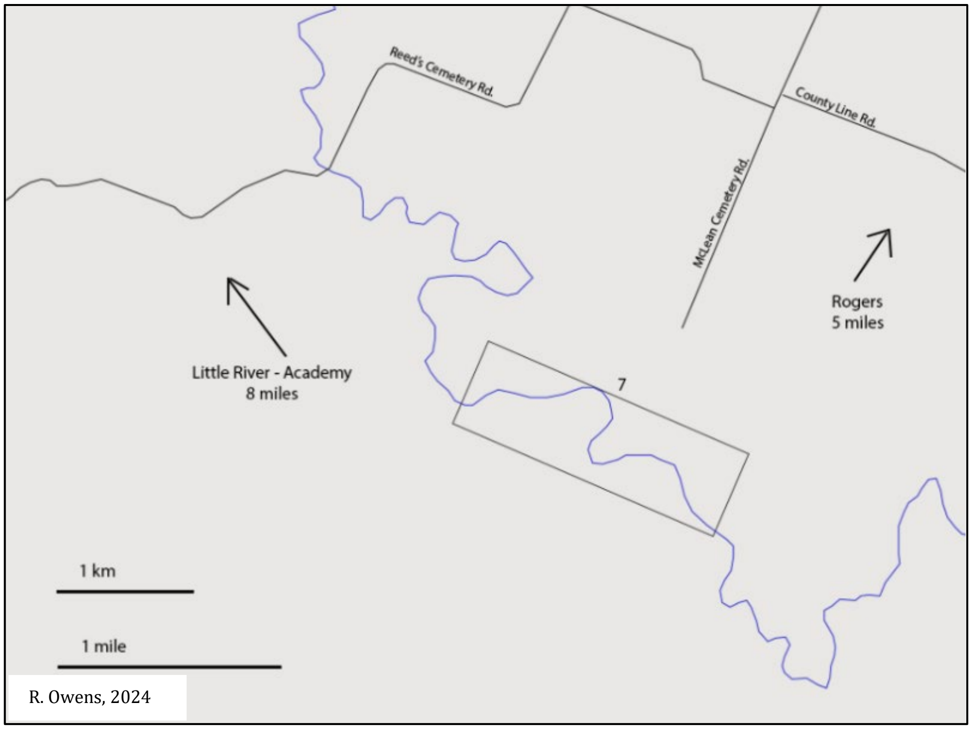

Figure 5-20. Location of Segment Seven.

5.3.7 Segment Seven

Location: 30.8824 N, 97.29659 W

In this segment, the river trends again to the east-southeast. Meander bends are less sinuous (1.74), but site 7 marks a rapidly advancing meander in this stretch. The stream is furcated to multiple branches by growing central and lateral bars and flow is slowed by the presence of LWD (Figure 5-21). The average channel width in this stretch is 78.7 ft (24 m). Banks are lightly to moderately vegetated. The locations for segments 8-12 are presented in Figure 5-22.

Figure 5-21. **Furcation of the river channel in Segment Seven.**

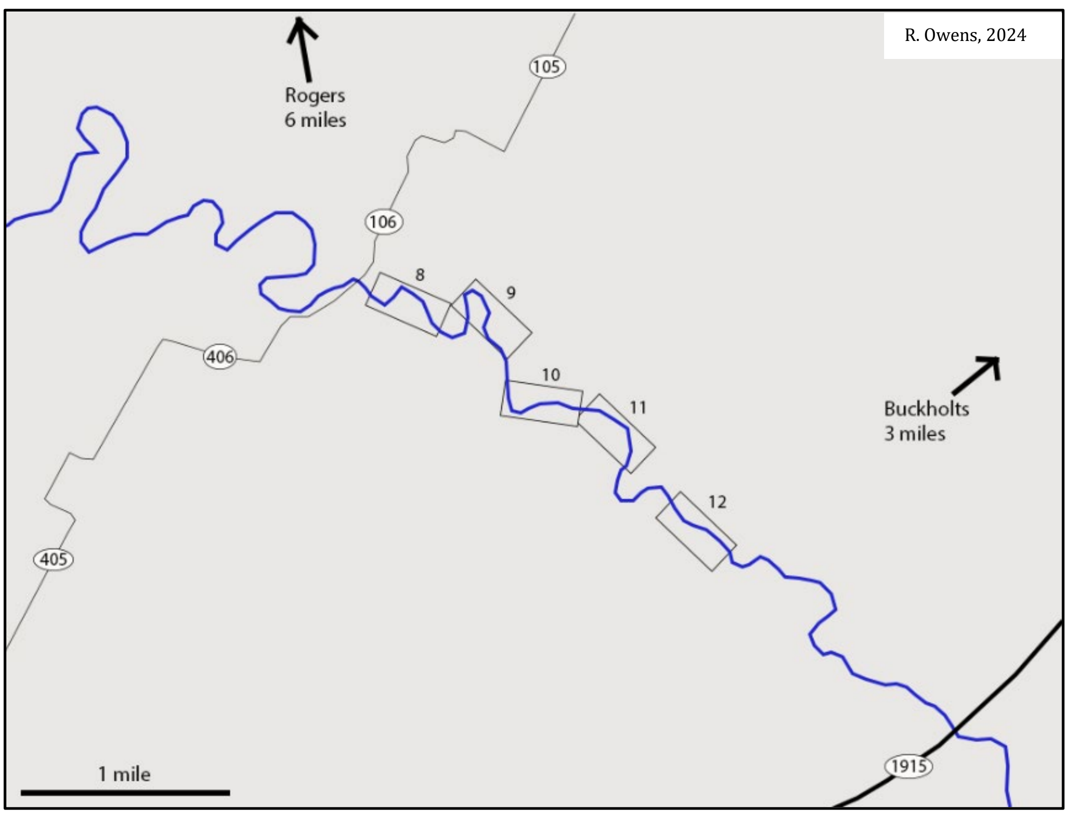

Figure 5-22. **Location of Segments 8-12.**

5.3.8 Segment Eight

Location: 30.84638 N, 97.19323 W

This is a sinuous (1.75) easterly-trending segment of the river exhibiting slowly migrating meanders and stable slopes. Slopes exhibit an angle of 24^{o} and are heavily vegetated (Figure 5-23).

As the river progresses to the east, sediment accumulation has created significant central bars, LWD appears, and bank erosion becomes more pronounced. To the east, cutbanks support only light vegetation and show evidence of undercutting the uppermost regolith layer.

The easternmost segment of this stretch includes a meander that was in the ten most rapidly migrating meanders for the years 1953-2022, according to ArcGIS Pro calculations. The rapidly-moving meander bend is one on which vegetation has been cleared to the channel for agriculture. In other areas on this stretch, moderate to heavy wooded vegetation remains. Where vegetation has been removed for agriculture, however, the meander bends are rapidly migrating. The rapidly-moving bend in the eastern part of this segment migrated ~413.4 ft (126 m) between the years 1953-2022.

Figure 5-23. **Stable, vegetated banks on Segment Eight.**

5.3.9 Segment Nine

Location: 30.84788 N, 97.1854 W

The eastward trending series of meanders culminates in a rapidly-moving lateral meander to the north. This sharp bend is progressing to the north and undercutting trees, creating LWD deposits and barren cutbanks with scalloped bedding (Figure 5-24).

Figure 5-24. Severe erosion in Segment Nine.

5.3.10 Segment 10

Location: 30.839456 N, 97.180549 W

After flowing south-southeast for 0.75 mi (1.2 km), the Little River makes another abrupt bend to the east. This rapidly progressing meander has lightly vegetated cutbanks and an established point bar with moderately large trees.

5.3.11 Segment 11

Location: 30.83777 N, 97.17082 W

Another rapidly progressing cutbank. Established, moderately vegetated bar. Here, the river turns back south. Immediately after this southward bend in the river, a significant bar is forming and LWD is accumulating. This segment ends with an abrupt turn to the northeast. Significant lateral erosion is occurring on this cutbank (Figure 5-25).

Figure 5-25. Bar development and erosion in Segment 11.

Looking upstream from the rapidly eroding cutbank in Figure 38 (5-25), the sudden change in vegetative cover is apparent. The rapid erosion is occurring where natural tree cover has been cleared for agricultural purposes. Original vegetation is seen in Figure 5-26.

Figure 5-26. Original vegetation in Segment 11, where it has not been cleared for agriculture.

5.3.12 Segment 12

Location: 30.83238 N, 97.16296 W

Between sites 11 and 13, the Little River progresses again to the southeast, exhibiting an average sinuosity of 1.2. In this stretch, the river channel exhibits evidence of moderate erosion. Light to moderate vegetation persists, though curved tree trunks are common. On some meanders, tree roots are exposed and gravel bars are developing in the channel. One rapidly progressing cutbank exists at 30° 48' 39.49" N, 97° 8' 5.06" W, exhibiting barren banks and talus slope formation. The point bar is moderately developed with LWD present.

Locations of segments 13-15 are presented in Figure 5-27.

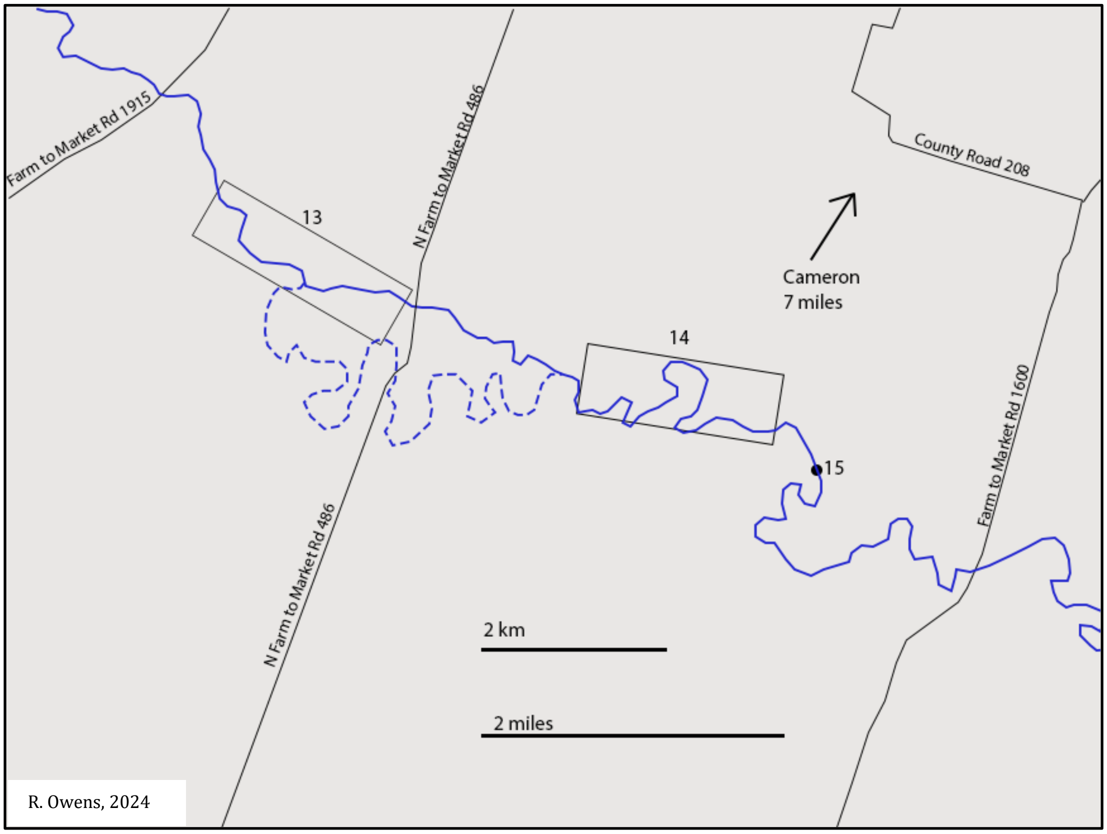

Figure 5-27. Locations of Segments 13-15.

5.3.13 Segment 13

Location: 30°48'14.3"N 97°07'41.1"W

Clays Creek enters the Little River at 30°48'14.3"N 97°07'41.1"W. At the confluence, LWD has accumulated and a bar approximates half the channel width. Approximately 0.35 mi (0.57 km) downstream from the confluence of Clays Creek, at 30° 48' 5.04" N, 97° 7' 27.66" W, the main river channel has formed a cutoff from an older meander bend. This is a significant cutoff, creating a parcel of land 0.96 mi^2 in area (2.5 km^2) now to the south of the Little River. The cutoff point has been infilled with sediment, forming an established plug (Figure 5-28). The start of the cutoff is at the beginning of a cutbank whose associated point bar is well developed and extends halfway across the river channel (Figure 5-29).

Figure 5-28. Photo taken from the wide point bar at Segment 13.

Figure 5-29. The channel in the background is the previous channel, which has been infilled since approximately 2018.

The chute channel is a rapidly eroding channel (Figure 5-30).


Figure 5-30. Evidence of rapid erosion in the new channel.

The eastern endpoint of the chute cutoff, located at 30°47'37.08" N, 97° 5'58.86" W is infilled and blocked by a LWD jam. Here, the river returns to a more stable channel and exhibits moderate to heavy vegetation cover, although occasional LWD persists (Figure 5-31).


Figure 5-31. Downstream of the cutoff, the river is again stable. The opening in the vegetation in the background of the left photo is the former channel.

5.3.14 Segment 14

Location: 30° 47' 37.72" N, 97° 4' 51.74" W

A rapidly migrating meander exists at 30° 47' 37.72" N, 97° 4' 51.74" W. The cut bank is barren and exhibits evidence of mass wasting. The point bar consists of both sediment and accumulations of LWD.

5.3.15 Segment 15

Location: 30° 46' 54.00" N, 97° 3' 56.34"

A channel-spanning log jam begins at 30° 46' 54.00" N, 97° 3' 56.34" W and completely blocks the channel for approximately 232.9 ft (71 m). Based on remote imagery, this jam formed between March of 2022 and May of 2023 (Figure 5-32). This timeline is supported by the plastic debris, such as a blue kayak trapped in the log jam, which was neither sun-faded nor cracked as of August of 2023 (Figure 5-33). A photo from above is presented in Figure 5-34.

Figure 5-32. The channel during March of 2022 (left) and May of 2023 (right). A channel-blocking log jam has formed between the taking of these two images and is encircled in the right photo.

Figure 5-33. Closeup of debris in the log jam. Note that the blue plastic ice chest and kayak are neither sun-faded nor cracked, although the kayak is in direct sunlight. This shows how recently and quickly the jam formed.

Figure 5-34. Drone photo of the channel-spanning log jam.

Locations of segments 16 and 17 are presented in Figure 5-35.

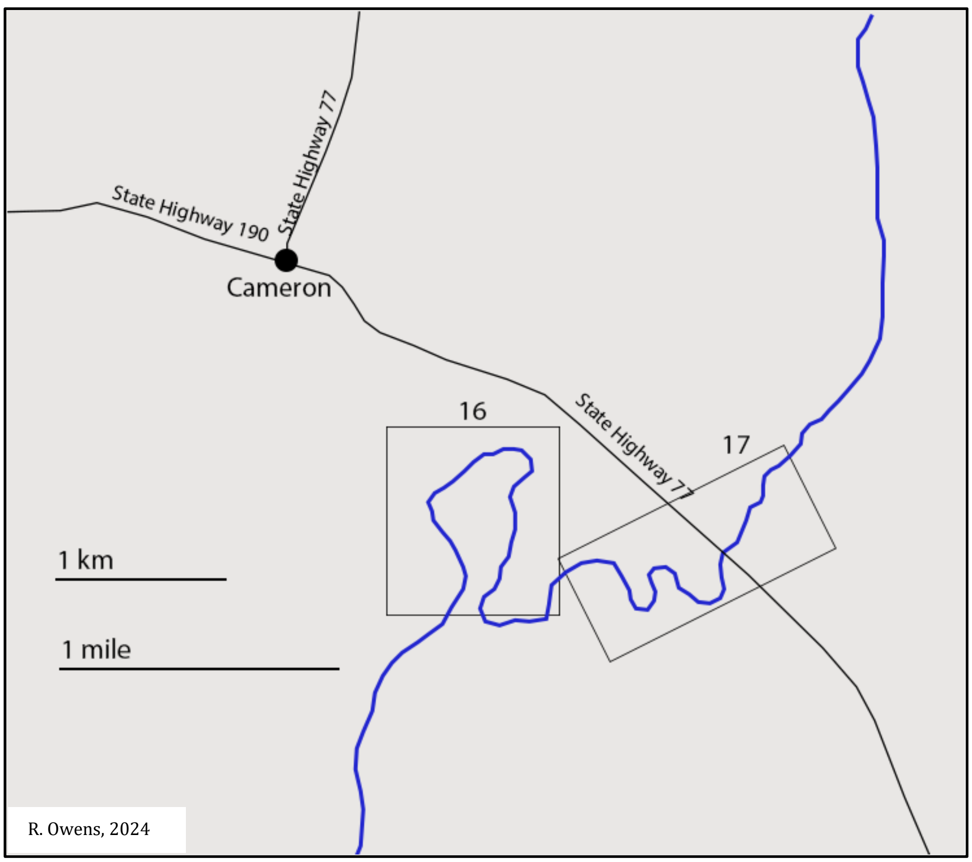

Figure 5-35. Locations of Segments 16 and 17.

5.3.16 Segment 16

Location: 30° 50' 25.41" N, 96° 57' 52.79" W

A weir and gage station at 30° 50' 25.41" N, 96° 57' 52.79" W near Cameron, Texas, slows the flow of the Little River locally, but regional land cover alteration encourages lateral growth of a northward-trending meander.

5.3.17 Segment 17

Location: 30° 50' 6.47" N, 96° 57' 16.96" W

From Segment 16, the Little River undulates with an average sinuosity of 1.75. Segment 17 exhibits active meander-bends with moderate vegetation, channel bars, and abundant LWD.

Locations of segments 18-23 are presented in Figure 5-36.

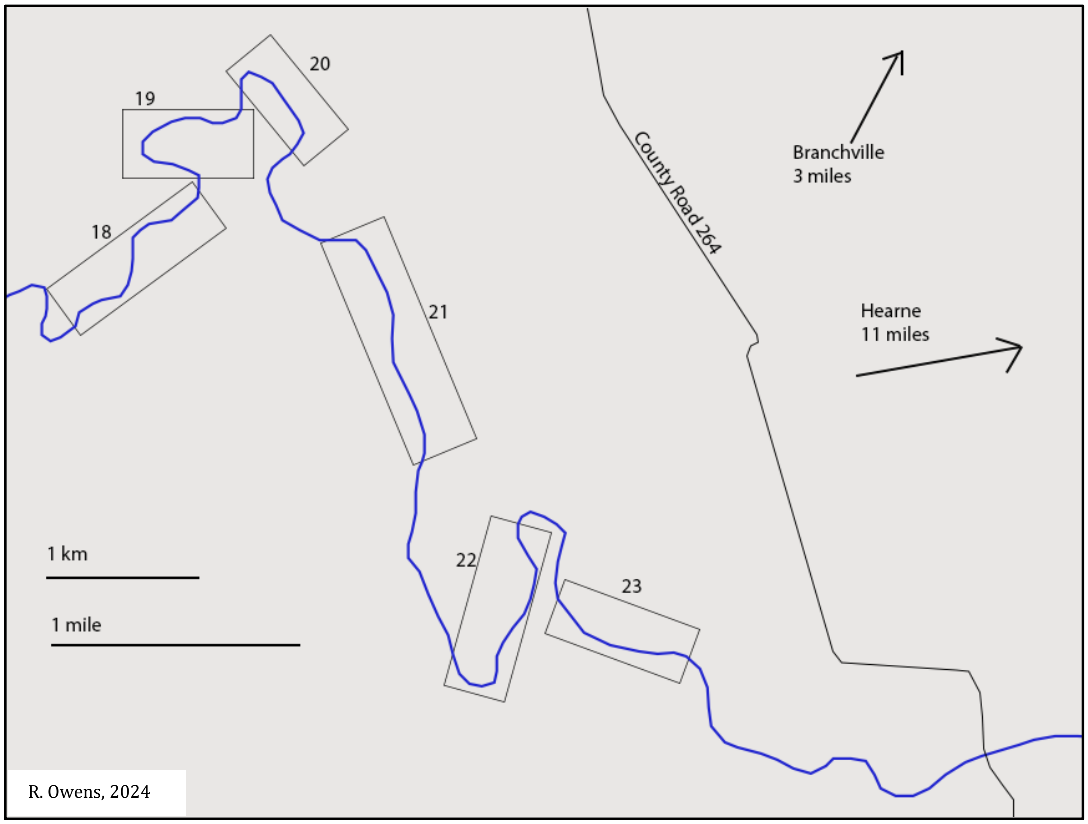

Figure 5-36. Locations of Segments 18-23.

5.3.18 Segment 18

Location: 30° 51' 14.83" N, 96° 48' 11.63" W

This stretch of the river exhibits moderate erosion rates.

5.3.19 Segment 19

Location: 30° 51' 48.53" N, 96° 47' 54.53" W

Stable banks with heavy vegetation, significant central bar development (Figure 5-37).

Figure 5-37. In Segment 19, the channel has divided around a significant central bar.

5.3.20 Segment 20

Location: 30° 51' 59.26" N, 96° 47' 40.78" W

In this stretch, the river cuts into well-cemented bedrock that includes a seam of lignite coal (Figure 5-38).

Figure 5-38. Bedrock banks including a seam of lignite in Segment 20. Closeup of lignite seam in right photograph.

Vegetation is well-established on the land surrounding this segment and the river channel is free of flow disruptors in most of the segment. An exception exists where blocks of limestone bedrock are exposed in the channel.

5.3.21 **Segment 21**

Location: 30° 50' 58.09" N, 96° 47' 3.26"W

Downstream of the exposed bedrock channel, the river returns to a stable state with well-established, mature vegetation and no flow disruptors. Bank slope angle is approximately 31° and the channel width is approximately ~180.5 ft (55 m). The sinuosity is approximately 1.1 in this segment.

5.3.22 Segment 22

Location: 30° 49' 46.7" N, 96° 46' 42.53" W

At the end of Segment 21, the Little River makes an abrupt turn to the north. This is a rapidly migrating meander, as evidenced by extensive slope failure. Debris is accumulating in the river here as a result of this failure (Figure 5-39).


Figure 5-39. Earthen blocks indicate slope failure in Segment 22 (left), and debris accumulations (right).

Erosion is exacerbated where vegetation has been cleared to the channel. In these sites, root overhang is common and barren banks support no vegetation (Figure 5-40).

Figure 5-40. Significant root overhang resulting from bank undercutting in Segment 22.

5.3.23 Segment 23

Location: 30° 49' 58.01" N, 96° 46' 13.44" W

This segment marks a portion of the river that has turned back to the south after a sudden northward turn and exhibits extensive bedrock in the channel (Figure 5-41). Banks are heavily vegetated in this stretch and bank slope averages 30 degrees. Channel width is approximately ~137.8 ft (42 m).

Figure 5-41. Bedrock channel in Segment 23.

Locations of segments 24-29 are presented in Figure 5-42*.*

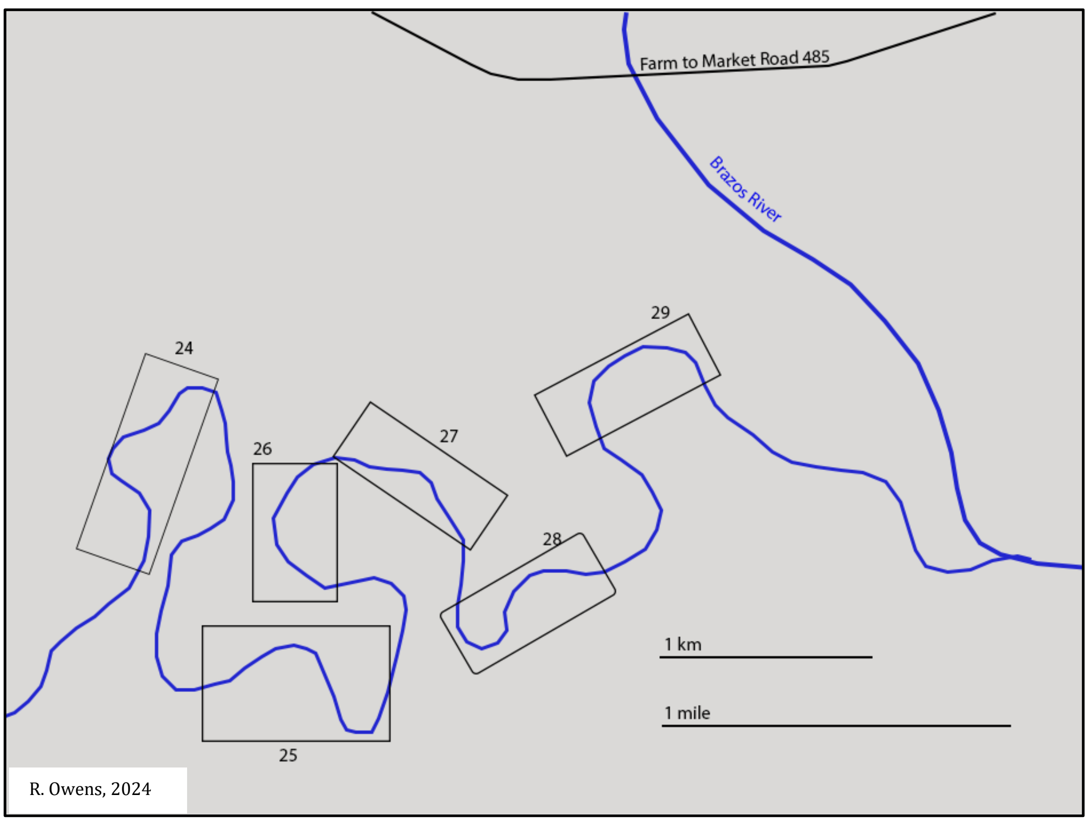

Figure 5-42. Locations of Segments 24-29.

5.3.24 Segment 24

Location: 30° 50' 34.08" N, 96° 43' 14.02" W

Segment 24 represents a complex meander that is rapidly migrating. Vegetation has been cleared to the edge of the channel. Erosion is evidenced by the earthflows at the base of banks and gully formation in the banks (Figure 5-43).

Figure 5-43. Rapidly-eroding banks in Segment 24.

5.3.25 Segment 25

Location: 30° 50' 10.61"N, 96° 42' 38.27" W

Segments 24-29 are all within a series of consecutive meanders that form as the Little River approaches the Brazos River. All are rapidly moving, but in Segment 25 the river has achieved stability and does not show evidence of rapid adjustment. Vegetation is mature and well-established, and the channel is mostly free of debris.

5.3.26 Segment 26

Location: 30° 50' 31.96" N, 96° 42' 47.84" W

Typical of the entirety of the Little River, stability of the channel diminishes where vegetation has been cleared. In Segment 26, agriculture has cleared vegetation to the edge of the channel. Barren banks support no vegetation and are developing gullies. Where vegetation is present, significant root overhang is present (Figure 5-44).

Figure 5-44. Severe root overhang from bank undercutting on Segment 26.

5.3.27 Segment 27

Location: 30° 50' 45.38" N, 96° 42' 31.46" W

Segment 27 is in the midst of a meander bend, but vegetation remains intact on the land surrounding the channel. The channel in this region is stable, exhibiting mature vegetation and no significant bank failure. Some flow disruptions exist in the form of bedrock blocks in the river channel (Figure 5-45).

Figure 5-45. Bedrock outcrops, Segment 27.

5.3.28 Segment 28

Location: 30° 50' 19.1"N, 96° 42' 15.95" W

This segment is a slow-moving meander. Vegetation remains intact to the river's edge and into the channel. A bar has begun forming on the inside of the meander, but it remains narrow. No flow disruptors nor bank failure is noted.

5.3.29 Segment 29

Location: 30° 51' 0.25" N, 96° 41' 51.29" W

This rapidly-moving meander is the last bend in the Little River before its confluence with the Brazos river. Agriculture has cleared most vegetation to the banks of the river. Where vegetation exists, root overhang is significant. Gullies and earthflows indicate significant erosion in the banks here

5.4 Summary of Migration Rates

The results of the stream power assessment, GIS assessment, and qualitative assessment were compared with one another for each segment assessed. Results are presented in Table 7. Higher qualitative stability scores indicated lower channel stability.

Table 5-3. Qualitative Stability Scores for Segments 1-29 of the Little River.

Segment	Bank soil texture	Avg. Bank angle (°)	Vegetative bank protection	Bank cutting	Mass wasting	Bar dev.	Debris jam pot.	Stream power (W/ft²)	Qualitative stability score
1	3	10	12	12	9	12	9	43.38	49.4
2	3	10	9	12	7	7	7	39.48	42
3	3	10	10	10	7	6	6	32.52	40.2
4	4	9	7	7	9	7	4	29.17	38.4
5	4	4	3	3	3	3	3	24.8	21.2
6	4	9	9	10	10	4	10	26.57	40.4
7	4	9	5	9	7	10	10	26.85	38
8	4	5	2	2	2	10	10	30.66	27.4
9	4	11	11	11	11	6	10	47.01	47.6
10	4	7	7	7	6	4	3	49.61	33.8
11	4	7	9	9	5	10	10	53.42	40.4
12	4	4	6	9	9	10	8	59.46	40
13	4	10	11	12	8	9	7	72.74	47.2
14	4	10	11	11	10	7	9	52.02	46.6
16	4	10	10	12	8	6	4	68.1	44
17	4	9	9	10	6	10	10	71.9	43.8
18	4	9	9	9	9	9	6	49.05	43.4
19	3	4	4	4	4	10	9	19.88	28
20	1	7	5	5	7	6	9	51.47	32.8
21	3	4	6	4	6	4	4	20.07	26.6
22	4	9	10	10	10	6	10	51.28	44.4
23	1	4	4	4	4	4	10	20.16	23.4
24	4	10	10	10	9	10	9	58.71	47.4
25	4	4	4	4	4	4	4	24.99	24
26	4	10	10	12	8	6	6	20.35	40.4
27	4	5	3	3	3	3	7	13.19	21.6
28	4	6	4	6	6	6	10	13.19	29
29	4	11	9	12	9	10	6	13.56	42.4

Avg. = average; Dev. = deviation; Pot. = potential

5.5 Stream Power, Stream Power Index, and Compound Topographic Index

Calculating stream power using the ArcGIS Pro tools and the workflows previously described here, helps in the investigation of stream energy and sediment transport in a watershed. Field verification of the computations is necessary (Gartner, 2016).

Stream power in segment 12 of the Little River reaches 59.46 W/ft² (640 W/m²) (Table 5-3) indicating potential for high erosion. A field visit conducted on August 12, 2024, provided verification of areas of high stream power where sediment transport is taking place along the river. Figures 5-46 and 5-47 show some areas of high erosion in segment 12 of the Little River.

Figure 5-46. A moderately developed point bar with LWD present in Segment 12 of the Little River.

Figure 5-47. A rapidly progressing cutbank exhibiting barren banks and talus slope formation in Segment 12 of the Little River.

The Flow Accumulation (Figure 5-48) and Flow Direction (Figure 5-49) maps generated by adapting Gartner (2016)'s workflow, are inputs necessary to calculate Stream Power, Stream Power Index, and Compound Topographic Index. The details in these maps are not observable at the scale presented in the figures within this report. Thus, the ArcGIS files are shared with the Texas Water Development Board through Dropbox. Zooming into the different segments of the river or smaller areas of the watershed allows the user to view the detail in these maps.

An artificial stream linear network was created for the Little River watershed using a flow accumulation value >= 42 (Figure 5-50). This map is useful to identify areas in the watershed in which water is more likely to flow.

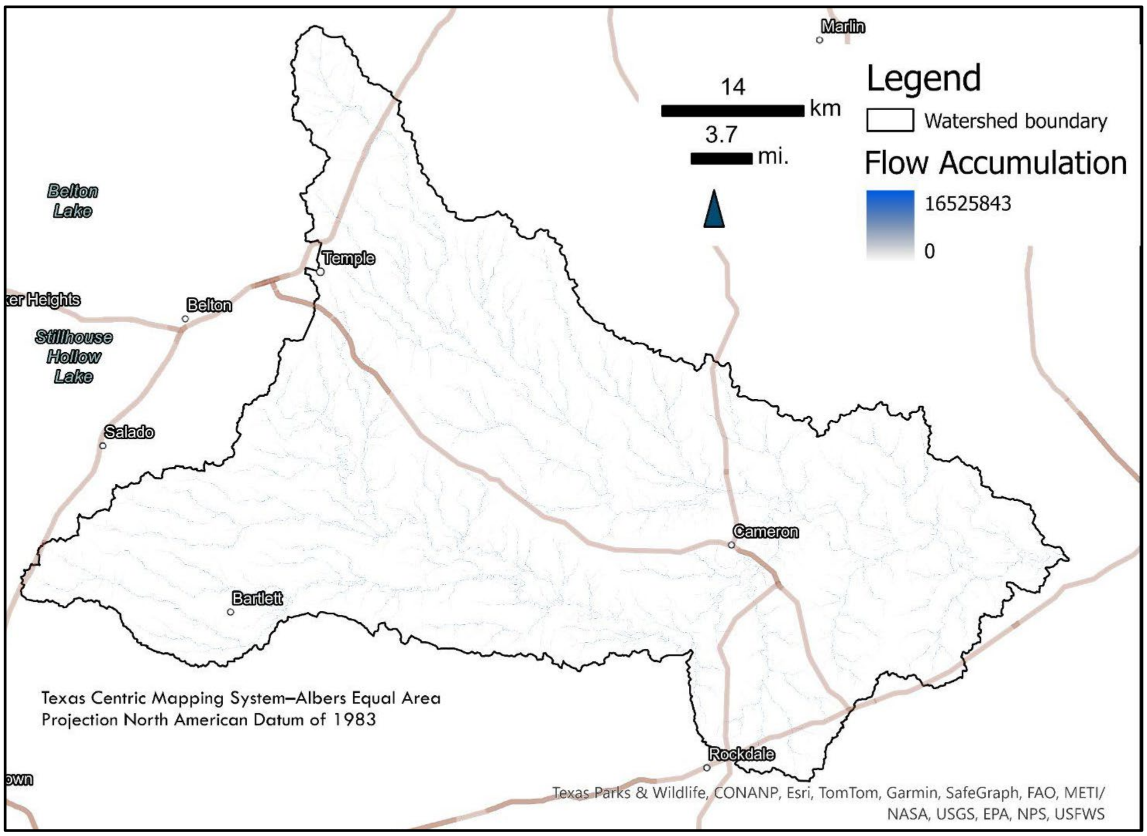

Figure 5-48. Flow Accumulation map for the Little River watershed.

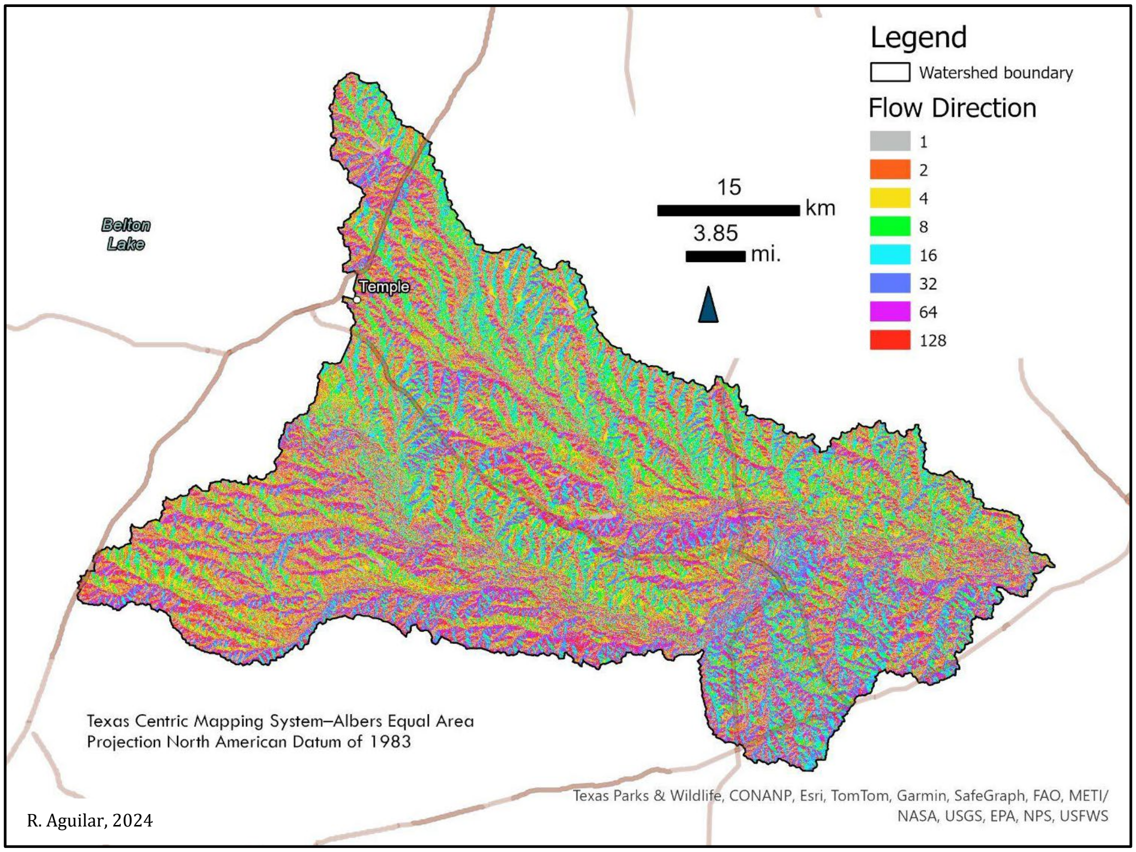

Figure 5-49. Flow Direction map for the Little River watershed.

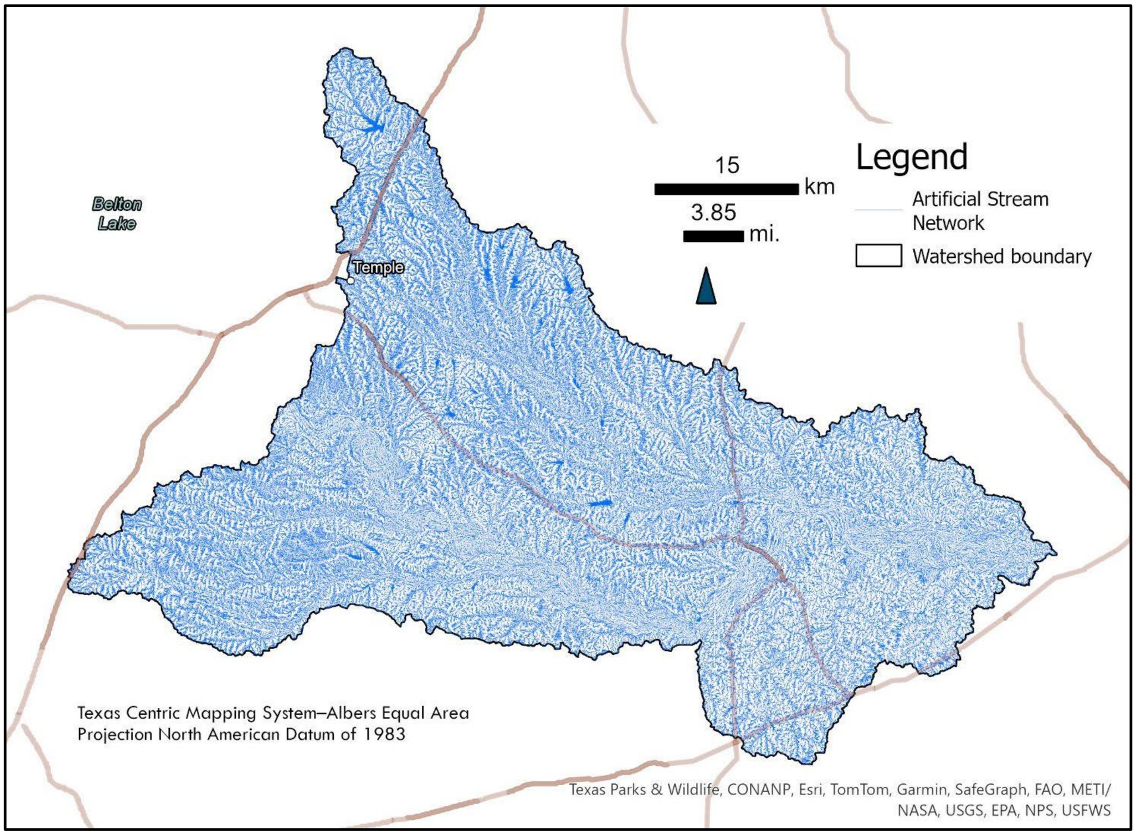

Figure 5-50. Artificial Stream Network for the Little River watershed.

Modeling stream power index (SPI) aids in the visualization of high slope areas and areas where flows accumulate, which can lead to increased erosion and potentially cause the formation of erosive features such as gullies and ravines (Timm, 2016).

In the Little River watershed, 81% of the area corresponds with slope values of 0 to 5%, greater than 5 to 10% slopes cover about 16% of the watershed, with only about 3% of the basin showing slopes greater than 10%, as shown in Figure 5-51.

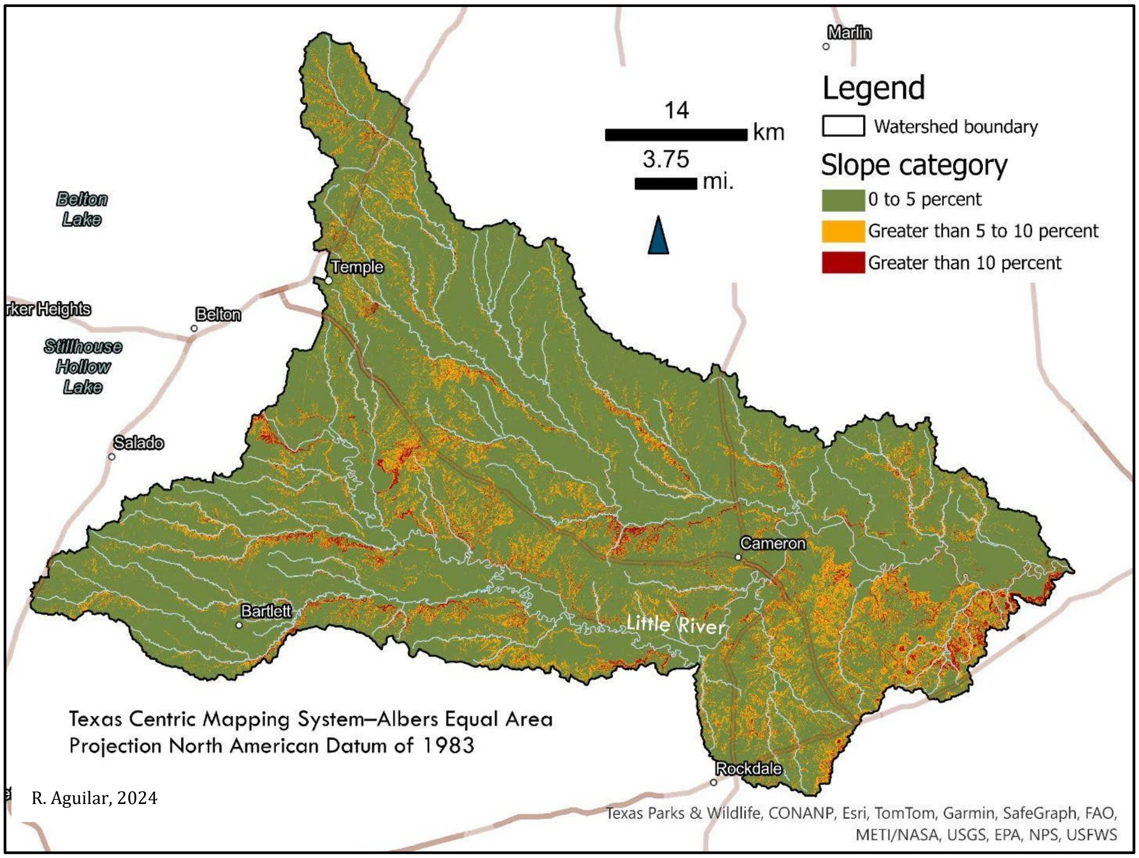

Figure 5-51. Slope map for the Little River watershed.

SPI signatures for the Little River watershed are shown in Figure 5-52. The details of the SPI map are not observable at the scale presented in this report; thus, the ArcGIS Pro files are shared with the Texas Water Development Board through Dropbox.

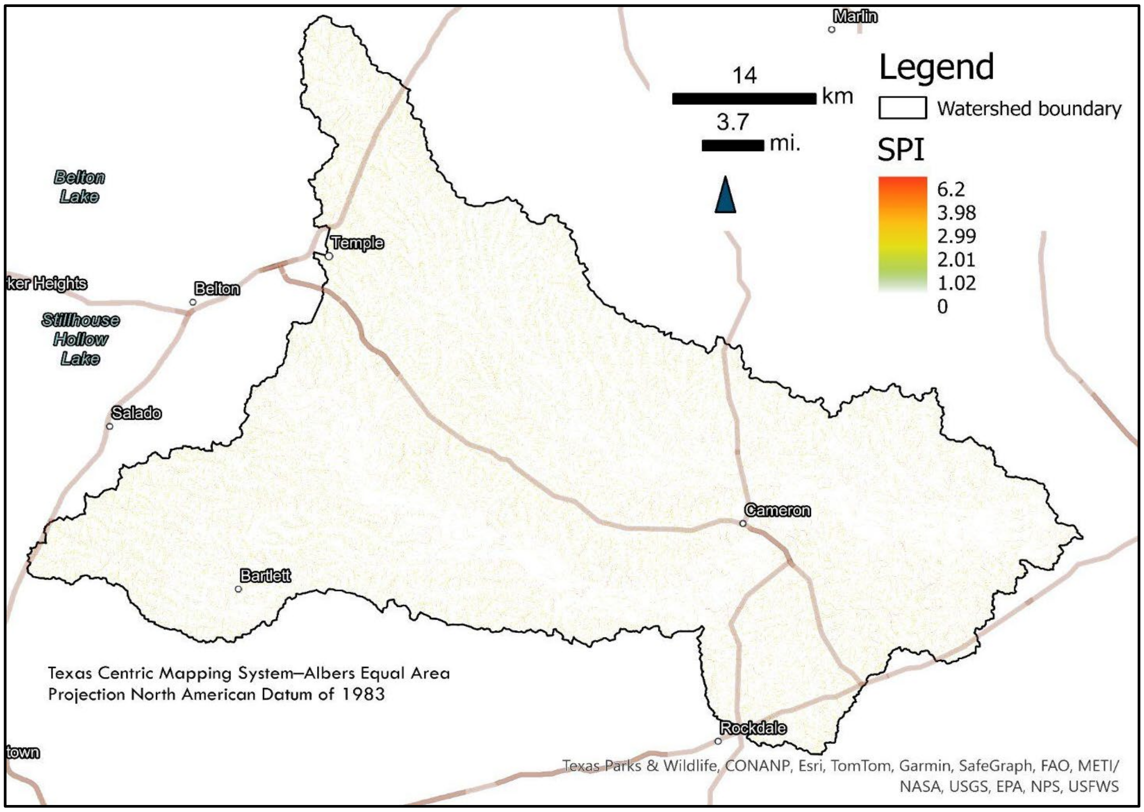

Figure 5-52. SPI map for the Little River watershed.

The Flow Accumulation and Slope rasters were used to produce the CTI map, which helps identify areas where water is likely to accumulate. Figures 5-53 shows the CTI map for the Little River watershed indicating potential areas of impounded water. Note the dendritic pattern of the CTI signatures on the surface.

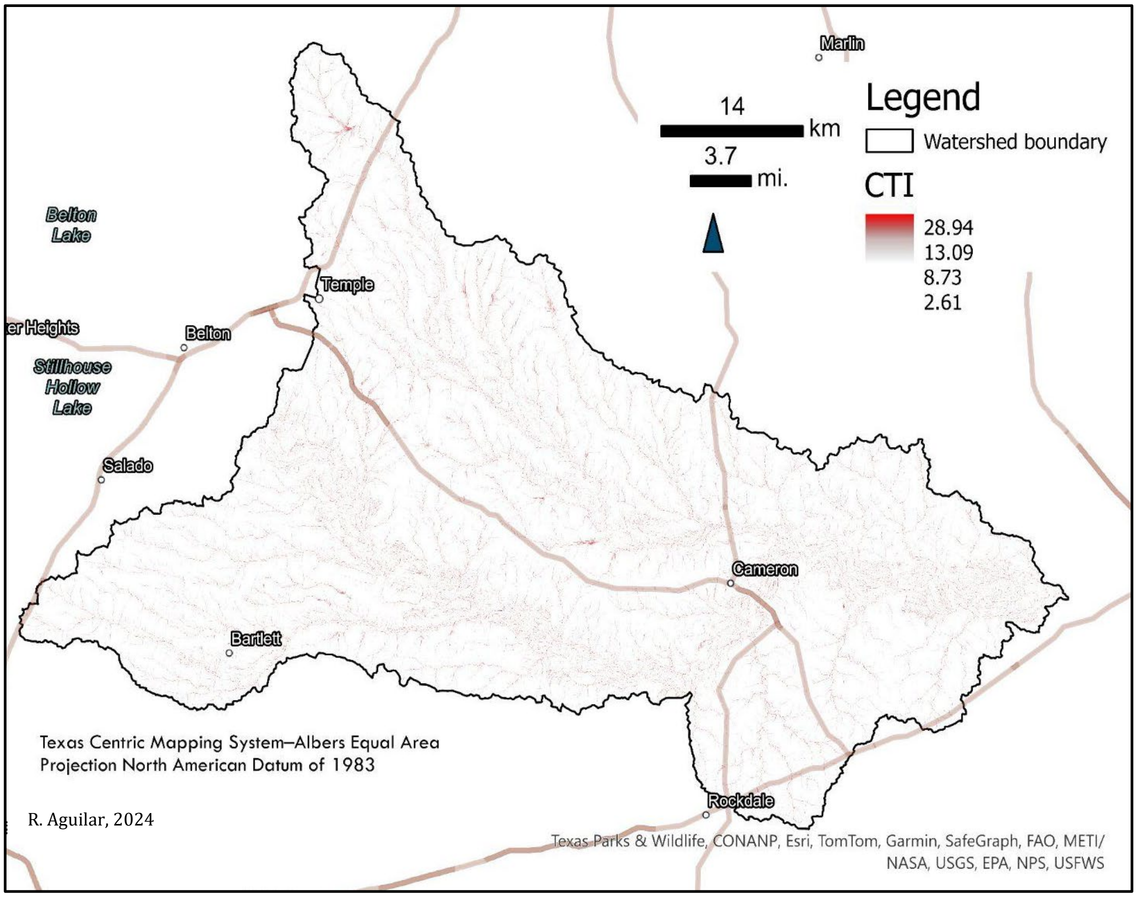

Figure 5-53. CTI map for the Little River watershed.

Combining the CTI and SPI signatures with field visits, and high-resolution aerial imagery, it is possible to identify areas in which overland flow accumulates and has the potential to move sediment within the Little River watershed. This information can be combined with land use data to inform best practices in areas where increased erosion is identified.

5.6 Assessment of Oxbow Development

This study assessed the development of oxbow lakes along the Little River. Aerial photography from 1953 to 2023 was utilized to identify current oxbow lakes and identify their date of cutoff. Elevation data from the cutoff plug and the main channel, were used with aerial imagery analysis to calculate the cutoff ratio and sedimentation rate of each oxbow lake.

Eight current oxbow lakes were identified along the ~107 mi (~172 km) course of the Little River (Figure 5-54). Of the eight, four separated from the main channel prior to 1953. For this reason, no aerial photography was available to document its date of cutoff, nor are topographic maps available for this region during that time. Those oxbows were assigned a cutoff date of 1953, but because it is known that the cutoff occurred before 1953, the sedimentation rates reported will be higher than their actual values. One oxbow remnant, located at 96°42'8"W 30°50'51"N (OL8), has been partially covered by the modern migration of the Little River, erasing the record of elevation at its plug.

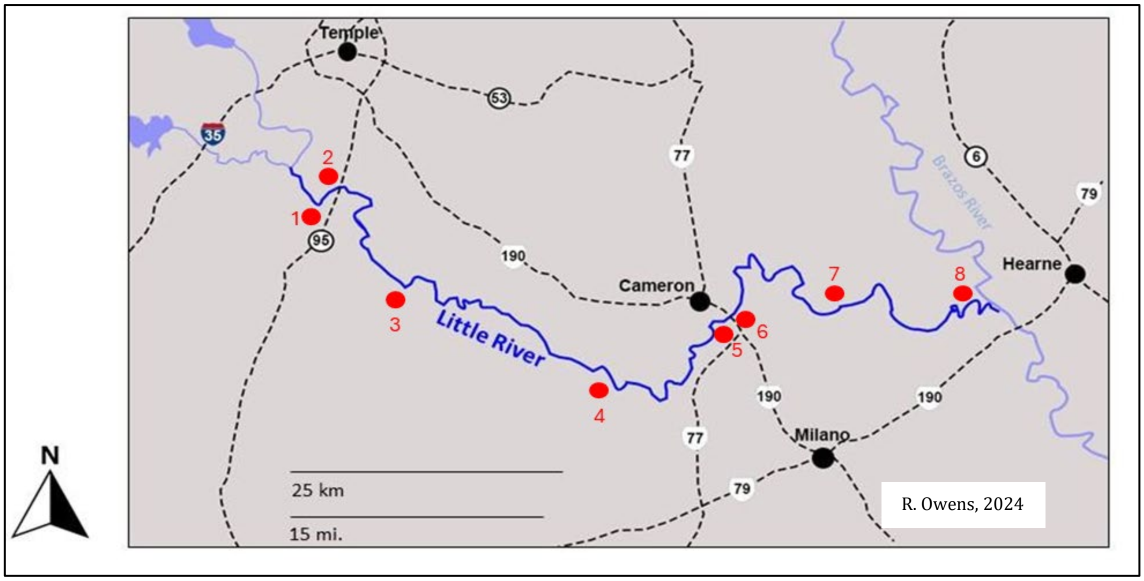

Figure 5-54. Location of oxbow lakes along the Little River.

The data for the eight oxbows assessed are presented in Table 5-4. Those with an assigned cutoff date of 1953 have a cutoff date that actually predates 1953, but no maps nor aerial photography are available for this region before that year. OL4 is an outlier, as this represents the chute cutoff. It has been included as a new oxbow lake, however, as it does represent a vast abandoned meander bend.

Table 5-4. Oxbow Lakes Near the Little River.

Oxbow	Coordinates	Cutoff date	Oxbow length (ft)	Meander length (ft)	Cutoff ratio
OL1	97°21’43” W 30°56’57” N	1953 [a]	2745.9	3678.11	0.75
OL2	97°21’20” W 30°57’46” N	1988	2407.8	471.23	5.11
OL3	97°16’24” W 30°51’51” N	1953 [a]	1540.5	1079.7	1.43
OL4	97°7’28” W 30°48’5” N	2018	37204.7	2517.77	4.50
OL5	96°57’29” W 30°49’42” N	1953 [a]	5811.2	251.64	23.09
OL6	96°56’58” W 30°49’54” N	2000	2133.9	594.22	3.59
OL7	96°50’53” W 30°50’53” N	2007	6060.5	1066.04	5.69
OL8	96°42’8” W 30°50’51” N	1953 [a]	6658.17	1463.18	4.55

[a] cutoff date predates 1953 but is assigned based on map/aerial photography available for the area.

6 Discussion

In this section, detailed discussion of the results of each objective are presented.

6.1 Meander Migration Analysis

A summary of qualitative assessment ratings, stream power values, and GIS-calculated migration rates are presented in Table 6-1.

Table 6-1. Summary of Qualitative Assessment Scores, Stream Power, and Migration Rate.

Segment	Average stream power (W/ft^2)	Qualitative stability score	Migration (ft) 2018-2022 calculated using GIS
1	43.4	49.4	102.0
2	39.5	42	48.6
3	32.5	40.2	49.6
4	29.2	38.4	42.7
5	24.8	21.2	22.1
6	26.6	40.4	50.9
7	26.9	38	50.0
8	30.7	27.4	31.5
9	47.0	47.6	34.4
10	49.6	33.8	37.6
11	53.4	40.4	50.0
12	59.5	40	64.0
13	72.7	47.2	1100
14	52.0	46.6	82.2
16	68.1	44	88.6
17	71.9	43.8	98.2
18	49.0	43.4	59.4
19	19.9	28	24.0
20	51.5	32.8	50.0
21	20.1	26.6	22.6
22	51.3	44.4	44.6
23	20.2	23.4	23.5
24	58.7	47.4	103
25	25.0	24	30.6
26	20.4	40.4	51.6
27	13.2	21.6	25.5
28	13.2	29	14.9
29	13.6	42.4	102

Qualitative assessment produced a positive correlation with GIS-enabled migration measurement (R^2=0.6) and is effective as a general assessment of a river channel's stability, particularly if it incorporates quantitative data such as stream power or shear stress ratios. It should be noted that the R^2 reported herein is based on the dataset from Table 5-3 but excludes the outlier segment 13. Segment 13 includes the chute cutoff that reduced the course of the Little River by approximately 4.6 mi (7.5 km) and has a migration polygon of over 600 ac (242.8 ha).

All segments with a qualitative assessment score less than 30 (n=6 segments) exhibited less than 32.8 ft (10 m) of migration during the years 2018-2022. Of the 15 segments with qualitative assessment scores of 40 or higher, all exhibited migration of 32.8 ft (10 m) of or more (Figure 6-1).

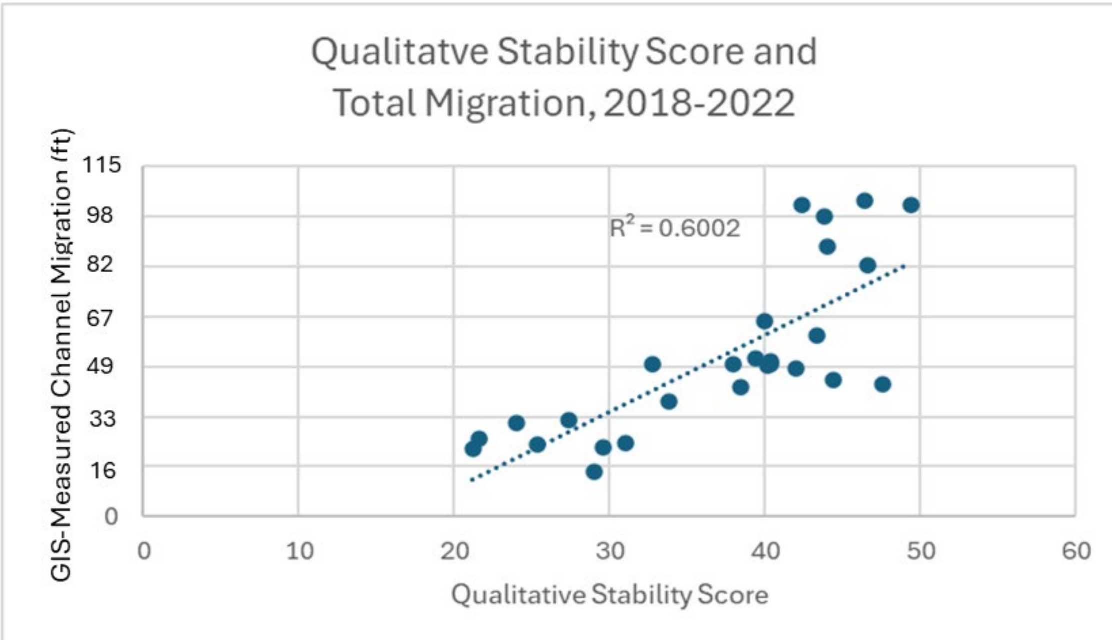

Figure 6-1. **Relationship of qualitative stability scores and GIS-calculated migration for the years 2018-2022.**

Stream power shows a positive correlation with migration (R^2=0.67), and is useful in determining the most unstable, thus rapidly migrating, channel bends (Figure 6-2).

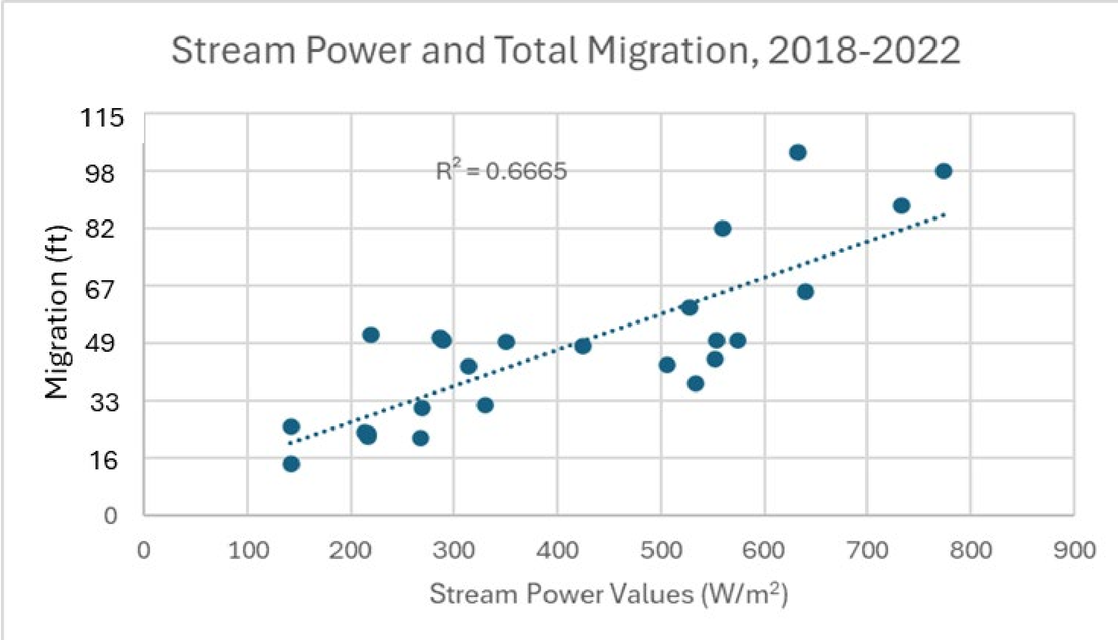

Figure 6-2. Relationship between stream power calculations and GIS-calculated migration totals for the years 2018-2022.

Comparison of the three methods of migration assessment indicates that the following segments of the Little River are experiencing the most significant channel migration, based upon remote sensing data from the year 2022 and field data from the year 2023:

1) Chute cutoff with endpoints at 30° 48' 5.04" N, 97° 7' 27.66" W and 30° 47' 38.76" N, 97° 5' 57.91". The cutoff has created a parcel of land approximately 618 ac (250 ha) in area which sits south of the new Little River channel and north of the former channel. This has the potential of causing frustration among landowners whose property boundaries are defined by the river channel. Based on remote sensing data, it is estimated that this cutoff was established in the year 2018.

2) Segment 24, with endpoints at 96°43'14.02"W, 30°50'34.08"N and 96°43'7"W, 30°51'N. This segment has migrated over 98.4 ft (30 m) since 2018, according to GIS analysis, and has an average stream power value of 58.71 W/ft^2 (632 W/m^2). Qualitative assessment also marked this stretch as unstable, with a score of 47.4. In this region, agriculture has cleared land cover to the channel's edge in some stretches. Even those stretches that have retained their original vegetative cover, however, are responding to channel adjustment.

3) Immediately after the confluence of the Leon and Lampasas rivers, the Little River flows through a wide meander that flows from southeast to southwest. This initial meander is rapidly advancing, having migrated approximately 101.7 ft (31 m) between the years 2018-2022 (Table 6-2). Its annual migration rate has increased since 2012:

Table 6-2. Increase in migration values at the first meander bend immediately after the confluence of the Leon and Lampasas rivers.

Years	Total migration (ft)	Annual migration rate (ft/yr)
1996-2004	30	3.7
2004-2012	44	5.4
2012-2018	122	20
2018-2022	102	26

4) A meander sequence southeast of Cameron, Texas, has exhibited regular migration historically. Aerial photography for this study area was available only to 1953, making migration assessment before the 1950s unfeasible. An oxbow located at 96°56'58" W, 30°49'54" N separated from the main channel as recently as the year 2000. Although migration has slowed since 2018, the stretch with endpoints at 96°57'55" W 30°49'57" N and 96°56'52"W 30°50'8" N exhibits an average stream power of 71.9 W/ft^2 (774 W/m^2) and a qualitative stability score of 43.8.
5) A meander sequence at the end of the Little River as it joins the Brazos River, beginning at approximately 96°43'27"W, 30°50'20"N, has exhibited progressively more active erosion since 1982, with the exception of the span from 2004-2012 (Table 11). The stream power values decrease from 64.47 W/ft^2 to 13.47 W/ft^2 (694 W/m^2 to 145 W/m^2) as the Little River approaches the Brazos River, with an average stream power over the entire stretch of 40.32 W/ft^2 (434 W/m^2).

Table 6-3. Increasing migration values near the confluence of the Little River and the Brazos River.

Years	Total migration (ft)	Annual migration rate (ft/yr)
1982-1996	66	4.7
1996-2004	60	7.6
2004-2012	28	3.5
2012-2018	76	12.8
2018-2022	50	12.5

The most dramatic change on the Little River since 2018 has been the formation of a chute cutoff with endpoints at 30° 48' 5.04" N, 97° 7' 27.66" W and 30° 47' 38.76" N, 97° 5' 57.91". The cutoff has created a parcel of land approximately 618 ac (250 ha) in area which sits south of the new Little River channel and north of the former channel. Before this cutoff formed, the most actively meandering portion of the channel was the region east of the transition from Cretaceous-aged limestone bedrock to Eocene-aged sandstone, roughly in the region of Buckholts, Texas. The most rapidly migrating meanders, with the exception of the chute cutoff, are those upon which vegetation has been cleared to the channel's edge for agricultural use.

The changes in migration patterns are portrayed through wavelet analysis in MStaT, as well. Most of the changes from 2018-2022 occurred 24.8-43.5 mi (40-70 km) downstream of the headwaters of the Little River, in the region of the chute cutoff. Prior to this cutoff, the 2012-2018 wavelet analysis identifies migration near the river's confluence with the Brazos River. The most rapid migration occurred over a shorter segment of the river but with slightly higher power levels.

Trends in migration have changed in response to land cover alteration and as cascading responses to prior change. When the channel is considered as a series of individual meanders, the most rapidly-migrating meanders are those on which the native vegetation has been cleared to the channel's edge.

6.2 Oxbow Development

Eight current or recent oxbow lakes were assessed in the Little River watershed, and four of the eight have formed since the mid-1980s. This is not an exhaustive list of oxbow lakes, but those recent ones found closest to the main channel. Of those most recent four, flow rate has been high enough to reconnect the oxbow to the main channel 3-489 times since 2008. Connection flows and the number of days of connection since initial separation are correlated (R^2 = 0.91) and in this region, can be predicted using the equation:

(Number of days of connection) = 5E + 9*(Connection flow in cms)$^{-3.233}$ Eq. 12

A strong correlation (R^2 = 0.69) was also established between the cutoff ratio and the sedimentation rate of each oxbow lake. This relationship is defined by the equation:

(Sedimentation rate in m/yr) = .0403*(Cutoff ratio)^2 + .0742*(Cutoff ratio) - .0063 Eq. 13

Elevation data from the main channel and the upstream end of each oxbow lake were obtained from DEMs through Google Earth®. Comparison of these elevation values over the existence of the oxbow lake provided the sedimentation rate in feet per year (ft/yr). Connection flow, or the discharge value required to reconnect the oxbow lake with its former channel, was calculated from Equation 11.

Daily discharge data from the United States Geological Survey (USGS) from nearest stream gages to each oxbow for the years 2000-2024 were collected to determine how often connection flow was achieved during that time span to provide the number of days of connection since the year 2000. These data are presented in Table 6-4. As the modern river channel has migrated over the upstream portion of OL8, elevation data could not be obtained and thus sedimentation rate could not be calculated.

Table 6-4. Hydrologic Data of Oxbow Lakes along the Little River since the year 2000

Oxbow	Coordinates	Cutoff Date	Sed. rate (ft/yr)	Number of days of connection since 2000	C. flow (cfs) [a]	Diversion angle (°)	Distance to channel (ft)	Lake area (ac)
OL1	97°21’43” W 30°56’57” N	1953 [b]	0.52	1	29000	139	2700	21
OL2	97°21’20” W 30°57’46” N	1988	6.56	532	4500	125	1300	4.8
OL3	97°16’24” W 30°51’51” N	1953 [b]	0.46	1	31000	170	880	4.5
OL4	97°7’28” W 30°48’5” N	2018	4.98	258	6200	138	1300	85
OL5	96°57’29” W 30°49’42” N	1953 [b]	0.22	1	48000	88	1700	12
OL6	96°56’58” W 30°49’54” N	2000	0.88	15	21000	149	2400	11
OL7	96°50’53” W 30°50’53” N	2007	4	118	7700	113	1800	39
OL8	96°42’8” W 30°50’51” N	1953 [b]	-	-	-	116	1300	1

[a] C. Flow is the connection flow in cubic feet per second
[b] cutoff date predates 1953 but is assigned based on map/aerial photography available for the area.
Sed. rate = sedimentation rate

Data were grouped into four-year increments for further analysis of reconnections (Table 6-5). Because some data for 2007 were missing and the year 2024 is not yet complete, data from 2008-2023 were compiled for the incremental analysis. OL8 is not included in the incremental analysis because the connection flow cannot be calculated.

Table 6-5. Number of Days of Connection to the Main Channel in Each Time Interval.

Oxbow	Coordinates	C. flow (cfs) [a]	2008-2011	2012-2015	2016-2019	2020-2023	Total
OL1	97°21’43” W 30°56’57” N	29000	0	0	0	0	0
OL2	97°21’20” W 30°57’46” N	4500	73	83	293	40	489
OL3	97°16’24” W 30°51’51” N	31000	0	0	0	0	0
OL4	97°7’28” W 30°48’5” N	6200	55	32	146	16	249
OL5	96°57’29” W 30°49’42” N	48000	0	0	0	0	0
OL6	96°56’58” W 30°49’54” N	21000	1	6	0	8	15
OL7	96°50’53” W 30°50’53” N	7700	34	10	71	0	115

[a] C. Flow is the connection flow in cubic feet per second

Several analyses of these data are presented in the following graphs. A strong (R^2 = 0.9) correlation was found between flood flows (connection flows) and the number of days of connection since 2000, with lower flood flows (connection flows) corresponding with more frequent connections (Figure 6-3).

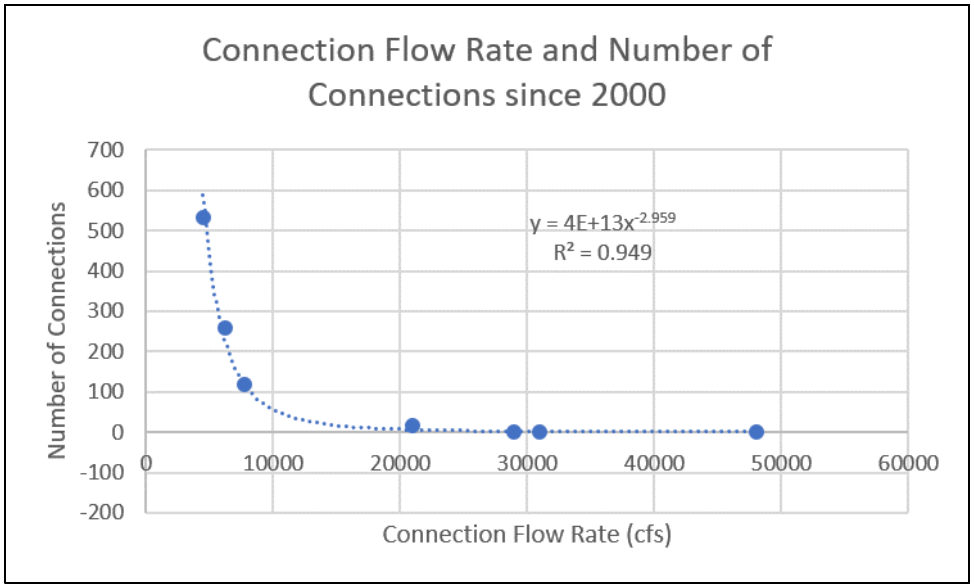

Figure 6-3. **Relationship between connection flow and the number of days of connection since 2000. (Number of Connections = Number of Days of Connection).**

A strong (R^2 = 0.7) correlation was also found between the sedimentation rate and cutoff ratio of oxbow lakes in the region (Figure 6-4).

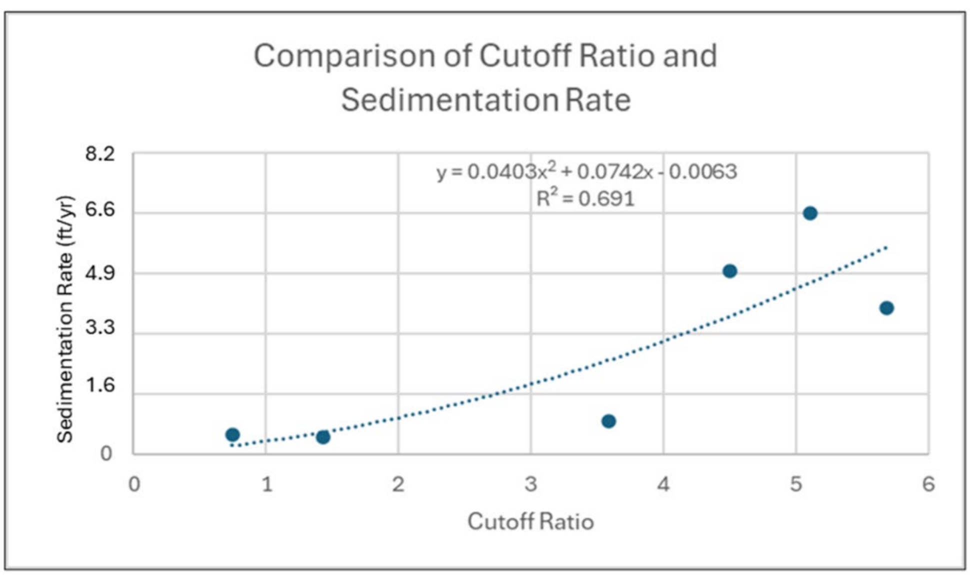

Figure 6-4. **Comparison of cutoff ratio and sedimentation rate for oxbow lakes on the Little River.**

There were not strong correlations between sedimentation rates and distance to the main channel ($R^2 = 0.2$) or sedimentation rates and lake area ($R^2 = 0.2$). These relationships are presented in Figures 6-5-6-7.

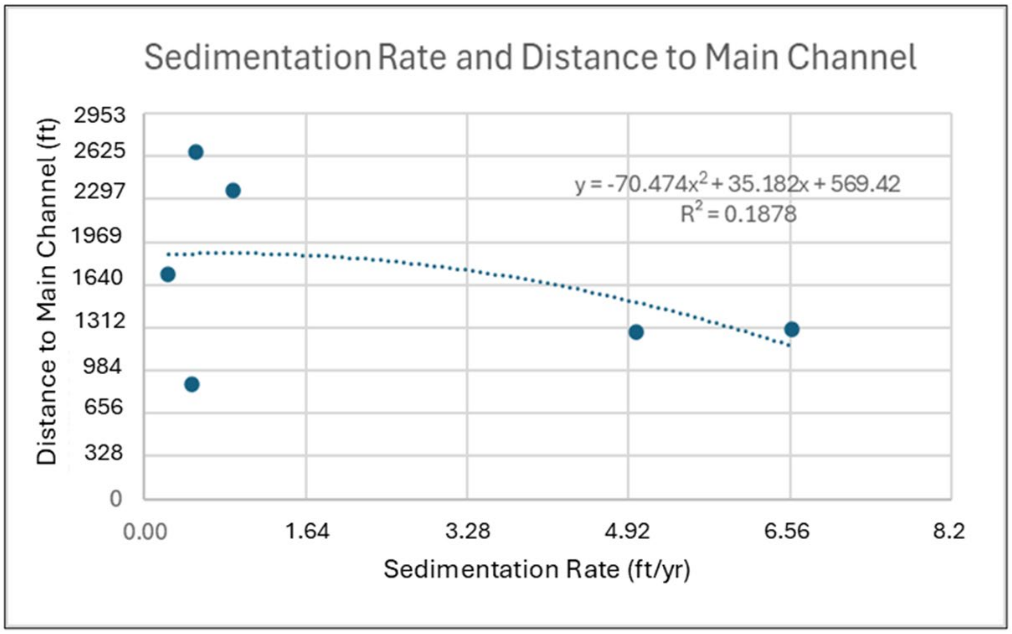

Figure 6-5. **Relationship of sedimentation rate and distance to the main channel for oxbow lakes on the Little River.**

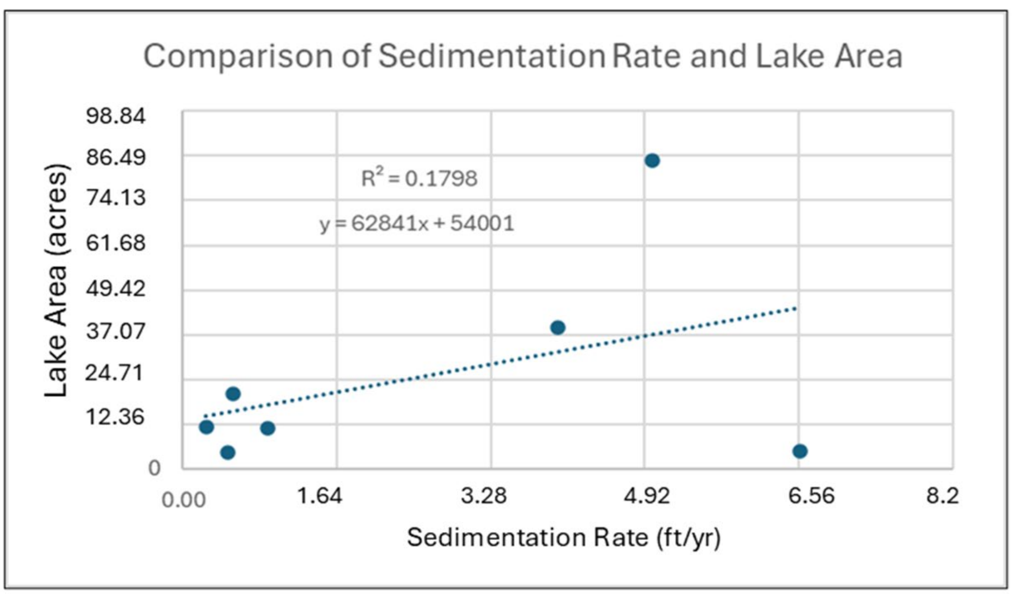

Figure 6-6. **Relationship of sedimentation rate and lake area for oxbow lakes on the Little River.**

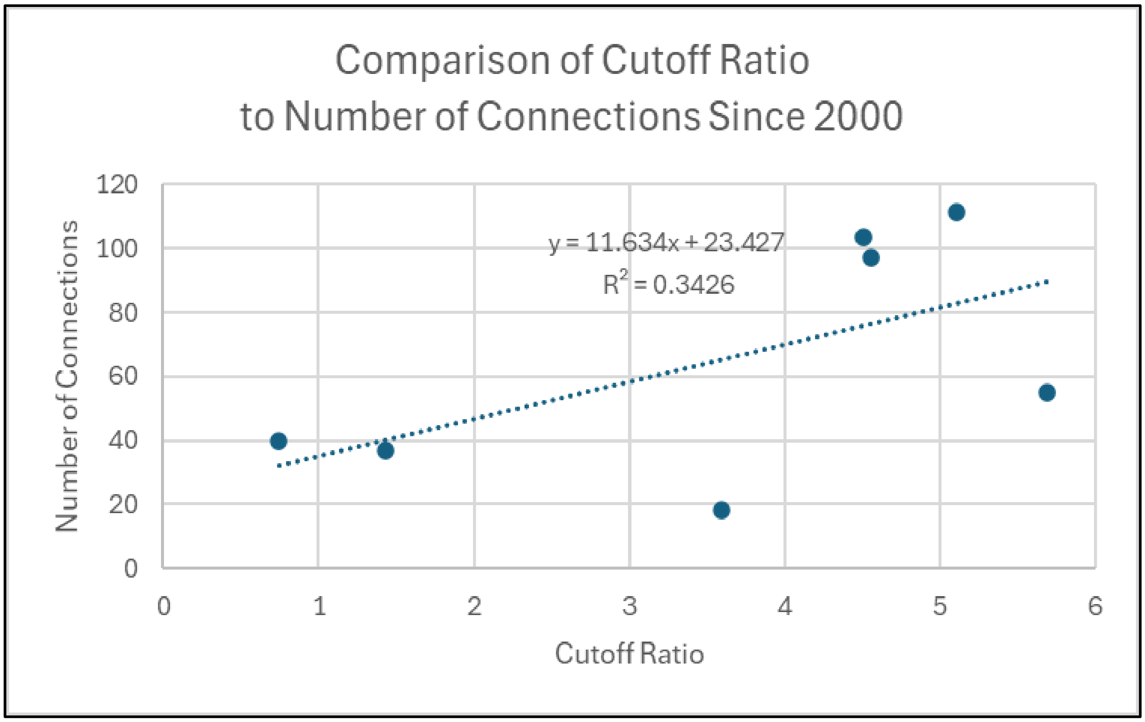

Figure 6-7. **Relationship of cutoff ratio and number of days of connection to the main channel for oxbow lakes on the Little River. (Number of Connections = Number of Days of Connection.)**

6.3 LiDAR Collection

LiDAR imagery in the form of DEMs and raw point cloud data are provided to the Texas Water Development Board through Dropbox. LiDAR scans using the 3D Scanner App effectively showed erosional gully formation in the vicinity of bridge support columns, especially when viewed in a color ramp with discrete boundaries. It is recommended to collect data of erosion around bridge support columns in late summer when the water is lowest, thus exposing more of the bank. Upper levels of banks, however, are best assessed during winter when less vegetation is present and risk of technology overheating is much lower. Separate scans of adjacent regions can be easily merged in CloudCompare if proper care has been taken to include location markers in the scans. CloudCompare will easily merge georeferenced point clouds automatically after manual alignment brings them sufficiently close.

7 Conclusion

This study addressed rates of channel migration influenced by varying flow regimes of the Little River from its headwaters at the confluence of the Leon and Lampasas rivers southeast of Belton, Texas, to its confluence with the Brazos River southwest of Hearne, Texas. The project assessed meander migration rates and patterns, river-bank stability, and landscape ecological factors associated with river-bank stability for the length of the river. The specific objectives of this project were:

1) Calculate rates of meander migration along selected reaches of the Little River and correlate these values with varying discharges.
2) Determine the mechanism of channel migration at temporal intervals (i.e., 1950s, 1960s, to 2020.) for each selected reach.
3) Categorize channel banks for erosion occurrence/potential by examining hydrologic shear stress, bank structure, associated flow, landscape ecological patterns, and sediment category along banks.
4) Compile LiDAR Imagery of the Little River Drainage Basin for management use
5) Quantify rates of planform oxbow development.
6) Quantify rates of meander cutoff for selected sites along the Little River.
7) Categorize oxbows and meander scrolls based on morphologic and hydrologic properties.

The Little River experienced migration every 1.24-2.49 mi (2-4 km) in the stretch ~13-~31 mi (20-50 km) from its headwaters. Most of the most rapidly migrating meanders occur west of Cameron, Texas, where the geology changes from Cretaceous-aged limestone to Paleocene—and Eocene-aged sandstones and mudstones. Using GIS, ten meander bends exhibiting the highest rates of migration during the years 1953-2022 were identified, eight of these meander bends occurred to the west of Cameron.

Channel erosion is most prominent where natural vegetation has been cleared for agriculture and has produced large woody debris (LWD) in the more actively migrating meander bends, including jams. As of summer of 2023, in fact, a significant log jam begins at 30° 46' 54.00" N, 97° 3' 56.34" W, and completely blocks the channel for approximately ~232.9 ft (71 m).

A chute cutoff with endpoints at 30° 48' 5.04" N, 97° 7' 27.66" W and 30° 47' 38.76" N, 97° 5' 57.91" has created a parcel of land, ~ 618 ac (~250 ha) in area, which sits south of the new Little River channel and north of the former channel. This has the potential to cause frustration among landowners whose property boundaries are defined by the river channel. The new channel was a small creek until 2011, based on remote imagery, at which time it became comparable to the former channel. By 2015, significant sedimentation began to create a plug separating the old channel from the new. As of 2023, the old channel has been plugged, and the cutoff is the main river channel.

Aerial LiDAR imagery at ~3.3 ft (1 m) resolution is available for most of the Little River except for its headwaters through the United States Geological Survey National Map Viewer. Aerial LiDAR imagery at ~33 ft (10 m) resolution is available for the entire Little River watershed through the United States Geological Survey National Map Viewer. Ground LiDAR imagery was compiled in this study at specific points of interest along the channel. These points of interest included overpasses and some rapidly migrating meander bends. All LiDAR imagery is provided through Dropbox.

The Little River is an actively meandering river typical of rivers in this region. Human activity has exacerbated erosion and increased migration rates, however, where extensive agriculture has modified the riparian zone adjacent to the channel. This has led to rapid erosion and cutoff of some meander bends and buildup of woody material in the channel, creating frequent and often significant log jams. This presents a series of cascading effects upstream and downstream in the channel, as water is slowed upstream of the jams and produces in-stream bars, and flow is temporarily reduced downstream. Bedrock geology also plays a role in migration rates, as many rapidly-migrating bends occur past the transition from Cretaceous-aged limestone to early Cenozoic sandstones. Vegetative cover is an effective defense, however, against accelerated erosion and, thus, against the cascading effects to the channel system.

Future studies should continue building a LiDAR database of imagery for the most rapidly eroding meanders in this channel, utilizing georeferenced field markers as reference points. Given the rapid erosion of some meanders, field scans could realistically be taken each year (winter is advisable) to monitor erosion rates, especially in regions where agriculture has cleared native vegetation to the edge of the channel.

The abundance of woody debris and prevalence of log jams also presents an interesting biogeomorphological research opportunity. An inventory of woody debris should be taken and compared to channel migration rates and sedimentation rates within the channel. Similarly, an inventory of channel-spanning or nearly channel-spanning log jams could be taken and compared to sinuosity of the river channel, flow rates, and erosion rates.

From a biological perspective, the impact of these log jams on the fluvial ecosystem would be an interesting research opportunity. Limited public access to the Little River contributes to abundant wildlife on its course, both aquatic and terrestrial. As log jams alter the flow of water and rate of sedimentation, it is reasonable to assume that novel aquatic communities are developing in their midst.

The equations utilized in this report for connecting flow of oxbow lakes were developed by Giardino and Lee (2012), based upon study of 17 oxbow lakes along the Brazos River. Future research could be centered on refining and improving the accuracy and applicability of these equations by assessing more oxbow lakes on different rivers in various physiographic or geologic settings and incorporating these new data into the current body of knowledge. The methods described by Giardino and Lee (2012) could be repeated with relative ease on other rivers, such as the Little River, and the equations reassessed and altered, as needed based on these data.

8 Acknowledgements

The authors sincerely thank Mike Owens for his assistance in gathering field data and Joe Prather for his assistance shuttling between many take-outs and put-ins.

The authors are grateful to Benjamin Bayless of Tyler Junior College and Luna Yang of the Texas Water Resources Institute for their advice regarding GIS methodology and stream power calculations used in this work.

9 References

Abbe, T. B., & Montgomery, D. R. (1996). Large woody debris jams, channel hydraulics and habitat formation in large rivers. Regulated Rivers: research & management, 12(2-3), 201-221.

Abbe, T. B., & Montgomery, D. R. (2003). Patterns and processes of wood debris accumulation in the Queets river basin, Washington. Geomorphology, 51(1-3), 81-107.

Abernethy, B., & Rutherfurd, I. D. (1998). Where along a river's length will vegetation most effectively stabilise stream banks? Geomorphology, 23(1), 55-75.

Alho, P., Vaaja, M., Kukko, A., Kasvi, E., Kurkela, M., Hyyppä, J., Hyyppä, H. & Kaartinen, H. (2011). Mobile laser scanning in fluvial geomorphology: Mapping and change detection of point bars. Zeitschrift fur Geomorphologie-Supplementband, 55(2), 31.

Ali, M., Sterk, G., Seeger, M., Boersema, M., & Peters, P. (2012). Effect of hydraulic parameters on sediment transport capacity in overland flow over erodible beds. Hydrology and Earth System Sciences, 16(2), 591-601.

Allen, G. H., Barnes, J. B., Pavelsky, T. M., & Kirby, E. (2013). Lithologic and tectonic controls on bedrock channel form at the northwest Himalayan front. Journal of Geophysical Research: Earth Surface, 118(3), 1806-1825.

Asquith, W.H., and Thompson, D.B. (2008). Alternative regression equations for estimation of annual peak streamflow frequency for undeveloped watersheds in Texas using PRESS minimization: U.S. Geological Survey Scientific Investigations Report 2008–5084, 40 p. https://doi.org/10.3133/sir20085084.

Baas, A. C. (2006). Wavelet power spectra of aeolian sand transport by boundary layer turbulence. Geophysical Research Letters, 33(5).

Bagnold, R. A. (1980). An empirical correlation of bedload transport rates in flumes and natural rivers. Proceedings of the Royal Society of London. A. Mathematical and Physical Sciences, 372(1751), 453-473.

Bagnold, R.A. (1966). An approach to the sediment transport problem from general physics: US Geological Survey, Professional Paper 422.

Bizzi, S., & Lerner, D. N. (2015). The use of stream power as an indicator of channel sensitivity to erosion and deposition processes. River research and applications, 31(1), 16-27.

Bobrowski, R., Winczek, M., Zięba-Kulawik, K., & Wężyk, P. (2023). Best practices to use the iPad Pro LiDAR for some procedures of data acquisition in the urban forest. Urban Forestry & Urban Greening, 79, 127815.

Brice, J. C. (1982). Stream channel stability assessment (No. FHWA/RD-82/021). United States. Federal Highway Administration.

Brookes, A. (1987). River channel adjustments downstream from channelization works in England and Wales. *Earth Surface Processes and Landforms*, *12*(4), 337-351.

Camporeale, C., Perona, P., Porporato, A., & Ridolfi, L. (2005). On the long-term behavior of meandering rivers. Water resources research, 41(12).

Candel, J. H., Kleinhans, M. G., Makaske, B., Hoek, W. Z., Quik, C., & Wallinga, J. (2018). Late

Holocene channel pattern change from laterally stable to meandering–a palaeohydrological reconstruction. Earth Surface Dynamics, 6(3), 723-741.

Cawthon, T. (2007). Log Jam Characterization, Distribution, and Stability on the San Antonio River, Texas. (Doctoral dissertation).

Chen, G., & Zhang, H. (2023). Wavelets in geosciences. In *Encyclopedia of Mathematical geosciences* (pp. 1626-1636). Cham: Springer International Publishing.

Chong, K. L., Lai, S. H., & El-Shafie, A. (2019). Wavelet transform based method for river stream flow time series frequency analysis and assessment in tropical environment. Water Resources Management, 33, 2015-2032.

Coco, G., Bryan, K. R., Green, M. O., Ruessink, B. G., van Enckevort, I. M. J., & Turner, I. L. (2005, January). Video observations of shoreline and sandbar coupled dynamics. In Coasts and Ports 2005: Coastal Living-Living Coast; Australasian Conference; Proceedings (pp. 471-476). Barton, ACT: Institution of Engineers, Australia.

Curran, J. C. (2010). Mobility of large woody debris (LWD) jams in a low gradient channel. Geomorphology, 116(3-4), 320-329.

Curtis, J. A., & Whitney, J. W. (2003). Geomorphic and hydrologic assessment of erosion hazards at the Norman Municipal Landfill, Canadian River floodplain, central Oklahoma. Environmental & Engineering Geoscience, 9(3), 241-253.

Dane, C. H., & Stephenson, L. W. (1928). Notes on the Taylor and Navarro Formations in east-central Texas. AAPG Bulletin, 12(1), 41-58.

Doyle, M. W., Harbor, J. M., Rich, C. F., & Spacie, A. (2000). Examining the effects of urbanization on streams using indicators of geomorphic stability. Physical geography, 21(2), 155-181.

Dutnell, R. C. (2000). Development of bankfull discharge and channel geometry relationships for natural channel design in Oklahoma using a fluvial geomorphic approach (Doctoral dissertation, University of Oklahoma).

Ferguson, R. I. (1975). Meander irregularity and wavelength estimation. Journal of Hydrology, 26(3-4), 315-333.

Finlayson, D. P., & Montgomery, D. R. (2003). Modeling large-scale fluvial erosion in geographic information systems. Geomorphology, 53(1-2), 147-164.

Fischenich, J. C. (2001). Stability thresholds for stream restoration materials (p. 10). US Army Engineer Research and Development Center [Environmental Laboratory].

Fonstad, M. A. (2003). Spatial variation in the power of mountain streams in the Sangre de Cristo Mountains, New Mexico. Geomorphology, 55(1-4), 75-96.

Gao, P., & Li, Z. (2024). Exploring meandering river cutoffs. Geological Society, London, Special Publications, 540(1), SP540-2022.

Gartner, J. (2016). Stream power: origins, geomorphic applications, and GIS procedures. Water Publications. 1. University of Massachusetts Amherst. Retrieved from https://scholarworks.umass.edu/entities/publication/e26f6228-3b61-42cc-878c-f715a5669643

Gartner, J. D., Dade, W. B., Renshaw, C. E., Magilligan, F. J., & Buraas, E. M. (2015). Gradients in stream power influence lateral and downstream sediment flux in floods. Geology, 43(11), 983-986.

Gautier, E., Brunstein, D., Vauchel, P., Roulet, M., Fuertes, O., Guyot, J. L., Darozzes, J. and Bourrel, L. (2007). Temporal relations between meander deformation, water discharge and sediment fluxes in the floodplain of the Rio Beni (Bolivian Amazonia). *Earth Surface Processes and Landforms*, *32*(2), 230-248.

Giardino, J. R., & Lee, A. A. (2012). Evolution of oxbow lakes along the Brazos River. Texas Water Development Board. Contract Number 0904830969, 27 p.

Giardino, J. R., & Rowley, T. (2016). Evaluating channel migration of the lower Guadalupe River: Seguin, TX, to the San Antonio River confluence. Texas Water Development Board. Contract Number 1548311790, 117 p.

Gollob, C., Ritter, T., Kraßnitzer, R., Tockner, A., & Nothdurft, A. (2021). Measurement of forest inventory parameters with Apple iPad pro and integrated LiDAR technology. Remote Sensing, 13(16), 3129.

Govers, G. (1992). Relationship between discharge, velocity and flow area for rills eroding loose, non-layered materials. Earth surface processes and landforms, 17(5), 515-528.

Govers, G., & Rauws, G. (1986). Transporting capacity of overland flow on plane and on irregular beds. Earth surface processes and landforms, 11(5), 515-524.

Graf, W. L. (1983). Downstream changes in stream power in the Henry Mountains, Utah. Annals of the Association of American Geographers, 73(3), 373-387.

Grenfell, M., Aalto, R., & Nicholas, A. (2012). Chute channel dynamics in large, sand-bed meandering rivers. Earth Surface Processes and Landforms, 37(3), 315-331.

Griffith, G. E., Bryce, S., Omernik, J., & Rogers, A. (2004). Ecoregions of Texas. Reston, Virginia, USA: US Geological Survey.

Güneralp, I., & Marston, R. A. (2012). Process–form linkages in meander morphodynamics: Bridging theoretical modeling and real world complexity. Progress in Physical Geography, 36(6), 718-746.

Güneralp, I., & Rhoads, B. L. (2009). Planform change and stream power in the Kishwaukee River watershed, Illinois: geomorphic assessment for environmental management. Management and Restoration of Fluvial Systems With Broad Historical Changes and Human Impacts: Geological Society of America Special Paper, 451, 109-118.

Güneralp, I., & Rhoads, B. L. (2011). Influence of floodplain erosional heterogeneity on planform complexity of meandering rivers. Geophysical Research Letters, 38(14).

Guo, X., Gao, P., & Li, Z. (2021). Morphological characteristics and changes of two meandering rivers in the Qinghai-Tibet Plateau, China. Geomorphology, 379, 107626.

Guo, X., Gao, P., & Li, Z. (2023). Hydrologic connectivity and morphologic variation of oxbow lakes in a pristine alpine fluvial system. Journal of Hydrology, 623, 129768.

Gurnell, A. M., Piégay, H., Swanson, F. J., & Gregory, S. V. (2002). Large wood and fluvial processes. Freshwater biology, 47(4), 601-619.

Gutierrez, R. R., & Abad, J. D. (2014). On the analysis of the medium term planform dynamics of meandering rivers. Water Resources Research, 50(5), 3714-3733.

Hickin, E. J. (1974). The development of meanders in natural river-channels. American journal of science, 274(4), 414-442.

Hickin, E. J., & Nanson, G. C. (1984). Lateral migration rates of river bends. Journal of hydraulic engineering, 110(11), 1557-1567.

Hodgetts, D. (2009). LiDAR in the environmental sciences: geological applications. *Laser scanning for the environmental sciences*, 165-179.

Hooke, J. M. (1995). River channel adjustment to meander cutoffs on the River Bollin and River Dane, northwest England. Geomorphology, 14(3), 235-253.

Hooke, J. M. (2007). Spatial variability, mechanisms and propagation of change in an active meandering river. Geomorphology, 84(3-4), 277-296.

Jain, V., Preston, N., Fryirs, K., & Brierley, G. (2006). Comparative assessment of three approaches for deriving stream power plots along long profiles in the upper Hunter River catchment, New South Wales, Australia. Geomorphology, *74*(1-4), 297-317.

Jha, M. K., Asamen, D. M., Allen, P. M., Arnold, J. G., & White, M. J. (2022). Assessing streambed stability using D50-based stream power across contiguous US. Water, 14(22), 3646.

Johnson, P. A., Gleason, G. L., & Hey, R. D. (1999). Rapid assessment of channel stability in vicinity of road crossing. Journal of Hydraulic Engineering, 125(6), 645-651.

Julian, J. P., Thomas, R. E., Moursi, S., Hoagland, B. W., & Tarhule, A. (2012). Historical variability and feedbacks among land cover, stream power, and channel geometry along the lower Canadian River floodplain in Oklahoma. Earth Surface Processes and Landforms, 37(4), 449-458.

Julien, P.Y. (2002) River Mechanics. Cambridge University Press, 434p

Karimova, L., Kuandykov, Y., Makarenko, N., Novak, M. M., & Helama, S. (2007). Fractal and topological dynamics for the analysis of paleoclimatic records. Physica A: Statistical Mechanics and its Applications, 373, 737-746.

Keller, E. A., & Swanson, F. J. (1979). Effects of large organic material on channel form and fluvial processes. Earth Surface Processes 4 (4): 361–380.

Knighton, A. D. (1999). Downstream variation in stream power. Geomorphology, 29(3-4), 293-306.

Lagasse, P. F., Zevenbergen, L. W., Spitz, W., & Arneson, L. A. (2012). Stream stability at highway structures (No. FHWA-HIF-12-004). United States. Federal Highway Administration. Office of Bridge Technology.

Lecce, S. A. (1997). Nonlinear downstream changes in stream power on Wisconsin's Blue River. Annals of the Association of American Geographers, 87(3), 471-486.

Li, Y., Lark, M., & Reeve, D. (2005). Multi-scale variability of beach profiles at Duck: A wavelet analysis. Coastal Engineering, 52(12), 1133-1153.

Liu, X., Zhang, Z., Peterson, J., & Chandra, S. (2007). LiDAR-derived high quality ground control information and DEM for image orthorectification. *GeoInformatica*, *11*, 37-53.

Liu, Y., San Liang, X., & Weisberg, R. H. (2007). Rectification of the bias in the wavelet power spectrum. Journal of Atmospheric and Oceanic Technology, 24(12), 2093-2102.

Lombardo, U. (2017). River logjams cause frequent large-scale forest die-off events in southwestern Amazonia. Earth System Dynamics, 8(3), 565-575.

Luetzenburg, G., Kroon, A., & Bjørk, A. A. (2021). Evaluation of the Apple iPhone 12 Pro LiDAR for an Application in Geosciences. Scientific Reports, 11.

Magilligan, F. J. (1992). Thresholds and the spatial variability of flood power during extreme floods. Geomorphology, 5(3-5), 373-390.

Mokroš, M., Mikita, T., Singh, A., Tomaštík, J., Chudá, J., Wężyk, P., ... & Liang, X. (2021). Novel low-cost mobile mapping systems for forest inventories as terrestrial laser scanning alternatives. International Journal of Applied Earth Observation and Geoinformation, 104, 102512.

Montgomery, D. R., Collins, B. D., Buffington, J. M., & Abbe, T. B. (2003). Geomorphic effects of wood in rivers. In American Fisheries Society Symposium (Vol. 37, pp. 21-47).

Morét, S. L. (1997). An assessment of a Stream Reach Inventory and Channel Stability Evaluation: predicting and detecting flood-induced change in channel stability.

Mount, N. J., Tate, N. J., Sarker, M. H., & Thorne, C. R. (2013). Evolutionary, multi-scale analysis of river bank line retreat using continuous wavelet transforms: Jamuna River, Bangladesh. Geomorphology, 183, 82-95.

Nanson, G. C., & Hickin, E. J. (1983). Channel migration and incision on the Beatton River. Journal of Hydraulic Engineering, 109(3), 327-337.

NOAA. National Weather Service Climate Data. National Weather Service website, https://www.weather.gov/wrh/climate. Accessed on 8/15/24.

Owens, R. (2020). The Effects of Urbanization on Channel Morphology of Rivers in Texas (Doctoral dissertation). Texas A&M University.

Parker, C., Thorne, C. R., & Clifford, N. J. (2014). Development of ST: REAM: a reach-based stream power balance approach for predicting alluvial river channel adjustment. Earth Surface Processes and Landforms, 40(3), 403-413.

Pfankuch, D. J. (1978). Stream reach inventory and channel stability evaluation. Rep., U.S. Department of Agriculture, Forest Service, Northern Region.

Phillips, J. D. (1989). Fluvial sediment storage in wetlands 1. JAWRA Journal of the American Water Resources Association, 25(4), 867-873.

Phillips, J. D., & Slattery, M. C. (2007). Downstream trends in discharge, slope, and stream power in a lower coastal plain river. Journal of Hydrology, 334(1-2), 290-303.

Phillips, J.D., 2013. Flow modifications and Geomorphic Thresholds in the lower Brazos River. Austin: Texas Instream Flow Program, Report No. 1248311367.

Post Oak Savannah. (n.d.) Texas Parks and Wildlife. Retrieved from https://tpwd.texas.gov/wildlife/wildlife-diversity/wildscapes/wildscapes-plant-guidance-by-ecoregion/post-oak-savannah/

Reinfelds, I., Cohen, T., Batten, P., & Brierley, G. (2004). Assessment of downstream trends in channel gradient, total and specific stream power: a GIS approach. Geomorphology, 60(3-4), 403-416.

Rosgen, D. L. (2001, March). A stream channel stability assessment methodology. In Proceedings of the seventh federal interagency sedimentation conference (Vol. 2).

Ruben, L. D., Naito, K., Gutierrez, R. R., Szupiany, R., & Abad, J. D. (2021). Meander Statistics Toolbox (MStaT): A toolbox for geometry characterization of bends in large meandering channels. SoftwareX, 14, 100674.

Ruessink, B. G., Coco, G., Ranasinghe, R., & Turner, I. L. (2007). Coupled and noncoupled behavior of three-dimensional morphological patterns in a double sandbar system. Journal of Geophysical Research: Oceans, 112(C7).

Short, A. D., & Trembanis, A. C. (2004). Decadal scale patterns in beach oscillation and rotation

Narrabeen Beach, Australia—time series, PCA and wavelet analysis. Journal of Coastal Research, 20(2), 523-532.

Słowik, M. (2016). The influence of meander bend evolution on the formation of multiple cutoffs: findings inferred from floodplain architecture and bend geometry. Earth Surface Processes and Landforms, 41(5), 626-641.

Stacey, M., & Rutherfurd, I. (2007, May). Testing specific stream power thresholds of channel stability with GIS. In 5th Annual Australian Stream Management Conference, Albury, Australia (pp. 384-389).

Sturm, T. W. (2001). Open channel hydraulics (Vol. 1, p. 1). New York: McGraw-Hill.

Tebbens, S. F., Burroughs, S. M., & Nelson, E. E. (2002). Wavelet analysis of shoreline change on the Outer Banks of North Carolina: An example of complexity in the marine sciences. Proceedings of the National Academy of Sciences, 99(suppl_1), 2554-2560.

Texas Water Development Board (2012). Water for Texas: 2012 State Water Plan.

Thompson, B. C. (2011). Post Oak Savanna in Transition: Juniper Encroachment and Climate Change Alter Grassland Soil Respiration (Doctoral dissertation, Texas A & M University).

Thorne, C. R., Allen, R. G., & Simon, A. (1996). Geomorphological river channel reconnaissance for river analysis, engineering and management. Transactions of the Institute of British Geographers, 469-483.

Timm, D. (2016). Identifying critical source areas for best management practice targeting in impaired Zumbro River watersheds using digital terrain analysis. Retrieved from the University Digital Conservancy, https://hdl.handle.net/11299/185105

Timm,D., Klang, J., Wilson, G. (2014). Zumbro River Watershed Restoration Prioritization & Sediment Reduction Project. Digital Terrain Analysis Technical Manual.

Turnipseed, C. (2017). Characterizing the hydrodynamics of a meandering river neck cutoff. Louisiana State University and Agricultural & Mechanical College.

USGS, 20211103, USGS 1/3 Arc Second n31w098 20211103: U.S. Geological Survey.

USGS, 20211103, USGS 1/3 Arc Second n32w097 20211103: U.S. Geological Survey.

USGS, 20211103, USGS 1/3 Arc Second n32w098 20211103: U.S. Geological Survey.

USGS, 20240229, USGS 1/3 Arc Second n31w097 20240229: U.S. Geological Survey.

USGS. (2007) Geologic Database of Texas. USGS. https://webapps.usgs.gov/txgeology/

Van Gerven, L. P. A., & Hoitink, A. J. F. (2009). A new method to analyze the geometry of a river: Wavelet analysis on the curvature series. Application to the Mahakam River indicates geometric zoning.

Volder, A., Briske, D. D., & Tjoelker, M. G. (2013). Climate warming and precipitation redistribution modify tree–grass interactions and tree species establishment in a warm-temperate savanna. Global Change Biology, 19(3), 843-857.

Wallerstein, N., & Thorne, C. R. (1996). Impacts of woody debris on fluvial processes and channel morphology in stable and unstable streams (p. 0115). US Army Research Development & Standardization Group.

Whipple, K. X., & Tucker, G. E. (1999). Dynamics of the stream-power river incision model: Implications for height limits of mountain ranges, landscape response timescales, and research needs. Journal of Geophysical Research: Solid Earth, 104(B8), 17661-

17674.

Wohl, E. (2000). Substrate influences on step-pool sequences in the Christopher Creek drainage, Arizona. The Journal of geology, 108(1), 121-129.

Wohl, E. (2013). Floodplains and wood. Earth-Science Reviews, 123, 194-212.

Wu, B., Wang, Z., Shen, N., & Wang, S. (2016). Modelling sediment transport capacity of rill flow for loess sediments on steep slopes. Catena, 147, 453-462.

Wu, B., Wang, Z., Zhang, Q., Shen, N., Liu, J., & Wang, S. (2018). Evaluation of shear stress and unit stream power to determine the sediment transport capacity of loess materials on different slopes. Journal of Soils and Sediments, 18, 116-127.

Yang, C. T. (1972). Unit stream power and sediment transport. Journal of the Hydraulics Division, 98(10), 1805-1826.

Zimmermann, J., Higgins, S. I., Grimm, V., Hoffmann, J., Münkemüller, T., & Linstädter, A. (2008). Recruitment filters in a perennial grassland: the interactive roles of fire, competitors, moisture and seed availability. Journal of Ecology, 96(5), 1033-1044.

10 Appendix A

1982-1996 Reaches with Migration > 32.8 ft

X Value of Centroid (W)	Y Value of Centroid (N)	Migration (ft)	Migration Rate (ft/yr)
-96.72194672	30.84576416	174.53435	12.46674
-96.94147491	30.88381958	146.92771	10.49484
-96.80142212	30.86196899	142.99299	10.21378
-96.84687805	30.84776878	142.07113	10.14794
-97.07974243	30.79004478	140.33379	10.02384
-97.08441162	30.78927803	136.83408	9.77386
-96.94065857	30.87645149	133.12322	9.50880
-96.92459869	30.89307785	129.86814	9.27630
-97.07900238	30.78767014	127.64811	9.11772
-96.71147156	30.84408951	122.71295	8.76521
-97.08740997	30.78862572	118.96113	8.49722
-96.92844391	30.88316345	108.40033	7.74288
-96.95034027	30.83303261	107.61185	7.68656
-96.84893799	30.84779549	104.87929	7.49138
-96.85037994	30.84590721	104.05883	7.43277
-96.80747986	30.85250092	101.60685	7.25763
-97.0623703	30.77531624	98.77153	7.05511
-96.774086	30.83778763	93.13587	6.65256
-96.77644348	30.83559036	90.38581	6.45613
-96.71890259	30.84910011	90.23340	6.44524
-96.89382172	30.88070488	83.97490	5.99821
-97.07157898	30.77861404	83.90283	5.99306
-96.93757629	30.85491562	79.80827	5.70059
-96.80164337	30.85679436	79.28472	5.66319
-97.24787903	30.86541557	75.67581	5.40542
-97.02345276	30.75767326	75.17237	5.36945
-97.09001923	30.7894268	73.31720	5.23694
-97.18694305	30.84596825	69.45446	4.96103
-97.05480194	30.77501869	67.54973	4.82498
-96.72184753	30.84328651	66.82422	4.77316
-97.32157135	30.9073658	66.39678	4.74263
-96.6962738	30.84933853	65.81991	4.70142
-96.70425415	30.83934021	63.96706	4.56908
-96.69577026	30.8426342	61.46344	4.39025
-97.32180786	30.90915108	60.79992	4.34285
-97.12559509	30.79485321	59.59781	4.25699
-97.02206421	30.75887871	59.58015	4.25573
-96.92684937	30.89113235	58.02427	4.14459
-96.87669373	30.86319542	57.57806	4.11272
-96.79159546	30.86235237	56.42171	4.03012

-96.72678375	30.83725357	56.24373	4.01741
-96.79434967	30.86642647	55.43982	3.95999
-96.73228455	30.8339138	54.25560	3.87540
-96.73355103	30.83017921	54.00122	3.85723
-97.09325409	30.79083061	53.97761	3.85554
-96.71899414	30.84012413	53.47633	3.81974
-97.06758881	30.78106308	53.09697	3.79264
-96.94792938	30.8349781	52.37045	3.74075
-96.94206238	30.87809372	51.33336	3.66667
-97.04656219	30.77438736	50.67957	3.61997
-97.07184601	30.77647972	50.58250	3.61304
-97.27118683	30.87419701	50.53843	3.60989
-96.72093201	30.84771156	50.13568	3.58112
-97.05617523	30.77653122	49.94400	3.56743
-97.05324554	30.77344894	49.68626	3.54902
-97.08260345	30.79344559	49.42050	3.53004
-96.79647827	30.86363602	49.33709	3.52408
-96.79048157	30.85745621	49.25011	3.51786
-96.95522308	30.83446312	48.99427	3.49959
-96.92616272	30.88945389	47.89315	3.42094
-97.13156891	30.80749321	47.25822	3.37559
-97.23483276	30.85356331	47.21949	3.37282
-97.12823486	30.80422974	47.16609	3.36901
-96.84637451	30.84425735	47.08509	3.36322
-96.79869843	30.86011124	46.88017	3.34858
-97.13652039	30.81706619	46.52868	3.32348
-97.24018097	30.85071564	45.88248	3.27732
-97.17098999	30.83529091	45.81029	3.27216
-97.12078094	30.79378891	45.69393	3.26385
-96.75279236	30.82418823	44.56603	3.18329
-96.98669434	30.80871391	43.63798	3.11700
-97.30114746	30.88152504	43.54900	3.11064
-97.32456207	30.91150475	43.39216	3.09944
-96.93729401	30.8732357	43.24727	3.08909
-96.84846497	30.84292984	43.20163	3.08583
-97.17346191	30.83856964	43.13378	3.08098
-96.78471375	30.85203552	42.47877	3.03420
-96.91680908	30.8846035	42.42391	3.03028
-97.12646484	30.80017281	42.34162	3.02440
-97.31853485	30.89582443	41.97901	2.99850
-97.24445343	30.85688019	41.92329	2.99452
-97.02472687	30.76106834	41.83346	2.98810
-97.26158905	30.87591553	41.77807	2.98415
-96.7820282	30.83934402	41.11128	2.93652
-97.12234497	30.79018593	41.07053	2.93361
-97.23635864	30.85005951	41.00064	2.92862
-97.24901581	30.87064171	40.95592	2.92542
-96.86864471	30.85037994	40.77446	2.91246
-97.14103699	30.82175446	40.75338	2.91096

-97.01229858	30.76813698	40.41580	2.88684
-96.79920197	30.85817719	39.80097	2.84293
-97.06982422	30.77500534	39.11695	2.79407
-97.264534	30.87691307	39.03156	2.78797
-96.96318817	30.84082031	38.80766	2.77198
-97.10968018	30.78969574	37.74297	2.69593
-97.19285583	30.84738922	37.56402	2.68314
-97.15383148	30.8274765	36.73959	2.62426
-97.18534088	30.84696198	36.14018	2.58144
-96.95288086	30.83425331	36.13746	2.58125
-96.96516418	30.83598709	35.86246	2.56160
-97.08255005	30.79193306	35.75051	2.55361
-97.21113586	30.85111618	35.60617	2.54330
-97.14766693	30.82406235	35.25192	2.51799
-96.70880127	30.84045029	35.04601	2.50329
-96.8425293	30.84461212	34.81390	2.48671
-97.03618622	30.7668457	34.65148	2.47511
-97.09860229	30.78997993	34.29693	2.44978
-96.70539093	30.84121323	34.02848	2.43061
-96.71452332	30.8381958	33.82316	2.41594
-97.20866394	30.85045242	33.76952	2.41211
-96.95928955	30.83328629	33.53915	2.39565
-96.97766876	30.81749916	33.48413	2.39172
-97.25653076	30.87427521	33.35170	2.38226
-96.9629364	30.83358765	33.32877	2.38063
-97.21352386	30.84963417	33.28553	2.37754
-97.1210556	30.78764534	33.15080	2.36791
-97.13251495	30.80963898	33.07774	2.36270
-96.98683167	30.80441856	32.90189	2.35014

1982-1996 Reaches with Migration 19.7- 32.8 ft

X Value of Centroid (W)	Y Value of Centroid (N)	Migration (ft)	Migration Rate (ft/yr)
-97.10309601	30.78882408	32.50612	2.32187
-97.03987885	30.77280807	32.43127	2.31652
-96.78304291	30.84773254	32.21701	2.30122
-96.96122742	30.83235931	31.74172	2.26727
-96.87506866	30.87436867	30.98610	2.21329
-97.16717529	30.83465576	30.58694	2.18478
-96.99411011	30.7797699	30.42310	2.17308
-96.92570496	30.88789749	30.39931	2.17138
-97.22123718	30.85730934	30.38915	2.17065
-96.96160126	30.83584976	30.12228	2.15159
-96.84089661	30.84736252	29.77928	2.12709
-97.11687469	30.79373932	29.66058	2.11861
-96.70056915	30.84101677	29.13892	2.08135
-97.24990082	30.87237358	29.12789	2.08056

-97.32167816	30.90213966	28.95187	2.06799
-97.02957916	30.76701355	28.85385	2.06099
-97.01449585	30.77491951	28.84984	2.06070
-97.11470032	30.78774071	28.62994	2.04500
-97.32137299	30.90042496	28.38865	2.02776
-97.03360748	30.77049255	28.38434	2.02745
-97.27638245	30.86767578	28.18583	2.01327
-96.83766937	30.84502411	27.75016	1.98215
-97.1992569	30.8456459	27.52723	1.96623
-97.26738739	30.87628937	27.44031	1.96002
-97.16253662	30.83227158	27.42611	1.95901
-96.77032471	30.83276558	27.21698	1.94407
-96.70773315	30.8384037	27.20532	1.94324
-97.30922699	30.88543892	26.71313	1.90808
-96.71704102	30.84509659	26.52685	1.89477
-97.20632935	30.84966087	26.49614	1.89258
-97.21828461	30.85700607	26.49355	1.89240
-96.99082184	30.79579735	26.21152	1.87225
-96.79260254	30.86559677	26.18336	1.87024
-97.15701294	30.8309021	26.14707	1.86765
-97.02951813	30.77080536	25.63535	1.83110
-96.81950378	30.8486824	25.55043	1.82503
-97.22122192	30.85381126	25.44234	1.81731
-96.98854828	30.78376007	24.88681	1.77763
-97.09463501	30.79279709	24.83550	1.77396
-97.01184845	30.77586555	24.82124	1.77295
-97.24623108	30.86132813	24.76893	1.76921
-96.76390076	30.83017731	24.76210	1.76872
-97.30849457	30.89292526	24.65380	1.76099
-96.98829651	30.80893135	24.50624	1.75045
-97.01873779	30.76023483	24.49366	1.74955
-97.2193985	30.85022736	24.37242	1.74089
-97.28482819	30.87024689	23.90394	1.70742
-97.23886871	30.84958267	23.81251	1.70089
-96.94621277	30.83828354	23.79494	1.69964
-97.06719208	30.78573227	23.78235	1.69874
-97.22709656	30.85028267	23.73239	1.69517
-97.29538727	30.87928581	23.50013	1.67858
-97.02746582	30.76559258	23.24470	1.66034
-97.01400757	30.76104546	23.11711	1.65122
-97.07299805	30.78718185	23.08128	1.64866
-97.32196045	30.90494919	23.06001	1.64714
-97.22499847	30.84918213	22.99656	1.64261
-97.10308838	30.79223061	22.92193	1.63728
-96.96535492	30.83250809	22.86838	1.63346
-97.28672791	30.87418175	22.56021	1.61144
-97.15202332	30.82569122	22.54381	1.61027
-97.03688049	30.76837921	22.24483	1.58892
-96.75043488	30.82343483	21.67168	1.54798

-97.27936554	30.86509132	21.65386	1.54670
-97.06977844	30.78746223	21.38820	1.52773
-97.02500916	30.76456642	21.31621	1.52259
-97.1346283	30.81162453	20.98404	1.49886
-97.11182404	30.79053879	20.77106	1.48365
-97.2026825	30.84537697	20.73720	1.48123
-97.03780365	30.77039337	20.41109	1.45793
-96.96759033	30.83067131	20.16954	1.44068
-97.1966629	30.84747124	19.86478	1.41891
-97.30314636	30.89105797	19.71846	1.40846

1996-2004 Reaches with Migration ≥ 32.8 ft

X Value of Centroid (W)	Y Value of Centroid (N)	Migration (ft)	Migration Rate (ft/yr)
-96.94903564	30.83253288	191.69675	23.96209
-96.85044861	30.84632111	108.14909	13.51864
-96.72159576	30.8433075	106.92879	13.36610
-96.77403259	30.83833122	98.70558	12.33820
-96.75289917	30.82464027	95.81556	11.97695
-96.72201538	30.84644318	91.70922	11.46365
-96.84615326	30.84757042	91.55671	11.44459
-96.94863892	30.83369637	90.22412	11.27802
-96.94473267	30.83988953	82.99675	10.37459
-96.7299881	30.83596802	80.22051	10.02756
-96.775383	30.83572769	79.05943	9.88243
-96.68054962	30.84242439	76.15556	9.51945
-96.72582245	30.83685684	76.02644	9.50331
-96.95446777	30.83376503	73.27884	9.15985
-96.71714783	30.8461132	72.98317	9.12290
-96.84794617	30.84819603	72.28748	9.03593
-97.13454437	30.81133842	67.35902	8.41988
-96.80988312	30.85260391	65.25468	8.15683
-96.94606018	30.83873558	62.93166	7.86646
-96.70867157	30.84333611	61.99175	7.74897
-96.69412994	30.85040855	60.26993	7.53374
-96.68318176	30.84474754	59.74776	7.46847
-96.7117691	30.83734322	59.26801	7.40850
-96.91278839	30.88034248	58.93690	7.36711
-96.80368042	30.85430336	58.80730	7.35091
-96.95298004	30.83375359	58.01210	7.25151
-96.70329285	30.83947754	57.10309	7.13789
-97.15333557	30.82896423	56.17289	7.02161
-96.71668243	30.83786011	54.58485	6.82311
-96.70856476	30.83838272	53.84860	6.73108
-96.94095612	30.87662125	50.67948	6.33494
-97.18663788	30.84626198	50.57833	6.32229
-96.73310089	30.83154297	50.16737	6.27092

-96.69547272	30.84440804	49.23655	6.15457
-96.80072784	30.8616333	49.02448	6.12806
-97.32662964	30.92760658	46.20991	5.77624
-96.94850159	30.83480644	45.42579	5.67822
-97.13269806	30.80955124	45.15987	5.64498
-96.7204895	30.84819221	44.95832	5.61979
-97.18505859	30.84699631	44.18733	5.52342
-96.68682861	30.84617805	42.98681	5.37335
-97.13378906	30.8101368	41.69987	5.21248
-96.78658295	30.85251236	41.13203	5.14150
-96.75868225	30.82583427	40.46044	5.05756
-97.13494873	30.81284904	40.38754	5.04844
-96.76286316	30.82887459	40.25468	5.03183
-97.16734314	30.83489799	40.04261	5.00533
-96.95149994	30.83481979	39.51528	4.93941
-96.80760956	30.85100174	39.50993	4.93874
-97.19274902	30.84721184	39.46901	4.93363
-97.22033691	30.85417747	38.65934	4.83242
-96.848526	30.84319878	36.54964	4.56870
-97.17365265	30.83922577	36.30284	4.53785
-97.35300446	30.96051979	35.11434	4.38929
-97.08872223	30.78963089	34.17813	4.27227
-97.33860779	30.95631599	34.00837	4.25105
-97.02577972	30.75976563	33.07433	4.13429

1996-2004 Reaches with Migration 19.7- 32.8 ft

X Value of Centroid (W)	Y Value of Centroid (N)	Migration (ft)	Migration Rate (ft/yr)
-97.32551575	30.92876625	32.35440	4.04430
-96.94306183	30.84177589	32.19272	4.02409
-96.75006866	30.82333755	31.57421	3.94678
-97.21623993	30.8484745	31.23202	3.90400
-96.87677002	30.86303329	30.79970	3.84996
-97.27891541	30.86480904	30.78505	3.84813
-97.13134766	30.80876923	30.69106	3.83638
-97.13134766	30.80876923	30.69106	3.83638
-97.09936523	30.79188919	30.31250	3.78906
-97.31975555	30.92563248	30.26141	3.78268
-97.39951324	30.97955894	30.01976	3.75247
-97.33480072	30.95722389	29.85651	3.73206
-97.16293335	30.83258057	29.77175	3.72147
-97.17058563	30.83513832	29.47264	3.68408
-97.15824127	30.83125496	29.39188	3.67399
-96.96427917	30.84062576	29.33063	3.66633
-97.15543365	30.83054352	28.77507	3.59688

-97.32151794	30.93059921	28.34276	3.54285
-97.19812012	30.84646225	27.98711	3.49839
-97.23538971	30.8507309	27.93103	3.49138
-97.36997223	30.95297432	27.65663	3.45708
-96.76865387	30.83230591	27.34961	3.41870
-96.95039368	30.83403587	27.28317	3.41040
-96.95838165	30.83446121	27.16813	3.39602
-97.35421753	30.95949364	27.14143	3.39268
-97.27676392	30.8683567	26.47650	3.30956
-96.79401398	30.86512184	25.91653	3.23957
-97.31645203	30.94685555	25.74027	3.21753
-97.20944977	30.85206985	25.38297	3.17287
-97.26309967	30.87830734	25.18949	3.14869
-97.19358826	30.84641266	25.03889	3.12986
-96.90943909	30.87543488	24.96010	3.12001
-97.08781433	30.79017258	24.71076	3.08884
-97.30405426	30.88197708	24.68471	3.08559
-96.92673492	30.89111328	24.67333	3.08417
-97.01280975	30.76819038	24.59351	3.07419
-97.16020203	30.83149147	24.51076	3.06384
-97.3428421	30.96403885	24.39198	3.04900
-96.71971893	30.84915543	24.29363	3.03670
-97.00219727	30.77369308	24.28407	3.03551
-97.30821991	30.89175034	24.27426	3.03428
-97.0395813	30.77292061	24.10679	3.01335
-96.96295166	30.83369064	23.93472	2.99184
-96.7190094	30.84947968	23.85899	2.98237
-96.91600037	30.88412857	23.83561	2.97945
-97.32384491	30.92856026	23.75927	2.96991
-97.32622528	30.92673492	23.42080	2.92760
-97.03032684	30.76804352	23.32665	2.91583
-97.22834778	30.84918404	23.01544	2.87693
-96.77789307	30.83102989	22.55939	2.81992
-97.025177	30.76107407	22.22633	2.77829
-97.25959015	30.87310791	22.08825	2.76103
-97.38365173	30.95783997	22.02834	2.75354
-97.23544312	30.85213089	21.99009	2.74876
-97.33013153	30.93992996	21.96414	2.74552
-97.32039642	30.89692879	21.69724	2.71215
-96.92553711	30.88698959	21.66807	2.70851
-97.112854	30.79188347	21.63402	2.70425
-97.37612915	30.95028114	21.61693	2.70212
-97.20436859	30.85092354	21.60892	2.70111
-96.88005829	30.88185501	21.59019	2.69877
-97.32038879	30.92899323	21.43733	2.67967
-97.30285645	30.8908329	21.36255	2.67032
-96.91547394	30.88238144	21.35120	2.66890
-97.36854553	30.95454216	21.10407	2.63801
-97.38653564	30.96208954	21.08865	2.63608

-97.07308197	30.77750397	21.07419	2.63427
-97.15323639	30.82599831	21.01420	2.62678
-96.6971817	30.84687996	20.98752	2.62344
-97.15403748	30.82723999	20.90596	2.61324
-97.31087494	30.89321518	20.76968	2.59621
-97.18977356	30.84624863	20.76192	2.59524
-97.07035065	30.7799511	20.76155	2.59519
-96.94689178	30.83633804	20.74157	2.59270
-96.77320862	30.83537674	20.66162	2.58270
-96.94176483	30.84286308	20.58136	2.57267
-96.80094147	30.85698891	20.55190	2.56899
-96.98688507	30.8038559	20.43867	2.55483
-97.21224976	30.85040283	20.30018	2.53752
-96.87760162	30.85922813	20.30013	2.53752
-97.18182373	30.84191704	20.03905	2.50488
-97.26157379	30.87423897	19.98773	2.49847

2004-2012 Reaches with Migration ≥32.8 ft

X Value of Centroid (W)	Y Value of Centroid (N)	Migration (ft)	Migration Rate (ft/yr)
-97.27852369	30.86423661	203.76131	25.47016
-96.94896599	30.83251149	203.32567	25.41571
-97.27468231	30.86953068	202.12004	25.26501
-97.27660967	30.86724461	162.03302	20.25413
-97.26755124	30.87612706	154.94751	19.36844
-96.84779841	30.84844129	132.81635	16.60204
-97.26469444	30.87624441	118.63035	14.82879
-96.80071149	30.8607653	116.57091	14.57136
-97.26166378	30.87567146	105.46286	13.18286
-96.72180608	30.84403017	94.52533	11.81567
-96.72190885	30.8465373	92.33924	11.54240
-96.94862841	30.8337307	86.02478	10.75310
-96.94601227	30.83901143	74.07044	9.25881
-96.75248565	30.82434783	72.20458	9.02557
-96.85024424	30.84659441	69.85516	8.73190
-96.73204243	30.83412097	67.82637	8.47830
-96.77355557	30.83787227	67.74203	8.46775
-96.77564967	30.83687545	66.63775	8.32972
-96.94447105	30.84007847	63.00659	7.87582
-96.72955434	30.83599187	60.41342	7.55168
-96.9132575	30.881182	59.90292	7.48787
-96.71987838	30.84890087	59.16465	7.39558
-96.72572472	30.83687176	57.14935	7.14367
-96.84594402	30.84747458	56.31565	7.03946
-96.84929803	30.8412093	56.24761	7.03095

-97.18664371	30.84625201	55.17731	6.89716
-96.95442768	30.83344808	53.99323	6.74915
-96.8093575	30.85222541	53.64269	6.70534
-97.13450536	30.81126461	52.51274	6.56409
-96.7111837	30.83662228	52.05150	6.50644
-97.28071794	30.8669429	51.03702	6.37963
-96.80338861	30.85476043	51.01414	6.37677
-96.75521381	30.82526559	50.01975	6.25247
-96.95323943	30.83310005	47.78142	5.97268
-96.70526777	30.84173111	47.25042	5.90630
-96.68002604	30.84225085	47.18745	5.89843
-96.95250606	30.83489936	47.16664	5.89583
-97.17215681	30.83856291	46.69913	5.83739
-97.15377168	30.82930116	46.39725	5.79966
-97.27146279	30.87406159	45.79955	5.72494
-96.7169697	30.84453127	45.71033	5.71379
-97.27969084	30.86662703	45.14436	5.64304
-97.13271405	30.80954958	44.51434	5.56429
-97.32660049	30.92762771	44.38350	5.54794
-96.91170024	30.87902351	44.27883	5.53485
-97.40148631	30.98252915	43.54553	5.44319
-97.40148631	30.98252915	43.54553	5.44319
-96.80025413	30.85761397	42.72335	5.34042
-96.83986982	30.84522877	42.58663	5.32333
-96.71572175	30.83783218	41.55687	5.19461
-97.13380017	30.81016739	40.78162	5.09770
-96.79514161	30.86562037	39.60077	4.95010
-96.94121677	30.87739929	39.52378	4.94047
-97.1927377	30.8472822	38.42154	4.80269
-96.71721183	30.8482112	38.22354	4.77794
-97.18494613	30.84690256	38.05588	4.75699
-96.73563883	30.82747522	37.41873	4.67734
-96.92692843	30.89285791	37.34769	4.66846
-96.76040937	30.82626884	36.49372	4.56171
-96.96170737	30.83239469	36.43365	4.55421
-96.84927033	30.84382701	36.00931	4.50116
-96.78458615	30.85116787	35.83548	4.47944
-96.6826625	30.8440096	34.76252	4.34531
-96.70736651	30.84592651	34.60087	4.32511
-97.16293267	30.8325821	34.33523	4.29190
-96.69608463	30.84564953	33.16896	4.14612
-96.846313	30.84429652	33.01379	4.12672
-97.16728177	30.83491031	32.95266	4.11908

2004-2012 Reaches with Migration 19.7- 32.8 ft

X Value of Centroid (W)	Y Value of Centroid (N)	Migration (ft)	Migration Rate (ft/yr)
719695.4375	3414090.25	32.56531	4.07066
721377.75	3414826.75	32.47051	4.05881
674983.4375	3412765	32.46421	4.05803
666774.375	3417008.5	32.38589	4.04824
655688.125	3425495.25	32.21292	4.02661
696200.25	3413093	32.16703	4.02088
675949.375	3412376.5	31.58670	3.94834
682874.6875	3407845.75	31.17883	3.89735
678761.125	3409898.75	31.09800	3.88725
670161.6875	3414801	30.96308	3.87038
712019.6875	3414735	30.72221	3.84028
657312.1875	3426384.25	30.32072	3.79009
705844.75	3414138	29.90537	3.73817
710172.25	3415760.25	29.61970	3.70246
718379.375	3414817.25	29.54323	3.69290
696400.5625	3413367.25	29.14892	3.64361
660146.5625	3422889.25	29.14410	3.64301
718844.4375	3414660.25	29.10476	3.63809
699265.125	3418433	28.46113	3.55764
659050.8125	3426050.75	28.35173	3.54397
696719.5	3413895.5	28.22316	3.52790
720261.9375	3414400.25	27.96467	3.49558
720611.625	3415235	27.81423	3.47678
666595.5625	3416948	27.68929	3.46116
678408.8125	3410346.25	27.64218	3.45527
716392.8125	3412563	27.06393	3.38299
653135.4375	3428009.25	26.93366	3.36671
668729.1875	3414542.25	26.77672	3.34709
692653.75	3410083.25	26.57992	3.32249
657177.0625	3426258.25	26.43463	3.30433
719094.3125	3414165.75	26.41430	3.30179
679663.5625	3408290.5	26.38459	3.29807
688958.4375	3404642	26.36304	3.29538
696039.5625	3412998.5	26.23565	3.27946
667188.25	3416896.75	26.16431	3.27054
710543.125	3416557.25	26.12660	3.26582
706547.0625	3414744.75	26.06010	3.25751
713306.1875	3413171.5	25.88523	3.23565
654677	3425597	25.25806	3.15726
691187.625	3406227	25.20743	3.15093
676148.875	3412354	25.09781	3.13723
685950.1875	3406650	24.96118	3.12015
681843.25	3408142.75	24.94330	3.11791

669409.625	3414230.25	24.78447	3.09806
680886.25	3407822.25	24.51479	3.06435
679138.375	3408989.75	24.22463	3.02808
696889.125	3414055.75	23.97157	2.99645
684655.375	3406747.5	23.93774	2.99222
670128	3414924	23.56132	2.94516
692456.3125	3407169.5	23.34764	2.91845
712486.9375	3412890	23.06625	2.88328
687939.9375	3405572.5	23.04055	2.88007
711445.25	3415771.25	22.92249	2.86531
671214.6875	3414579	22.91145	2.86393
661716.75	3418814.75	22.77305	2.84663
683484.5625	3408098.75	22.47993	2.80999
715239.5625	3412188	22.32861	2.79108
660193.625	3421339.75	22.17894	2.77237
672295.1875	3413971.75	21.59434	2.69929
668674.6875	3414348.25	21.46294	2.68287
689145.6875	3404976	21.41985	2.67748
701958.5625	3418660	21.18198	2.64775
660930.625	3419092.75	21.17904	2.64738
674335.1875	3413359	21.15765	2.64471
659023.9375	3425860	21.09772	2.63722
719139.875	3413642	20.97381	2.62173
672151.5	3414314.75	20.96379	2.62047
660379.625	3423121	20.87165	2.60896
713976	3412791	20.83521	2.60440
677199.375	3411585	20.76516	2.59565
660010.875	3422929	20.70924	2.58866
670513.1875	3414155.5	20.69727	2.58716
706870.5625	3414486.75	20.45424	2.55678
672942.9375	3414106.5	20.43369	2.55421
698303.4375	3418797	20.42279	2.55285
709098.25	3415193.5	20.41677	2.55210
718175.9375	3413832.5	20.21243	2.52655
694913.75	3413580.75	20.20866	2.52608
660823.5625	3424932.5	20.17645	2.52206
670953.4375	3414397	20.13953	2.51744
682996.875	3407889	20.04370	2.50546
712074.4375	3414305.25	19.91978	2.48997
669067.1875	3414627	19.80843	2.47605
718139.4375	3414211.5	19.78564	2.47320
703066.9375	3415749.5	19.72570	2.46571
692111	3407082.75	19.70668	2.46333

2012-2018 Reaches with Migration >32.8 ft

X Value of Centroid (W)	Y Value of Centroid (N)	Migration (ft)	Migration Rate (ft/yr)
-96.84822845	30.84573555	629.08900	104.84817
-96.72151184	30.84421539	236.16735	39.36122
-96.94896698	30.83252907	220.60578	36.76763
-97.27489471	30.86947823	207.22155	34.53693
-97.27846527	30.86406708	193.68688	32.28115
-96.71244049	30.84461594	188.39843	31.39974
-96.72180176	30.84685326	182.22442	30.37074
-97.27657318	30.86722755	173.65340	28.94223
-96.94834137	30.83404541	168.59863	28.09977
-96.75237274	30.82452202	168.49782	28.08297
-97.26767731	30.87630844	153.90440	25.65073
-96.84526062	30.84259605	149.55420	24.92570
-96.94443512	30.84023857	149.12043	24.85341
-96.77404022	30.83870125	147.53355	24.58893
-96.70336914	30.8389492	134.82766	22.47128
-96.75508881	30.82512665	134.33653	22.38942
-96.77523804	30.83628464	132.15969	22.02662
-97.18655396	30.84586334	129.24879	21.54147
-97.17053986	30.83492851	126.53468	21.08911
-96.71701813	30.84425354	124.40196	20.73366
-97.40131378	30.9822464	122.19951	20.36659
-96.913414	30.88113594	121.71326	20.28554
-96.70500183	30.84076691	115.84634	19.30772
-97.15323639	30.82891273	115.02363	19.17061
-97.26460266	30.87613106	114.00292	19.00049
-96.94583893	30.83906364	113.15297	18.85883
-96.84898376	30.8412571	112.00530	18.66755
-97.13235474	30.80942345	111.95994	18.65999
-96.95274353	30.83350563	109.63439	18.27240
-97.26177216	30.87584877	108.64864	18.10811
-96.72560883	30.83689499	106.46871	17.74479
-96.72979736	30.83613968	105.08430	17.51405
-96.72026062	30.84850693	102.34059	17.05677
-97.17173767	30.83797646	102.33655	17.05609
-96.80337524	30.85438156	100.64328	16.77388
-96.71675873	30.8375988	100.37043	16.72840
-96.80922699	30.85257721	100.22669	16.70445
-96.79008484	30.85709381	99.05412	16.50902
-96.80039978	30.86071014	98.82548	16.47091
-96.70906067	30.84075928	98.37103	16.39517
-96.71783447	30.84896851	97.77601	16.29600
-97.18495178	30.84699059	90.36941	15.06157
-96.95909119	30.83323288	89.47141	14.91190
-96.96114349	30.83856964	88.33005	14.72167

-96.95139313	30.8349514	85.44314	14.24052
-96.95441437	30.83387184	83.67993	13.94666
-96.71154785	30.83727455	83.53974	13.92329
-96.94285583	30.84186935	82.15644	13.69274
-97.19260406	30.84730911	79.35789	13.22631
-97.13119507	30.80862045	78.42684	13.07114
-96.94125366	30.8772068	77.92695	12.98783
-96.68270874	30.84429741	77.82967	12.97161
-96.69397736	30.85062408	76.28706	12.71451
-97.13443756	30.81112099	75.38792	12.56465
-96.80015564	30.85760689	74.08190	12.34698
-97.39083862	30.96971512	73.21950	12.20325
-97.2203598	30.85428238	72.10826	12.01804
-97.35421753	30.9594574	69.55997	11.59333
-96.70620728	30.84506607	69.12289	11.52048
-96.95015717	30.83382225	68.23682	11.37280
-97.15317535	30.82590675	66.82415	11.13736
-96.69553375	30.84464264	66.30584	11.05097
-97.22780609	30.84946251	65.56729	10.92788
-96.73199463	30.8337307	64.84066	10.80678
-97.05648041	30.77805328	63.93505	10.65584
-97.16043854	30.83145142	63.92332	10.65389
-96.96195984	30.83232307	63.68121	10.61354
-97.23511505	30.85190392	63.51039	10.58507
-96.8019104	30.85655594	63.22925	10.53821
-97.02375031	30.76264572	62.47620	10.41270
-97.1348877	30.81264687	62.08041	10.34674
-97.36989594	30.95299339	61.71115	10.28519
-96.70891571	30.83542061	61.51522	10.25254
-96.94150543	30.84308243	59.16148	9.86025
-97.16728973	30.83509445	55.41581	9.23597
-97.35286713	30.96044159	55.35111	9.22519
-97.27178955	30.87309647	54.21293	9.03549
-97.13362122	30.80994225	54.09535	9.01589
-97.08885193	30.78944016	54.00278	9.00046
-96.80725861	30.85111046	52.60682	8.76780
-96.76039886	30.82621384	52.28555	8.71426
-96.78348541	30.84785652	51.25396	8.54233
-96.96460779	30.83442713	46.18103	2.09914
-97.26838151	30.87790412	45.66714	2.07578
-97.38149436	30.95383517	45.29036	2.05865
-96.96075894	30.84115692	45.23787	2.05627
-97.08707861	30.7884668	45.21187	2.05508
-96.80182794	30.85663044	44.93276	2.04240
-97.05524255	30.77498466	43.77871	1.98994
-96.95818787	30.83464404	43.49374	1.97699
-97.31617496	30.89405416	43.11467	1.95976
-97.03942564	30.77289035	42.50167	1.93189
-97.09288532	30.78928083	42.11172	1.91417

-96.98774848	30.7935817	41.70759	1.89580
-97.09263026	30.79134968	41.53078	1.88776
-97.32713938	30.93198755	41.49307	1.88605
-97.24744324	30.86741904	41.32612	1.87846
-97.07119578	30.77859689	41.30367	1.87744
-97.27756822	30.86430284	41.08451	1.86748
-96.79534518	30.86572081	40.74567	1.85208
-97.05658358	30.7780787	40.17791	1.82627
-96.91169464	30.87907078	40.10296	1.82286
-97.33430726	30.95609758	40.01975	1.81908
-97.21946171	30.84769759	39.11198	1.77782
-97.087906	30.79021783	38.49812	1.74991
-97.13559993	30.81445582	38.45097	1.74777
-97.39075685	30.96961459	37.99961	1.72725
-97.32676804	30.92750809	37.67366	1.71244
-97.27656597	30.86446316	37.35022	1.69774
-97.08731252	30.78740576	37.17616	1.68983
-97.12577556	30.80090182	37.12038	1.68729
-97.38792106	30.96282884	36.96248	1.68011
-97.12029918	30.79078191	36.38606	1.65391
-96.91543852	30.8823109	35.94484	1.63386
-97.03598789	30.76816318	35.86526	1.63024
-97.39608954	30.97565771	35.63274	1.61967
-97.3148252	30.8934344	35.52791	1.61490
-97.19018097	30.84667137	35.44417	1.61110
-97.07041005	30.78024057	35.26258	1.60284
-97.11899348	30.78827538	34.70774	1.57762
-97.16198397	30.83210179	34.35625	1.56165
-97.36884672	30.95447905	33.81753	1.53716

2012-2018 Reaches with Migration 19.7- 32.8 ft

X Value of Centroid (W)	Y Value of Centroid (N)	Migration (ft)	Migration Rate (ft/yr)
-96.71878815	30.84241104	32.61472	5.43579
-97.0871582	30.78749084	32.25520	5.37587
-97.13578796	30.8146019	32.04443	5.34074
-97.08786774	30.79020119	31.73007	5.28834
-97.03370667	30.76840401	31.57318	5.26220
-97.06718445	30.78073692	31.56512	5.26085
-96.79781342	30.86350441	31.49517	5.24919
-96.98623657	30.80828094	31.28354	5.21392
-96.96986389	30.82745171	31.23121	5.20520
-97.3213501	30.93061638	31.20449	5.20075
-97.38800049	30.96280098	31.19156	5.19859
-97.39607239	30.97565842	31.15951	5.19325

-97.09936523	30.79181862	31.15948	5.19325
-97.01968384	30.76059723	31.09586	5.18264
-97.28126526	30.86673927	30.85001	5.14167
-97.36897278	30.95444298	30.57671	5.09612
-97.13204956	30.80663872	30.44492	5.07415
-97.20163727	30.84698105	30.18645	5.03108
-97.27626038	30.86518669	30.16405	5.02734
-96.93572235	30.86871529	29.91028	4.98505
-97.24108124	30.85025787	29.88341	4.98057
-97.21099091	30.85110283	29.78925	4.96487
-97.12804413	30.80011177	29.56078	4.92680
-97.25263214	30.87428093	29.46409	4.91068
-97.25564575	30.87463951	29.29195	4.88199
-97.12442017	30.7952137	29.12587	4.85431
-97.33032227	30.93934631	29.05704	4.84284
-96.94430542	30.87976265	28.99389	4.83232
-97.39390564	30.9756012	28.68286	4.78048
-97.07041931	30.78021812	28.55774	4.75962
-97.13165283	30.80588913	28.36167	4.72694
-96.91122437	30.87703705	28.36096	4.72683
-96.69968414	30.84140587	27.93493	4.65582
-97.02957916	30.76940727	27.73925	4.62321
-97.08181	30.7914772	27.56693	4.59449
-97.15653229	30.83062553	27.55589	4.59265
-97.21308136	30.85005951	27.39003	4.56501
-97.0377121	30.76784706	27.33179	4.55530
-97.23872375	30.85006714	26.79440	4.46573
-97.14724731	30.82422066	26.68160	4.44693
-97.05218506	30.77215767	26.52747	4.42124
-97.33345795	30.95889854	26.14002	4.35667
-97.10650635	30.79269981	26.09209	4.34868
-97.38117218	30.95362091	25.64502	4.27417
-97.08084869	30.78706932	25.62221	4.27037
-97.03907013	30.77025223	25.56131	4.26022
-97.11290741	30.79057884	25.49203	4.24867
-96.73724365	30.82639313	25.37769	4.22961
-96.92747498	30.89204216	25.25766	4.20961
-97.04059601	30.77230263	25.22148	4.20358
-96.78459167	30.85124588	25.17067	4.19511
-97.23547363	30.85338402	24.97737	4.16289
-96.95835114	30.8345871	24.82772	4.13795
-96.9465332	30.83692741	24.78225	4.13038
-97.02366638	30.75744629	24.54810	4.09135
-97.0535202	30.77480125	24.31806	4.05301
-96.82201385	30.84881783	24.28645	4.04774
-97.19487	30.84751511	24.27154	4.04526
-96.96630859	30.83892059	24.23171	4.03862
-96.7762146	30.83287239	24.17420	4.02903
-97.14006805	30.82138443	24.07002	4.01167

-96.88526917	30.8849678	24.06873	4.01145
-97.23285675	30.85396576	23.82772	3.97129
-97.37637329	30.94919777	23.78526	3.96421
-97.04005432	30.77682877	23.64164	3.94027
-96.77115631	30.83306122	23.53866	3.92311
-97.27959442	30.86701584	23.50416	3.91736
-97.05069733	30.77357101	23.33076	3.88846
-96.92594147	30.89304161	23.31964	3.88661
-97.20085907	30.85123444	23.15286	3.85881
-97.2352829	30.85072708	23.00662	3.83444
-96.85227203	30.8418045	22.81212	3.80202
-97.12765503	30.79596329	22.72048	3.78675
-96.92559052	30.88505363	22.65028	3.77505
-96.98521423	30.80675888	22.55136	3.75856
-97.23809052	30.84888077	22.34359	3.72393
-97.34481812	30.96609116	22.34030	3.72338
-97.11134338	30.79083633	22.22208	3.70368
-97.16519928	30.83345222	22.17197	3.69533
-97.12360382	30.78953171	22.13990	3.68998
-97.10227203	30.78944778	22.09853	3.68309
-96.71168518	30.84106827	21.76548	3.62758
-97.01540375	30.75979614	21.75317	3.62553
-96.88937378	30.88338852	21.74568	3.62428
-96.84191895	30.84611702	21.56704	3.59451
-97.02246857	30.75888443	21.24700	3.54117
-97.0993042	30.79407883	21.14354	3.52392
-97.11916351	30.79321289	21.12141	3.52024
-97.19302368	30.84619331	20.96455	3.49409
-97.11086273	30.78660202	20.83341	3.47224
-97.10063171	30.78874779	20.79906	3.46651
-96.79508972	30.86630821	20.78360	3.46393
-96.96286011	30.8337307	20.57646	3.42941
-96.99154663	30.7964592	20.55908	3.42651
-97.07922363	30.7922554	20.45822	3.40970
-97.11372375	30.7883358	20.45555	3.40926
-97.3780365	30.95014191	20.45200	3.40867
-97.01477814	30.77492523	20.44331	3.40722
-96.98935699	30.79414749	20.43613	3.40602
-97.19910431	30.84574699	20.38868	3.39811
-97.34041595	30.96123123	20.35961	3.39327
-96.96065521	30.84103394	20.29834	3.38306
-96.8409729	30.84767723	20.26728	3.37788
-97.22175598	30.85656548	20.22755	3.37126
-96.97001648	30.8212471	20.17004	3.36167
-96.69750214	30.84745979	20.02039	3.33673
-97.31471252	30.893507	19.78862	3.29810

1996-2018 Reaches with Migration >32.8 ft

X Value of Centroid (W)	Y Value of Centroid (N)	Migration (ft)	Migration Rate (ft/yr)
-96.84817472	30.84551817	651.72132	29.62370
-96.72145806	30.84385492	228.04715	10.36578
-96.77432887	30.83870415	215.35926	9.78906
-96.71242376	30.84441042	215.10661	9.77757
-96.94903184	30.83254861	209.59034	9.52683
-96.75255755	30.82462645	195.01477	8.86431
-96.72184712	30.84682711	176.80502	8.03659
-96.94453151	30.84015385	171.83848	7.81084
-96.94834979	30.83399014	168.24954	7.64771
-96.7752236	30.83600219	162.36500	7.38023
-96.71703365	30.84442416	161.82292	7.35559
-96.84523083	30.84260748	147.40011	6.70000
-96.70342247	30.83905328	139.91636	6.35983
-96.95277231	30.83353017	136.48112	6.20369
-96.71694021	30.83763945	133.65733	6.07533
-97.18653459	30.84586933	132.68880	6.03131
-96.72998198	30.83608731	132.68602	6.03118
-96.91354736	30.88116863	132.11663	6.00530
-97.17061578	30.83492588	130.12454	5.91475
-96.71799431	30.8489962	129.53159	5.88780
-96.80349367	30.85427963	129.02298	5.86468
-96.75525967	30.82506343	123.81522	5.62796
-96.70545868	30.84235687	115.08567	5.23117
-97.27928424	30.86476321	114.68871	5.21312
-97.13234148	30.80942693	111.30656	5.05939
-97.15320879	30.82890973	110.01744	5.00079
-96.80960797	30.85270547	109.50821	4.97765
-96.68297033	30.84463072	105.90250	4.81375
-96.95144216	30.83494117	104.49775	4.74990
-96.94592727	30.83876878	100.95322	4.58878
-97.17171943	30.83802448	99.56711	4.52578
-97.40130597	30.98227657	99.32277	4.51467
-96.71183966	30.8376396	96.27463	4.37612
-96.69546829	30.84410066	95.91199	4.35964
-96.69438785	30.8502894	94.78677	4.30849
-96.95437561	30.83390055	94.37081	4.28958
-96.70884795	30.838854	94.00615	4.27301
-96.94113529	30.87683871	92.83659	4.21985
-96.72030818	30.84832665	88.34233	4.01556
-96.94291639	30.84180379	87.55272	3.97967
-96.72564867	30.83693808	86.18002	3.91727
-97.13445098	30.81117136	85.41817	3.88264
-97.22029775	30.85426761	82.03269	3.72876
-97.192613	30.84727594	81.53055	3.70593

-97.13117867	30.80865464	81.25985	3.69363
-96.96115959	30.83855624	77.88216	3.54010
-96.78793698	30.8542695	76.07276	3.45785
-96.80745216	30.85104307	75.85138	3.44779
-97.13488119	30.81274047	74.99327	3.40878
-96.84879104	30.84129559	73.41332	3.33697
-96.79544911	30.8639501	70.87669	3.22167
-96.96049205	30.83277021	69.28021	3.14910
-96.94164379	30.84301714	68.06295	3.09377
-96.68654315	30.84609271	66.97348	3.04425
-97.15317155	30.82590739	66.95459	3.04339
-97.35413402	30.95951595	66.61666	3.02803
-96.77816149	30.83033833	63.72527	2.89660
-97.38021434	30.95249747	63.24424	2.87474
-96.98907636	30.78262618	62.67364	2.84880
-96.9502123	30.83384599	61.82757	2.81034
-97.2278041	30.84944718	61.34157	2.78825
-97.32631578	30.92673766	61.33908	2.78814
-97.28090773	30.86692963	61.20042	2.78184
-96.92677076	30.89289372	60.96319	2.77105
-97.16042458	30.83143914	58.95119	2.67960
-96.80013416	30.86094942	58.62661	2.66485
-97.36987886	30.95306893	57.90717	2.63214
-97.23508716	30.85188997	57.63407	2.61973
-97.02575727	30.75971977	56.72769	2.57853
-97.1336256	30.80993935	56.10265	2.55012
-97.18488717	30.84684084	56.09683	2.54986
-97.08880771	30.78946885	55.70706	2.53214
-97.3528908	30.96047443	53.33619	2.42437
-96.7603925	30.82620767	52.89914	2.40451
-96.76280867	30.82875253	51.94929	2.36133
-97.27973272	30.86651482	48.98325	2.22651
-97.15804711	30.83119109	48.89849	2.22266
-96.9257016	30.88817686	48.69168	2.21326
-97.16743179	30.83516503	48.29478	2.19522
-96.83991042	30.8475567	47.12745	2.14216
-97.02375547	30.7626008	47.07891	2.13995
-96.73225983	30.83279431	46.89380	2.13154
-96.96118482	30.83683819	20.71876	0.94176
-97.19486875	30.84756001	20.64362	0.93835
-97.05348029	30.77478456	20.56408	0.93473
-96.7166573	30.84671311	20.56377	0.93472
-96.93572883	30.85879928	20.50209	0.93191
-96.97276249	30.81838308	20.42122	0.92824
-97.14722277	30.82421439	20.34814	0.92492
-96.97017259	30.82436388	20.34122	0.92460
-96.81865699	30.84915545	20.33249	0.92420
-97.34486374	30.96610501	20.30332	0.92288
-96.7192984	30.84038702	20.28510	0.92205

-97.05225976	30.77206894	20.25742	0.92079
-97.34249257	30.96337267	20.12016	0.91455
-96.98953648	30.79424768	20.08124	0.91278
-97.12319094	30.78887299	20.01333	0.90970
-97.33485636	30.95748269	20.00763	0.90944
-96.6906384	30.84817052	19.90259	0.90466
-97.02958449	30.7711512	19.79933	0.89997
-96.97000488	30.82134381	19.78954	0.89952

1996-2018 Reaches with Migration 19.7- 32.8 ft

X Value of Centroid (W)	Y Value of Centroid (N)	Migration (ft)	Migration Rate (ft/yr)
-96.96631103	30.83904545	32.63145	1.48325
-97.3253368	30.92571683	32.56911	1.48041
-97.0295166	30.76942039	32.54573	1.47935
-96.75050058	30.82330536	32.52897	1.47859
-96.98934544	30.80891034	32.11531	1.45979
-97.38625181	30.96201861	32.05823	1.45719
-97.21096826	30.85114619	31.64450	1.43839
-97.25796801	30.87334837	31.43092	1.42868
-97.26155089	30.87435733	31.20568	1.41844
-96.79107769	30.86238271	31.00136	1.40915
-97.39387456	30.97560989	30.32788	1.37854
-97.29505742	30.87964316	29.50308	1.34105
-96.96288584	30.83373252	29.07736	1.32170
-97.15656233	30.83062643	29.03001	1.31955
-97.22683384	30.84858363	28.63942	1.30179
-97.0252327	30.76127016	28.32295	1.28741
-97.260884	30.8733515	27.96221	1.27101
-97.26262492	30.87797807	27.70623	1.25937
-97.27610853	30.8695339	27.34809	1.24309
-97.3203997	30.92955458	26.91056	1.22321
-97.20175564	30.84694317	26.78790	1.21763
-96.70024367	30.8413939	26.24571	1.19299
-96.94706469	30.83625877	26.11473	1.18703
-97.23871443	30.85002007	25.97127	1.18051
-96.8768566	30.86288259	25.89523	1.17706
-97.08138254	30.78721663	25.83770	1.17444
-97.23530338	30.85071789	25.77177	1.17144
-96.71880909	30.84245526	25.64562	1.16571
-97.04055531	30.77227596	25.58398	1.16291
-97.32005203	30.92598432	25.42268	1.15558
-96.99207271	30.78188782	25.39347	1.15425
-97.1246003	30.79539767	25.34328	1.15197
-97.03035976	30.76796729	25.22728	1.14669

-96.91116667	30.8767733	25.20935	1.14588
-97.12802643	30.80025776	25.09383	1.14063
-97.06742675	30.78078024	24.90460	1.13203
-97.22240131	30.85098342	24.43723	1.11078
-97.32964185	30.95568101	24.38385	1.10836
-97.26507063	30.87535633	24.27386	1.10336
-97.32037807	30.89677015	24.27159	1.10325
-97.13203519	30.80665527	24.14943	1.09770
-97.37821671	30.95026664	23.98278	1.09013
-97.20097844	30.85133026	23.82493	1.08295
-96.94430285	30.87980725	23.78961	1.08135
-97.21988921	30.85487319	23.65687	1.07531
-97.21299231	30.85011864	23.46097	1.06641
-96.76974347	30.83306429	23.36759	1.06216
-97.09929323	30.79177459	23.36034	1.06183
-97.0730573	30.77742703	23.31622	1.05983
-97.14006986	30.82138522	23.21550	1.05525
-97.1128405	30.79053369	23.19293	1.05422
-97.0336777	30.76836271	23.18518	1.05387
-97.1979464	30.84652709	23.15464	1.05248
-97.10658771	30.79273837	23.02740	1.04670
-97.23554418	30.85334188	23.01400	1.04609
-97.11424192	30.78639082	22.89527	1.04069
-97.32176715	30.93053989	22.86570	1.03935
-97.329945	30.9397981	22.77310	1.03514
-97.05068055	30.77357652	22.77190	1.03509
-97.02472189	30.75795844	22.73691	1.03350
-97.01313873	30.76864722	22.65226	1.02965
-96.85220547	30.84180104	22.64760	1.02944
-97.11125532	30.79094136	22.61538	1.02797
-97.03722798	30.76734977	22.47204	1.02146
-96.92641212	30.89024269	22.23382	1.01063
-97.08175602	30.7914959	22.15895	1.00722
-97.23836855	30.84888543	22.07317	1.00333
-97.16510425	30.83342029	22.01819	1.00083
-97.13111536	30.80548052	21.92715	0.99669
-97.32740455	30.93944725	21.86787	0.99399
-96.83846642	30.84487384	21.77754	0.98989
-97.11092922	30.7865433	21.76748	0.98943
-96.77629879	30.83280947	21.65318	0.98424
-97.37639794	30.94922436	21.52831	0.97856
-96.79257971	30.86539404	21.47348	0.97607
-96.94230972	30.87831423	21.41226	0.97328
-97.27637033	30.86743313	21.38248	0.97193
-97.3230039	30.91428116	21.31888	0.96904
-97.33765674	30.95588812	21.23184	0.96508
-97.19323679	30.84621112	21.17996	0.96273
-97.02251391	30.75882238	21.00854	0.95493
-96.96989553	30.82740855	20.98732	0.95397

2018-2022 Reaches with Migration 19.7- 32.8 ft

X Value of Centroid (W)	Y Value of Centroid (N)	Migration (ft)	Migration Rate (ft/yr)
-96.94374847	30.84084511	32.70651	8.17663
-97.0206604	30.75998497	32.70228	8.17557
-96.695961	30.84589195	32.64918	8.16230
-96.92556	30.88637924	32.42057	8.10514
-97.33078003	30.95369911	32.33358	8.08339
-97.14354706	30.8228302	32.20011	8.05003
-97.13725281	30.81944847	31.98105	7.99526
-96.798172	30.86358452	31.48318	7.87079
-97.01346588	30.77429581	31.41337	7.85334
-97.13619995	30.81492424	31.38039	7.84510
-97.37620544	30.94914246	31.20039	7.80010
-96.72522736	30.83703613	31.08019	7.77005
-97.30486298	30.88092232	30.97299	7.74325
-96.98854828	30.78395081	30.86407	7.71602
-96.70458984	30.84150887	30.83362	7.70841
-97.1625824	30.83236504	30.62104	7.65526
-96.7110672	30.83706093	30.59576	7.64894
-97.16387177	30.83304214	30.47978	7.61994
-97.09879303	30.79430771	30.03389	7.50847
-97.18483734	30.84704018	30.02455	7.50614
-96.78179932	30.83540726	30.02271	7.50568
-97.38606262	30.96180916	29.75613	7.43903
-97.39250183	30.97403526	29.51171	7.37793
-97.1818161	30.84216881	29.41180	7.35295
-97.22756958	30.84962273	29.41026	7.35256
-96.73561096	30.82777977	29.31950	7.32987
-96.70576477	30.84475517	29.18249	7.29562
-97.3300705	30.9396801	29.10786	7.27696
-97.33492279	30.95923233	28.98462	7.24615
-97.37014771	30.95236969	28.98315	7.24579
-97.27971649	30.86605835	28.73685	7.18421
-97.33649445	30.95594597	28.52855	7.13214
-97.02583313	30.75949478	28.41285	7.10321
-96.73182678	30.83366013	28.37759	7.09440
-97.31760406	30.94510841	28.31230	7.07808
-96.99320221	30.78058243	28.31062	7.07765
-97.20021057	30.85048676	28.30166	7.07541
-97.24288177	30.85135269	28.20077	7.05019
-97.39221191	30.9732933	28.11599	7.02900
-97.31918335	30.92483902	27.62639	6.90660
-96.68545532	30.84581184	27.51386	6.87846
-97.08177185	30.79057121	27.34786	6.83697
-97.02531433	30.76126862	27.05376	6.76344

-96.91643524	30.88430977	26.95342	6.73835
-97.23540497	30.85235023	26.78724	6.69681
-96.96066284	30.84022141	26.50568	6.62642
-97.32383728	30.93862534	26.48980	6.62245
-96.99200439	30.7959671	26.42153	6.60538
-96.78643799	30.85591698	26.40135	6.60034
-97.31796265	30.92142487	26.33457	6.58364
-97.27116394	30.8741703	26.28353	6.57088
-96.87597656	30.86329079	26.22927	6.55732
-97.02372742	30.75745583	26.21438	6.55360
-97.32617188	30.94007874	26.20563	6.55141
-97.39791107	30.97557831	25.98656	6.49664
-97.36712646	30.95538712	25.91203	6.47801
-97.31613159	30.918293	25.82760	6.45690
-97.33576202	30.95851898	25.73300	6.43325
-96.91349792	30.88084221	25.70654	6.42664
-97.32067871	30.90805054	25.68305	6.42076
-97.23888397	30.85038757	25.65963	6.41491
-96.98985291	30.80934906	25.58890	6.39722
-96.70772552	30.84592628	25.49373	6.37343
-97.15781403	30.83119774	25.46885	6.36721
-96.9358139	30.8687191	25.22235	6.30559
-97.20135498	30.84532356	24.98992	6.24748
-97.3812027	30.95352364	24.78174	6.19544
-97.13117218	30.80542183	24.57622	6.14406
-97.32230377	30.93041039	24.55899	6.13975
-97.32996368	30.95550156	24.41279	6.10320
-97.24201965	30.85045433	24.36086	6.09022
-96.91534424	30.88270569	24.19476	6.04869
-97.32259369	30.90938759	24.08013	6.02003
-97.02953339	30.76989746	24.05721	6.01430
-97.14846802	30.82420921	24.03648	6.00912
-96.72846985	30.83619118	24.02907	6.00727
-97.32263947	30.93613434	23.90558	5.97640
-97.3739624	30.94785881	23.89525	5.97381
-97.32065582	30.94305229	23.64972	5.91243
-96.98722839	30.79052925	23.56362	5.89091
-96.9648056	30.8402729	23.53028	5.88257
-97.27633667	30.86483765	23.49222	5.87306
-97.39163971	30.97111893	23.45766	5.86442
-97.03827667	30.77030754	23.32194	5.83048
-96.77294159	30.8347683	23.22881	5.80720
-96.83992004	30.84564781	23.05144	5.76286
-97.03417969	30.76750183	22.90752	5.72688
-96.9613266	30.83639717	22.87921	5.71980
-97.2574234	30.87372589	22.81044	5.70261
-96.71370697	30.84263229	22.68266	5.67066
-96.77836609	30.830616	22.63756	5.65939
-96.98516846	30.81415749	22.49170	5.62293

-97.36902618	30.9545002	22.44454	5.61113
-96.71255493	30.84175682	22.41500	5.60375
-96.75521088	30.82478523	22.38339	5.59585
-97.30371094	30.88906288	22.36040	5.59010
-96.91989136	30.89035606	22.34880	5.58720
-97.32281494	30.93741989	22.29113	5.57278
-97.3190155	30.95095825	22.26917	5.56729
-97.19621277	30.84768295	22.16424	5.54106
-97.19223785	30.84717941	22.11513	5.52878
-96.71906281	30.84177971	22.07512	5.51878
-97.33204651	30.95728683	21.95035	5.48759
-97.00170898	30.77365112	21.92848	5.48212
-97.00589752	30.77541733	21.86784	5.46696
-96.94809723	30.8350544	21.67041	5.41760
-96.94063568	30.87576103	21.62852	5.40713
-96.77633667	30.83283615	21.53012	5.38253
-96.91048431	30.87615204	21.49259	5.37315
-97.23684692	30.84981537	21.43185	5.35796
-96.98960876	30.79429436	21.38916	5.34729
-96.99225616	30.78141975	21.21866	5.30467
-96.95407104	30.83402824	21.19037	5.29759
-96.99054718	30.79720879	21.13088	5.28272
-97.40100861	30.98007393	21.12862	5.28215
-97.34075928	30.96145248	20.91278	5.22820
-96.8400116	30.84769058	20.77438	5.19359
-97.21071625	30.85166931	20.53774	5.13443
-97.22740173	30.84815216	20.52797	5.13199
-97.34836578	30.96494675	20.48597	5.12149
-96.98962402	30.79968643	20.43545	5.10886
-96.7822876	30.84346771	20.36904	5.09226
-97.08178711	30.78726959	20.36204	5.09051
-97.05535889	30.77514648	20.30907	5.07727
-96.87325287	30.85357475	20.30641	5.07660
-97.07035065	30.77916336	20.18031	5.04508
-97.28833008	30.87598419	20.05607	5.01402
-97.0589447	30.77671242	20.03717	5.00929
-97.07253265	30.77666855	20.03488	5.00872
-96.9743042	30.81893921	19.95883	4.98971
-96.94216156	30.88454056	19.92771	4.98193
-97.044487	30.77532768	19.87153	4.96788
-97.03926086	30.77431107	19.77065	4.94266
-97.21785736	30.84794617	19.68897	4.92224

2018-2022 Reaches with Migration ≥32.8 ft

X Value of Centroid (W)	Y Value of Centroid (N)	Migration (ft)	Migration Rate (ft/yr)
-97.11390686	30.79468346	1098.68956	274.67239
-96.7754364	30.83750916	103.47417	25.86854
-97.40089417	30.98189545	102.01738	25.50435
-96.84437561	30.8429966	101.62068	25.40517
-97.32501984	30.92541313	98.17358	24.54339
-96.71945953	30.84932899	89.52092	22.38023
-97.16016388	30.83114624	82.15388	20.53847
-97.1342392	30.81049156	80.29443	20.07361
-97.28436279	30.8689537	74.39691	18.59923
-97.40097809	30.98307037	72.37135	18.09284
-97.3957901	30.97576332	68.79165	17.19791
-97.32523346	30.91184616	67.67365	16.91841
-96.72154236	30.84758186	65.73056	16.43264
-97.32144928	30.91380882	64.07188	16.01797
-97.39080048	30.96929932	63.85578	15.96395
-97.3539505	30.95953178	63.01728	15.75432
-97.32534027	30.91344643	61.99819	15.49955
-96.84683228	30.84249496	61.80879	15.45220
-97.17082214	30.83517265	60.86350	15.21587
-97.17137909	30.83841705	59.35020	14.83755
-96.92546082	30.89324951	59.18958	14.79739
-97.32115936	30.90244293	59.12069	14.78017
-97.31295776	30.89422417	59.00575	14.75144
-97.32509613	30.92884254	56.34573	14.08643
-97.38738251	30.96255493	55.96076	13.99019
-97.16138458	30.83165741	55.82519	13.95630
-97.3265686	30.92744827	55.62745	13.90686
-97.32621765	30.92647362	53.70692	13.42673
-96.80323029	30.85420036	53.63535	13.40884
-96.80150604	30.85694885	53.15562	13.28891
-96.72117615	30.84448242	52.39144	13.09786
-96.71230316	30.84563446	51.63343	12.90836
-96.7742157	30.83939362	51.38665	12.84666
-97.31101227	30.8931675	51.33011	12.83253
-97.31934357	30.91540337	50.98518	12.74629
-96.7027359	30.83911133	50.84904	12.71226
-97.22039795	30.85456848	50.69353	12.67338
-96.80723572	30.85088921	50.28071	12.57018
-97.29515839	30.88070869	49.97179	12.49295
-96.69315338	30.85082626	49.87819	12.46955
-96.7158432	30.83747673	49.65234	12.41308
-97.32032013	30.89756012	49.09500	12.27375
-97.37985992	30.951931	48.67773	12.16943
-97.38982391	30.96787834	48.37335	12.09334

-97.3524704	30.96029472	48.01871	12.00468
-96.88495636	30.88508415	47.70691	11.92673
-97.31636047	30.89455223	46.60742	11.65185
-97.13091278	30.80849266	45.92684	11.48171
-96.94262695	30.87852859	45.72986	11.43246
-97.32376862	30.91460609	45.49998	11.37500
-96.84877014	30.84150505	45.31778	11.32945
-96.68235016	30.84415054	45.25754	11.31439
-96.81012726	30.85235977	43.52665	10.88166
-97.18695068	30.84562874	43.23613	10.80903
-96.98876953	30.78267097	43.21174	10.80293
-96.94549561	30.8390007	42.71424	10.67856
-97.31504822	30.89308929	42.68508	10.67127
-97.33900452	30.95903397	42.54039	10.63510
-96.78829193	30.85626411	41.87312	10.46828
-96.70864105	30.83874893	41.57227	10.39307
-97.3167572	30.9458046	41.19866	10.29967
-97.15652466	30.83049202	40.37231	10.09308
-97.28430939	30.87125969	40.28923	10.07231
-97.31022644	30.88677979	39.09221	9.77305
-97.22211456	30.8514843	38.41966	9.60491
-97.13475037	30.81221581	38.32196	9.58049
-96.78253174	30.84637451	37.98258	9.49565
-97.32293701	30.90624046	37.86966	9.46741
-96.95225525	30.83348846	37.80842	9.45210
-97.39186859	30.97217178	37.72618	9.43155
-97.17983246	30.83974838	37.59214	9.39804
-97.15283203	30.82571602	37.50602	9.37651
-97.32756042	30.9321003	37.32036	9.33009
-97.248909	30.870924	37.20130	9.30032
-97.32126617	30.92881584	36.81241	9.20310
-96.9118042	30.87895775	36.63260	9.15815
-96.71699524	30.84563065	36.28408	9.07102
-97.28088379	30.86683846	36.21343	9.05336
-96.75175476	30.82444191	36.19359	9.04840
-97.13208771	30.80914307	36.09683	9.02421
-97.3066864	30.89084816	35.86544	8.96636
-97.31944275	30.92338181	35.84336	8.96084
-96.84183502	30.84610748	35.49454	8.87364
-97.21979523	30.85476685	35.24913	8.81228
-97.31654358	30.94693565	35.15335	8.78834
-97.32383728	30.92474747	34.88210	8.72053
-97.0560379	30.77744484	34.55531	8.63883
-96.79131317	30.86222458	34.41005	8.60251
-96.79511261	30.86422348	34.39490	8.59873
-97.02400208	30.76240158	34.17468	8.54367
-97.24045563	30.85055161	34.08323	8.52081
-97.24688721	30.86123276	34.08200	8.52050
-97.09740448	30.79432106	33.96734	8.49184

-97.31723785	30.9487133	33.74166	8.43542
-97.15302277	30.8288517	33.71982	8.42995
-96.79951477	30.86020851	33.62829	8.40707
-97.39356232	30.97544479	33.59500	8.39875
-97.31376648	30.91951752	33.58274	8.39569
-97.23860168	30.84870148	33.26517	8.31629
-97.30835724	30.89241791	33.17629	8.29407
-97.24473572	30.85777664	33.13905	8.28476
-97.24788666	30.86502838	33.06035	8.26509
-97.28252411	30.86854744	32.99439	8.24860

1953-2022 Reaches with Migration 19.7- 32.8 ft

X Value of Centroid (W)	Y Value of Centroid (N)	Migration (ft)	Migration Rate (ft/yr)
-97.39390564	30.97545052	32.59717	0.47242
-97.27192688	30.87114716	32.58806	0.47229
-97.0721817	30.77851295	32.44004	0.47015
-97.27169037	30.87223434	31.04279	0.44990
-97.26164246	30.87688255	30.81825	0.44664
-97.27146912	30.87353516	30.44456	0.44123
-96.94499969	30.8400383	30.28383	0.43890
-97.0406189	30.77226448	29.65993	0.42985
-97.15814972	30.83141899	29.49203	0.42742
-96.69610596	30.85122108	29.27523	0.42428
-96.96483612	30.84020233	27.97141	0.40538
-97.30318451	30.88859177	27.86039	0.40377
-97.14201355	30.82201004	27.64656	0.40067
-97.31745911	30.94523811	27.52356	0.39889
-97.26438141	30.87766647	27.41861	0.39737
-97.08136749	30.78800392	27.09893	0.39274
-97.3077774	30.88233566	26.80451	0.38847
-97.24739838	30.86721802	26.61311	0.38570
-97.03782654	30.76807594	26.56711	0.38503
-97.24403381	30.85314941	26.31062	0.38131
-97.03739929	30.76732063	26.09442	0.37818
-97.3197937	30.8963871	26.07252	0.37786
-97.37091827	30.95103645	25.60418	0.37108
-96.79547882	30.86562538	25.45384	0.36890
-97.33429718	30.95941162	24.94217	0.36148
-97.35179138	30.95972061	23.78858	0.34476
-97.40100861	30.9801445	23.70053	0.34349
-97.32209778	30.90172005	23.23114	0.33668
-97.36712646	30.95540237	23.22297	0.33656
-97.25621033	30.87477303	22.17422	0.32137
-96.79955292	30.86098289	21.90041	0.31740

-97.38838959	30.96385002	21.86005	0.31681
-96.88498688	30.88491249	21.60560	0.31312
-97.39263916	30.97429657	21.29370	0.30860
-97.38622284	30.96224976	20.85952	0.30231
-97.30463409	30.88860893	20.57699	0.29822
-97.32524872	30.91340446	20.31167	0.29437
-97.24481964	30.8615036	20.05096	0.29059
-96.90465546	30.8785305	19.99677	0.28981

1953-2022 Reaches with Migration ≥32.8 ft

X Value of Centroid (W)	Y Value of Centroid (N)	Migration (ft)	Migration Rate (ft/yr)
-97.11408997	30.79491234	1156.52911	16.76129
-96.75370026	30.82924843	947.15283	13.72685
-96.84783936	30.84499168	681.34478	9.87456
-96.71380615	30.83856201	609.19987	8.82898
-96.72503662	30.83986282	574.30808	8.32331
-96.71140289	30.84334373	573.26004	8.30812
-96.70040894	30.8418045	570.03321	8.26135
-96.77873993	30.83460999	490.23967	7.10492
-97.18700409	30.8458004	413.52253	5.99308
-96.7872467	30.8547802	390.64204	5.66148
-96.70755005	30.84645081	330.18832	4.78534
-96.71720123	30.84499931	327.95261	4.75294
-96.80930328	30.85262489	315.73098	4.57581
-96.80410767	30.85435295	294.34577	4.26588
-96.69676208	30.84780312	282.61024	4.09580
-96.94987488	30.83262444	280.55588	4.06603
-96.82553864	30.84893227	278.75102	4.03987
-97.17034912	30.83509827	262.78457	3.80847
-97.18517303	30.84693527	259.42472	3.75978
-96.84877014	30.84078789	256.93124	3.72364
-96.7194519	30.84932327	253.44814	3.67316
-96.79303741	30.86615944	253.10738	3.66822
-96.95284271	30.83369255	249.47883	3.61564
-97.40143585	30.98250961	245.36683	3.55604
-96.92124176	30.88983154	244.85825	3.54867
-96.86322784	30.84672356	244.60427	3.54499
-97.17186737	30.83825302	243.92222	3.53510
-96.72174072	30.84699249	241.37217	3.49815
-97.15349579	30.828825	240.86067	3.49073
-96.94332886	30.87831497	239.47834	3.47070
-96.79161072	30.8621769	236.63776	3.42953
-96.92631531	30.88829422	219.54574	3.18182
-97.13168335	30.80803871	218.48319	3.16642
-97.35448456	30.96048737	218.21438	3.16253
-96.93762207	30.87293625	207.96811	3.01403

-96.93521118	30.8839798	205.05560	2.97182
-97.16033173	30.83162308	202.49784	2.93475
-96.96138	30.84093475	198.31771	2.87417
-97.15327454	30.82616043	192.22738	2.78590
-97.19269562	30.84746742	192.13854	2.78462
-96.95475769	30.83434677	179.33954	2.59912
-96.79811859	30.86392403	177.46940	2.57202
-97.08235168	30.79131699	170.01316	2.46396
-96.98925781	30.79454994	162.67247	2.35757
-97.13332367	30.81012535	162.03520	2.34834
-97.22766113	30.84971046	161.68817	2.34331
-96.95915222	30.83348656	160.57548	2.32718
-96.94720459	30.83644485	160.39670	2.32459
-97.13507843	30.81323814	159.01384	2.30455
-97.08746338	30.78902817	156.61800	2.26983
-97.32623291	30.92672157	156.15738	2.26315
-96.94348145	30.84144592	154.77726	2.24315
-96.96517944	30.83529282	153.79478	2.22891
-96.95161438	30.83492661	151.96746	2.20243
-97.0798645	30.79223061	151.40389	2.19426
-97.0565033	30.77744865	149.78458	2.17079
-96.78239441	30.84451103	146.94722	2.12967
-97.12843323	30.80451584	145.42931	2.10767
-97.09467316	30.79200363	138.23433	2.00340
-97.02391815	30.76268578	136.04926	1.97173
-97.08911133	30.78924179	134.16481	1.94442
-97.32178497	30.92863464	131.99942	1.91304
-97.27934265	30.86471939	131.82114	1.91045
-97.31834412	30.92152405	130.34354	1.88904
-97.39585876	30.97567177	129.54103	1.87741
-96.91023254	30.87603188	127.07454	1.84166
-97.02561951	30.75990295	126.95562	1.83994
-97.00286865	30.77651405	126.07464	1.82717
-97.27770996	30.86421204	125.73303	1.82222
-97.32653809	30.92779922	122.51702	1.77561
-97.32511902	30.9256649	122.00197	1.76814
-97.37846375	30.9505825	121.16043	1.75595
-97.09100342	30.78884888	120.63552	1.74834
-97.16365051	30.83261681	120.58789	1.74765
-96.84178162	30.84617615	120.12138	1.74089
-97.05358887	30.77390862	119.79827	1.73621
-97.32506561	30.93148613	119.05532	1.72544
-97.27503204	30.86955833	118.93458	1.72369
-97.31967926	30.9235611	117.85444	1.70804
-97.32277679	30.92554474	116.92042	1.69450
-97.19325256	30.84602165	115.11416	1.66832
-97.07051849	30.77529144	114.43751	1.65851
-97.16531372	30.83371353	114.41004	1.65812
-97.15628052	30.83070374	113.17172	1.64017

-97.22967529	30.85228348	113.16922	1.64013
-97.02420807	30.75769424	110.50869	1.60158
-96.70511627	30.84324646	110.47453	1.60108
-97.06288147	30.77515221	110.38656	1.59981
-97.1360321	30.81499481	108.40269	1.57105
-97.16749573	30.83504486	108.10483	1.56674
-97.07170105	30.78554916	105.18630	1.52444
-96.94120789	30.87632751	104.97607	1.52139
-97.32538605	30.91199303	104.49490	1.51442
-97.32391357	30.91440201	103.01336	1.49295
-97.22548676	30.8492794	102.42256	1.48438
-97.27980804	30.8664093	101.01870	1.46404
-97.32839203	30.9393959	100.84992	1.46159
-96.83971405	30.84679794	100.57137	1.45756
-96.9620285	30.83552361	100.07530	1.45037
-97.31665802	30.89471054	98.54400	1.42817
-97.31655121	30.91848564	98.31283	1.42482
-96.93694305	30.85477829	98.09133	1.42161
-96.93580627	30.86872101	96.25897	1.39506
-97.05909729	30.77671051	94.59661	1.37097
-97.28261566	30.86839104	94.33605	1.36719
-96.96609497	30.83927345	93.56653	1.35604
-97.39092255	30.96983147	92.51527	1.34080
-97.18983459	30.84616089	92.45784	1.33997
-97.1401062	30.82147217	92.20148	1.33625
-97.31317902	30.89413643	91.93327	1.33237
-96.88734436	30.88378525	91.55420	1.32687
-97.17861176	30.84019852	90.09501	1.30572
-97.32318878	30.94293976	90.06577	1.30530
-97.06121826	30.77597237	89.71491	1.30022
-97.32424927	30.935606	89.54152	1.29770
-97.20146179	30.84723663	89.42551	1.29602
-97.01765442	30.76009369	89.05188	1.29061
-96.91275787	30.88033104	89.02186	1.29017
-97.07052612	30.77980614	88.87190	1.28800
-97.28449249	30.86896896	88.34507	1.28036
-97.02526855	30.76136589	87.77365	1.27208
-97.14780426	30.82422638	87.38542	1.26646
-97.36979675	30.95301628	86.80724	1.25808
-97.13722992	30.81915665	86.33028	1.25116
-97.33643341	30.95595741	86.32431	1.25108
-97.03582001	30.76883698	85.85558	1.24428
-97.37411499	30.94810867	85.73171	1.24249
-97.38300323	30.95672989	84.92124	1.23074
-97.06861877	30.78180504	84.43771	1.22373
-97.32992554	30.95560837	83.57049	1.21117
-97.31658936	30.94717026	83.31690	1.20749
-97.36899567	30.95439339	83.25189	1.20655
-97.32279968	30.93755722	83.00902	1.20303

-97.08678436	30.78759575	82.39935	1.19419
-97.1987915	30.84637642	81.92645	1.18734
-96.89764404	30.88117409	80.48497	1.16645
-97.18191528	30.8421402	80.36688	1.16474
-97.32457733	30.95190811	79.56476	1.15311
-96.97663116	30.81898308	79.29765	1.14924
-97.05205536	30.77242088	78.92532	1.14385
-97.3877182	30.96272087	77.88668	1.12879
-97.2175827	30.84881783	77.55246	1.12395
-97.02957916	30.76946831	77.38357	1.12150
-97.22066498	30.8542347	77.26415	1.11977
-97.03823853	30.77037621	76.80687	1.11314
-97.27627563	30.86725426	76.48179	1.10843
-97.3407135	30.96154594	75.59583	1.09559
-97.26535034	30.87546921	74.88719	1.08532
-97.32152557	30.91376305	74.74930	1.08332
-97.23566437	30.85312653	74.60990	1.08130
-97.05510712	30.77490997	74.26420	1.07629
-96.98830414	30.78518105	74.09448	1.07383
-97.33177948	30.95728683	73.77456	1.06920
-97.29815674	30.88169861	73.55969	1.06608
-97.08420563	30.78897476	73.46831	1.06476
-97.30884552	30.88861656	73.23582	1.06139
-97.02693939	30.76564407	72.43222	1.04974
-97.034729	30.76717186	71.88655	1.04183
-96.91430664	30.88117599	71.63453	1.03818
-97.01284027	30.77050781	68.18488	0.98819
-97.32060242	30.89801788	67.45164	0.97756
-97.24103546	30.85035324	67.43770	0.97736
-97.20451355	30.85032463	66.66203	0.96612
-97.26856232	30.87796402	66.43412	0.96281
-97.31101227	30.89307976	66.17127	0.95900
-97.33908081	30.95891953	66.02650	0.95691
-97.31730652	30.94884682	65.64782	0.95142
-97.0393219	30.77401924	64.99855	0.94201
-97.21001434	30.85168266	64.63118	0.93668
-97.28113556	30.86675262	64.14693	0.92967
-97.22143555	30.85668373	63.37139	0.91843
-97.33585358	30.95922089	62.79175	0.91003
-97.23875427	30.85031319	62.45982	0.90521
-97.28853607	30.87528801	61.82030	0.89595
-97.31920624	30.92495728	61.60109	0.89277
-97.25881958	30.87346649	60.73340	0.88019
-96.9876709	30.8088932	60.16638	0.87198
-97.24803162	30.86286354	59.44344	0.86150
-97.31506348	30.89313698	59.44096	0.86146
-97.06639099	30.77370644	59.33718	0.85996
-97.30858612	30.89294815	58.22335	0.84382
-97.27648926	30.86446571	58.11219	0.84221

-97.23834991	30.84899139	57.33382	0.83092
-97.32116699	30.90323448	57.08053	0.82725
-96.98694611	30.80396271	55.71824	0.80751
-97.31934357	30.9153347	55.18509	0.79978
-97.05065155	30.77354431	55.12895	0.79897
-96.99061584	30.79734421	54.85729	0.79503
-97.32048798	30.90865898	54.62787	0.79171
-97.35256958	30.96038055	54.18479	0.78529
-97.04020691	30.77132416	52.93793	0.76722
-97.25045776	30.87239456	52.29194	0.75785
-97.30544281	30.89120865	51.55247	0.74714
-96.95042419	30.83407402	51.05637	0.73995
-97.32250977	30.90670395	50.59442	0.73325
-96.87538147	30.87251472	49.72989	0.72072
-97.18366241	30.84461212	49.71072	0.72045
-96.87602997	30.86362267	49.44087	0.71653
-97.06488037	30.77414894	49.30376	0.71455
-97.26152039	30.87457466	48.50530	0.70298
-97.21924591	30.85762215	48.14155	0.69770
-97.32545471	30.928936	47.98355	0.69541
-96.77375793	30.83939552	47.25071	0.68479
-97.30314636	30.8908844	47.07346	0.68222
-97.09938812	30.79401207	46.74181	0.67742
-97.20841217	30.85012627	46.72938	0.67724
-96.98695374	30.79094696	46.01167	0.66684
-97.34475708	30.96596527	45.87535	0.66486
-97.37216187	30.94912338	44.83790	0.64982
-97.38943481	30.96683502	44.42114	0.64378
-97.09237671	30.78887367	44.15410	0.63991
-97.33483124	30.95741081	43.66051	0.63276
-97.39942169	30.9773407	43.49639	0.63038
-97.03055573	30.77181053	42.61010	0.61754
-97.30797577	30.89057159	41.91254	0.60743
-97.23497772	30.85201836	41.33953	0.59912
-96.69422913	30.85150146	41.08737	0.59547
-96.88273621	30.88498878	40.54669	0.58763
-97.21789551	30.85392189	39.81116	0.57697
-97.37994385	30.95232391	38.82456	0.56267
-96.94225311	30.84274101	38.76440	0.56180
-97.32358551	30.9105587	35.98741	0.52156
-97.39187622	30.97226906	35.79039	0.51870
-96.98961639	30.80062103	34.50673	0.50010
-97.39212799	30.97317123	34.09813	0.49418
-97.03248596	30.77236748	33.50159	0.48553
-97.04451752	30.77533531	33.08779	0.47953
-97.27607727	30.86563492	33.07620	0.47937
-96.73199463	30.83501434	32.92502	0.47717